EUROPEAN COMMISSION
5th EURATOM FRAMEWORK PROGRAMME 1998-2002
KEY ACTION: NUCLEAR FISSION

IRRADIATION EFFECTS IN MARTENSITIC STEELS

UNDER NEUTRON AND PROTON MIXED SPECTRUM

SPIRE

CONTRACT N°FIKW – CT – 2000 - 00058

FINAL SCIENTIFIC AND TECHNICAL REPORT

Ana ALAMO

Project Coordinator

Commissariat à l'Energie Atomique

Deliverable n° 50 - Month 48

Dissemination level:
PU: public

Project Coordinator :

Commissariat à l'Energie Atomique	F

Contractors :

Centro de Investigationes Energeticas, Medioambientales y Tecnologicas	E
Centre National de la Recherche Scientifique, Institut National de Physique Nucléaire et de Physique des Particules	F
Centre National de la Recherche Scientifique Groupe de Physique des Matériaux UMR CNRS 6634	F
Nuclear Research and consultancy Group	NL
Ente per le Nuove Tecnologie, l'Energia e l'Ambiente	I
Paul Scherrer Institut	CH
Kungliga Tekniska Högskolan	S
Belgian Nuclear Research Centre	B
Forschungszentrum Karlsruhe	D
Centre National de la Recherche Scientifique, Centre d'Etudes de Chimie Métallurgique	F

Distribution list :

EC	V. Bhatnagar
CIEMAT	A.M. Lancha, D. Gomez-Briceño
CNRS/UMR 6634	P. Pareige
CNRS/IN2P3	M. O. Ruault, H. Bernas
CNRS/CECM	V. Pontikis
ENEA	M.F. Maday, G. Filacchioni
FZK	A. Moslang, P. Vladimirov, C. Fazio, J. Knebel
NRG	J.W. Rensman, B. van der Schaaf
KTH	J. Wallenius
PSI	Y. Dai, F. Groeschel
SCK•CEN	E. Lucon, H. Aït Abderrahim, A. Almazouzi
FzJ	P. Jung
ANSALDO	L. Cinotti
FRA-ANP	B. Giraud

CEA

DEN		P. Lederman
	DSOE	J.L. Boutard
	DDIN	D. Warin
	DTN	C. Latgé
	DER	G. Granget
	DPC	A. Terlain
	DMN	P. Le Poac, J. L. Séran
	/SRMA	F. Ravel, J. Henry, Y. de Carlan,
		J.C. Brachet, B. Marini, L. Vincent
	/SEMI	P. Yvon, X. Averty
	/SRMP	M. Guttman, R. Gupta

EXECUTIVE SUMMARY

SPIRE project dealing with the "irradiation effects in martensitic steels under neutron and proton mixed spectrum", started in August 2000 and finished in July 2004. It was carried out with participation of eleven European partners and had as a main objective the investigation of the specific irradiation effects undergone by the structural materials constituting the spallation target of an Accelerator Driven System (ADS).

The high Chromium martensitic steels, 9-12%Cr, appeared to be the most promising candidates to resist such as severe irradiation conditions. So, the selected candidates are:

- Conventional 9Cr and 12Cr martensitic steels : 9Cr-1Mo (EM10), 9Cr1MoVNb (T91) and 12Cr1MoVW (HT9)
- Experimental alternative clean steels: 7-9 Cr1-2WTa.

To study the evolution of the microstructure and mechanical properties of these materials under conditions simulating the spallation environment, a large number of experiments were performed using important facilities existing in Europe like SINQ spallation source facility, Materials Testing Reactors (HFR, BR2), Jülich compact cyclotron for He-implantations, other ions accelerators, the corresponding hot cells for Post-irradiation Examinations and also BOR60 fast reactor implanted in RIAR (Russia).

A particular attention has been paid to the microstructure assessment to get insight on the evolution of the mechanical properties under irradiation. Transmission Electron Microscopy (TEM) including X-ray Emission Dispersion Spectroscopy (XEDS) were used as well as Auger Electron Spectroscopy (AES), Tomographic Atom Probe (TAP), Small Angle Neutron Scattering (SANS).
Important calculation tools for numerical simulations were also implemented in different labs to provide basic understanding and predictions for high dose under spallation relevant spectrum.

The programme aimed to evaluating the different contributions to damage induced in structural materials in a spallation target environment: atomic displacements produced by high energy protons and neutrons, effects of gas production (hydrogen and helium) and other solid elements (Ca, Ti, P, S, etc.) produced by spallation reactions.

To complete the data concerning the mechanical behaviour of unirradiated conventional and experimental martensitic steels, tensile, creep, impact and fracture toughness tests were also performed. Round robin tests assessed the high confidence level of results obtained between different labs. Also, estimates of the fracture probability and cleavage stress level corresponding to EM10 and T91 steels were determined for temperatures of about -170/-150°C.

The effects of solid spallation elements were studied using two simulation techniques, i.e., doping during melting some ingots manufactured for this purpose or implanting with the element of interest. Results on doped materials showed the strong tendency of these elements to segregate in grain boundaries or precipitate with very fast kinetics, which should be the situation in-service conditions. The concurrent presence of Ti, P and S resulted in a significant degradation of toughness and impact properties in the unirradiated condition and after irradiation as well.
Tomography Atom Probe (TAP) examinations following implantation evidenced the trend of P and S to be associated in clusters of nanometric size. In contrast, neither clustering nor hardening was observed after implantation of Ca-ions up to 0.2% max.

The effects of hydrogen on tensile properties were investigated at room temperature for contents of 110-450 appm (2-8 wppm) introduced by cathodic charging techniques. Hydrogen induces a decrease of ductility and the occurrence of increasing intergranular decohesions and transgranular cleavage. T91 steel presented the higher resistance to this type of damage.

One of the most important concerns is the production of Helium whose effects were investigated in T91 and EM10 steels by implantation experiments performed at different temperatures (125-550°C) and He-contents (up to 5000 appm). These experiments have established the existence of a "low temperature Helium-embrittlement" occurring at temperatures about or lower than 250°C, where the ductility drops very

quickly with He-content simultaneously with the increasing hardening of the material. For He ≥ 2500 appm, elongations reached nearly zero values and an intergranular fracture mode was observed.
At higher temperatures, lower hardening and higher ductility was obtained. Moreover, the feasibility of He-implantation in Charpy specimens to study fracture toughness properties has been demonstrated.

The irradiations under mixed proton/neutron spectrum at SINQ facilities constituted a particularly relevant part of the programme, since it is the prototypical spectrum foreseen for the beam window of the spallation target. The experiments were carried out in nearly the same range of irradiation temperatures (100-350°C, up to 12 dpa) used in neutron and implantation experiments, which allows comparing the behaviour of 9-12Cr martensitic steels in different environments.

Important modifications of the microstructure were observed: point defect clusters, high density of He-bubbles, amorphisation of initial carbide particles. Irradiation induced hardening is equivalent to that obtained after neutron irradiation performed in similar conditions of dose and temperature. In contrast, a higher level of embrittlement was observed for all materials and in particular for T91 specimens irradiated in SINQ compared to results of neutron irradiation. This accelerated brittle behaviour could be attributed to He-effects even though the concentrations obtained (< 1000 appm) are lower than the critical concentration determined from tensile properties of implanted specimens. Further data from SINQ and neutron experiments are needed at various doses and temperatures to assess these phenomena.

An important database is available now from neutron irradiations to evaluate the effects of atomic displacements on the behaviour of 9-12%Cr martensitic steels in the range 200-325°C where previous existing data were quite limited. Comparable and consistent results originating from experiments in BR2 (200°C) and in HFR (250°C) at low doses (2-4 dpa) have shown the occurrence of increasing hardening with the dose, an increase of Ductile Brittle Transition Temperature (DBTT) with a slight decrease of the upper shelf energy. Facture toughness tests performed in the upper shelf region decreased 25-30% after irradiation, whereas the reference temperature T_o, determined from the Master Curve approach in the transition regime, increased faster than the DBTT. EM10 and 9Cr2WTaV steels displayed the least embrittlement after irradiation at low doses.

One open point is related to the applicability of the Master Curve approach to high chromium martensitic steels, since the T_o increase is greater than the DBTT shift which is not observed in other types of steels. This point should have important implications for designers and safety authorities.

For higher dose, close to that planned for the spallation target structures, the neutron experiment performed in BOR60 reactor at 325°C for doses of 32-42 dpa has shown: a very low deformation (0.2-0.6 % at 42 dpa) due to irradiation creep at this temperature determined for pressurised tubes of all 9Cr materials. T91 and EM10 specimens were prone to irradiation effects more rapidly as compared to 9Cr-1&2 W VTa experimental steels, i.e., much faster hardening and a more rapid decrease of their ductility. In particular, a nearly total loss of ductility was obtained for tensile specimens of EM10 and T91 tested at 20°C. This fact is probably related to the increase of DBTT above room temperature. This point will be assessed in the near future by Charpy tests (in progress).

But, the most important outcome from BOR60 irradiation is associated to the important effect of the irradiation temperature. The irradiation behaviour of EM10 and T91 steels was largely investigated in the range 400-550°C for high doses in Phenix reactor. Both materials displayed in these conditions a very low increase of yield stress and DBTT shift, but the decrease of the irradiation temperature to 325°C lead EM10 steel to a hardening (620 MPa) of about 4 times higher than that detected at 390°C (~ 150 MPa).

On the other hand, tasks of "Basic Studies" completed the experimental approach by theoretical simulations. In particular, calculations for the irradiation damage (displacement, heat deposition and gas & spallation elements production) in the beam window provided new estimates assuming a proton beam of lower energy (600 MeV) and lower current density compared to the values originally assumed when SPIRE project was initiated (1 GeV and ~70μA/cm^2). The maximum damage rate of the beam window will be about 32 dpa/fpy with lower hydrogen and helium production rates: 430 appm H/dpa and 35 appm He/dpa.

Other important achievements in this project are related to the development of FeCr many body potential to model the configuration and migration of radiation defects, clustering/ precipitation of chromium.

The evaluation of cohesion energy of segregated boundaries was performed taking into account different elements (H, He, Ti, V, Cr, Zr, Nb, Cl etc.). In particular for helium, calculations have concluded to the significant loss in grain boundary cohesion due to the chemical interaction of helium, which is essentially repulsive with neighbouring atoms. Calculations for the co-segregations of H and He in the grain boundary show that the synergistic effect is small.

All performed experiments have shown a very important degree of embrittlement in the temperature irradiation range of 100-325°C. This is a common feature to irradiations with mixed spectrum where both displacement damage and He-effects contributions operate, to neutron irradiations where only displacement damage is produced or to He-implantations.

So, the most important conclusion that could be drawn is related to the major role of the temperature in the activation of mechanisms responsible of materials properties degradation.

Consequently, to avoid a prohibitive level of hardening and embrittlement, it is recommended that in-service temperatures need to be higher than 350°C to optimise the lifetime of the beam window and other structures heavily irradiated of the spallation target or core components.

Finally, it must be pointed out that a significant contribution has been made by the SPIRE project to improve the scientific and technological knowledge related to the metallurgy of 9Cr martensitic materials.

In general, this project allowed fruitful cooperation with other European and international projects, like MEGAPIE, where data obtained in the frame of SPIRE has a direct application.

In particular, the main outcomes of SPIRE constituted the basic input for the definition of the research programme concerning the structural materials irradiation behaviour included in the IP-EUROTRANS (6^{th} FP) devoted to "Partitioning and Transmutation" field.

Also, connected fields such as materials community for fusion technology and advanced fission reactors will also benefit from the successful outcomes of the present work.

CONTENT

1. INTRODUCTION 10

1.1 Background and Objectives of SPIRE Project 10

1.2 The selection of 9Cr martensitic steels 11

1.3 SPIRE Work Programme 11

2. METALLURGY BEFORE IRRADIATION WORK-PACKAGE 2 14

2.1 Materials 14

2.2 Complementary studies on conventional 9Cr candidate materials 15
2.2.1 Metallurgical characterisation of conventional and experimental 9Cr martensitic steels 15
2.2.2 Interlaboratory comparison of mechanical test results 15
2.2.3 Mechanical characterisation of EM10 and T91 reference steels 16
2.2.4 Modelling of fracture mechanisms of conventional 9Cr steels using the local approach 17

2.3 Effects of spallation elements like Ti, P, and S on the behaviour of 9Cr steels 17
2.3.1 Effects on physical metallurgy 17
2.3.2 Mechanical properties of Ti, P, S doped steels 18

2.4 Effects of hydrogen on the tensile properties of candidate steels and doped materials 18

2.5 Summary and Conclusions 20

2.6 Reports produced in the frame of SPIRE project - WP2 21

3. EXPERIMENTAL SIMULATION OF IRRADIATION EFFECTS IN A SPALLATION SPECTRUM WORK-PACKAGE 3 22

3.1 He implantation of 9Cr-1Mo steels and related examinations 22
3.1.1 Materials, implantation and testing conditions 22
3.1.2 He-effects on tensile properties 23
3.1.3 He-effects on the microstructure 24
3.1.4 He-effects on fracture properties 25

3.2 Implantation of various spallation products (Ca, S, Ti) and related examinations 26

3.3 Conclusions 28

3.4 Reports produced in the frame of SPIRE project – WP3 29

4. NEUTRON-IRRADIATION AND POST-IRRADIATION EXAMINATION WORK-PACKAGE 4 31

4.1 Irradiation in BR2 reactor at 200°C and associated PIE (SCK•CEN) 31
4.1.1 Materials, specimens and irradiation conditions 31
4.1.2 Tensile properties 31
4.1.3 Impact properties 32
4.1.4 Fracture toughness 34

4.2 Irradiation in HFR reactor at 250°C and associated PIE 34
4.2.1 Materials, specimens and irradiation conditions 35
4.2.2 Evolution of tensile properties 35
4.2.3 Evolution of impact properties 36
4.2.4 Fracture toughness 38

4.3 Irradiation in BOR60 at 325°C and associated PIE 38
4.3.1 Materials, specimens and irradiation conditions 38
4.3.2 Tensile properties 39
4.3.3 Irradiation Creep 41

4.4 Summary and Main Conclusions 42

4.5 Reports produced in the frame of SPIRE project – WP 43

5. IRRADIATION UNDER MIXED PROTON-SPECTRUM AND POST-IRRADIATION EXAMINATION WORK-PACKAGE 5 44

5.1 Irradiations of SPIRE Materials in SINQ Facility 44

5.2 PIE of specimens irradiated in STIP-I 44
5.2.1 Investigation on the microstructure of martensitic steels T91 and F82H 44
5.2.2 Mechanical properties of T91 and others F/M specimens irradiated in STIP-I 46

5.3 PIE of specimens irradiated in STIP-II 49

5.4 Summary and Main Conclusions 50

5.5 Reports produced in the frame of SPIRE project – WP5 51

6. BASIC STUDIES: NUMERICAL SIMULATION OF IRRADIATION EFFECTS WORK-PACKAGE 6 **52**

6.1 Damage Characterisation of the ADS Beam Window **52**
6.1.1 Displacement damage 52
6.1.2 Heat production 53
6.1.3 Gas and spallation elements production rates 53
6.1.4 Conclusions 54

6.2 Molecular dynamic simulation of defects production and migration rates in FeCr alloys **55**

6.3 Modelling of the obstacle forces due to irradiation defects and the associated hardening **55**

6.4 Cohesion energy of segregated boundaries based on electronic structure **56**

6.5 Reports produced in the frame of SPIRE project – WP6 **57**

7. DISCUSSION **58**

8. CONCLUSIONS **64**

9. PROSPECTS FOR FUTURE PROGRAMME **66**

10. LIST OF DELIVERABLES **68**

11. PUBLICATIONS IN INTERNATIONAL SCIENTIFIC JOURNALS **73**

1. INTRODUCTION

The main purpose of the present report is to summarise the analyzed data and principal outcomes obtained during the development of SPIRE programme. This project started in 1st August 2000 and finished on 31 July 2004. It was conducted with the fruitful contribution of European partners of the consortium integrated by CEA, CIEMAT, CNRS, ENEA, FZK, KTH, NRG, PSI, SCK•CEN. Besides them, Forschungszentrum Jülich (Germany) and RIAR Dimitrovgrad (Russia), participated also as sub-contractors in the development of this programme.

After a general introduction outlining the background and the objectives planned at the beginning of SPIRE project, this report presents a scientific/technical review of the main experimentations, theoretical approaches used and results obtained. The presentation of such a huge amount of data, based on the progress and final reports produced by different participating institutions, is given in chapters 2 to 6 corresponding to the technical work-packages (WP2 to WP6) of the SPIRE project. Work package 1 (WP1) is related to the coordination activities of the project.

A general discussion, final conclusions and prospects for future programmes are also presented as well as the lists of technical reports released in the frame of this programme and the publications in international scientific journals.

1.1 BACKGROUND AND OBJECTIVES OF SPIRE PROJECT

The safety objectives of nuclear installations in Europe are strongly linked to a safe and effective management of radioactive wastes and final disposal. More specifically, the objectives of the Safety of the fuel cycle are the development of sound basis for policy choices on the management of high level and long-lived radioactive wastes and for evaluating the feasibility at industrial scale of partitioning and transmutation including design studies and associated research.

The Accelerator Driven Sytem (ADS) is an innovative concept destined to transmute with good efficiency long-lived radio nuclides to reduce their activity and radio-toxicity in the final storage.
One of key issues for ADS development is the design and validation of the liquid metal spallation target that produces neutrons. The liquid eutectic PbBi is the prime candidate foreseen as spallation material. The structure of the spallation target is commonly viewed as a container with a window to separate the vacuum of the proton accelerator from the spallation liquid metal.

For such a high power liquid metal target, the structural materials, and basically the beam window, will be exposed to intense fluxes of high energy protons and neutrons generating both high levels of radiation damage, but also significant quantities of impurities produced by spallation reactions occurring inside the window material. Therefore, severe and specific irradiation conditions are expected for the target structures coming from the higher recoil energy and the spallation elements production (He, H, P, S, Ti, V, Ca etc.) as well.

Assuming protons of 1GeV with a maximum current density of ~70 μA/cm^2 and a full calendar year of operation, the preliminary estimates of atomic displacements and spallation elements production were:

- The atomic displacements amount up to ~100 Displacements Per Atom (dpa) in the window and ~50 dpa in other structures of the target.

- In the window, the direct impingement of the proton beam, which results in the production of H (~90,000 appm), He (5,000 appm) and other spallation elements (such as Ca: ~1,000 appm, Ti: ~1,000 appm, V: ~1,000 appm, P: ~200 appm, S: ~600 appm).

It was believed that this particular environment should induce strong modifications in the microstructure, chemical composition, atomic and crystallographic structure, that will result in important changes of macroscopic properties such as significant hardening, embrittlement and loss of dimensional stability.

The main issues concerning the integrity and the lifetime of the spallation target structures were expected to be mainly brittle fracture by decrease in ductility and fracture toughness.

The main objective of SPIRE project was therefore the investigation of irradiation effects specific to a spallation target environment on the basic in-service properties (tensile, Charpy, fracture toughness, irradiation creep and swelling) of 9-12%Cr martensitic steels that appeared to be the most promising candidates to resist such a severe irradiation conditions.

In the perspective of a transmutation Demonstrator, the project was developed with the following general goals:

- Determine relevant properties of selected structural steels under irradiation conditions simulating the spallation target environment
- Provide the basic mechanisms and modelling for the phenomena observed under spallation conditions
- Provide basic data and guidance for conceptual design purposes
- Contribute to specify a reference material and give a path for the development of an advanced window material.

1.2 THE SELECTION OF 9CR MARTENSITIC STEELS

Taking into account the severe and rather new operating conditions, the selection of structural materials was one of the key issues to demonstrate the feasibility of safely operating spallation target of a transmutation Demonstrator.
The objectives of the selection was to obtain, in the operating temperature range from ~200°C to 550°C, materials that exhibit (i) heat resistance, (ii) sufficient strength with limited loss of ductility and fracture toughness under irradiation (iii) dimensional stability i.e. good resistance to swelling and limited irradiation creep and (iv) Pb-Bi compatibility.

The high chromium martensitic steels, 9-12%Cr, were selected as prime candidates, on the basis of the existing data base which comes essentially from fission and fusion programmes, so without taking into account the effect of spallation products.
The choice of 9-12 Cr martensitic steels was also based on the excellent compromise between fabricability, good resistance to heat deposition, excellent swelling resistance up to high atomic displacement dose under fission neutron spectrum (> 100 dpa), acceptable resistance to liquid Pb-alloys due to the low Ni content. It is important to notice that the higher the Cr-content, the better the resistance to corrosion but the higher the shift of the Ductile Brittle Transition Temperature (DBTT) after irradiation at least for temperatures above ~400°C.

The 9Cr1Mo presents very low DBTT after irradiation in the temperature range of 400-550°C and has been proved to be an excellent reference structural steel for the wrapper tube of the fuel subassembly of Phénix. It has a well documented data base. The 9Cr1MoVNb has been studied by the community of the Fast Reactor (FR) as a possible candidate for wrapper tubes and fuel cladding. This steel has therefore a significant but insufficient data base. The 12Cr1MoVW was extensively studied and proposed as cladding for FR, namely for Fast Flux Facility Testing Facility (FFTF). Although undergoing higher embrittlement, 12 Cr1MoVW should have somewhat higher corrosion resistance. The 7-9Cr1-2W type steels are emerging as the most promising among the experimental clean steels studied for the past ten years in the Fusion Technology Programme.

On this basis the following structural materials for the window and the target container were selected :

- Conventional 9Cr and 12Cr martensitic steels : 9Cr1Mo, 9Cr1MoVNb and 12Cr1MoVW.
- Experimental alternative clean martensitic steels : 7-9Cr1-2WTa

1.3 SPIRE WORK PROGRAMME

The irradiation conditions of spallation target steels are specific compared to fast neutrons, because of the higher recoil energy and spallation elements production that are completely absent in nuclear reactors.

Spallation products will affect both chemical composition and microstructure and induce therefore significant changes in the in-service properties. In martensitic steels, H and He will contribute to the nucleation and growth of bubbles and voids that will harden and embrittle the material and possibly

contribute to swelling. H could also induce embrittlement although the foreseen operating temperatures are rather high. P and S are well known to segregate to interface boundaries and induce intergranular brittleness.
Ti and V should harden the material via carbides precipitation. Ti and Ca could also contribute to the embrittlement via possible hydride formation.

The limited dose that can be achieved in irradiation facilities under prototypical neutron and proton mixed spectrum and the totally new and severe spallation effects in structural steels of the target resulted in adopting an analytical approach for SPIRE project to allow the simulation and evaluation of the various contributions (protons, neutrons, spallation elements production) to the material's behaviour.

On the other hand, most of existing data were obtained for temperatures in the range 400-550°C. Consequently, SPIRE project was mainly focused on the study of materials behaviour at temperatures lower than 400°C where more pronounced hardening and embrittlement could be expected.

In order to obtain comparable and consistent results, the experiments performed in the frame of SPIRE project were carried out using the same materials that were supplied by:
- CEA in the case of reference 9Cr1Mo (EM10) and 9Cr1MoVNb (T91) heats as well as Ti, P, S doped versions based in 9Cr1Mo alloy.
- NRG for 9Cr(1-2W)VTa experimental martensitic steels and doped nuances based in 9Cr2WVTa alloy with additions of B^{10}, B^{11}, low and high content of Ti-P-S.
- SCK-CEN for 12Cr1MoW V (HT9) steel.

The SPIRE project was organised in the following work-packages with the objectives described below.

- **Coordination Activities (WP1 Leader : A. Alamo – CEA)**

  The aim of the coordination work package was to ensure the progress of the project according to schedule and provide links with other projects such as networking (ADOPT), on design (PDS-XADS) and Pb-Bi corrosion activities (TECLA) etc.

- **Metallurgy before irradiation (WP2 Leader : A.M. Lancha – CIEMAT)**

The goal was to perform complementary characterisation of the mechanical behaviour of reference materials to complete their database. Another goal was to investigate the changes in physical metallurgy, microstructure and mechanical properties, induced by some spallation elements, introduced during melting like (P, S, Ti) or after cathodic charging in the case of Hydrogen.

- **Experimental simulation of irradiation effects in a spallation spectrum (WP3 Leader : J. Henry – CEA)**

The objective was to simulate the effects on microstructure and mechanical properties due to energetic spallation elements production by single beam implantation (He, Ca, Ti, S, H) or by successive implantations to test the possibility of Ca or Ti hydride formation using different complementary facilities. The mechanical properties were determined by either nano-hardness in the case of Ca, Ti, H (implantation of a few 100 nm) or tensile tests for He implantation (uniform implantation on ~100 µm). For He, a feasibility study to implant the notch of mini Charpy specimens on depth ~2 times the notch radius was carried out to test the effect of He on impact properties.

- **Neutron-irradiation and post-irradiation examination (WP4 Leader: J.W. Rensman – NRG)**

Fast neutron irradiations allow simulating reasonably well the atomic displacements in a spallation environment. The neutron irradiation experiments were designed to complete the data base of the effect of displacement damage on mechanical properties at low temperatures (below 380°C) and their evolution at high dose (comparable to dose received by the window of the target).

- **Irradiation under mixed proton-neutron spectrum and post-irradiation examination (WP5 Leader: Y. Dai – PSI)**

This part of the programme was very important, since the mixed proton-neutron spectrum is prototypical, even the dose achieved was in the range of a few dpa and the number of samples irradiated at one temperature was limited, due to high thermal gradient in the rig. The experiences were carried out in nearly the same range of irradiation temperatures used in neutrons and implantation experiments, which allow comparing the behaviour of 9-12Cr martensitic in different environments.

- **Basic studies : numerical simulation of irradiation effects (WP6 Leader: P. Vladimirov – FZK)**

The main objective was to provide the basic understanding and tools for reliable understanding and prediction of the behaviour of materials at high dose under spallation relevant spectrum.

The selected research subjects were : (i) Irradiation damage characterisation in the beam window, (ii) molecular dynamics prediction of irradiation damage, (iii) modelling, on an atomic basis, of the hardening due to radiation defects and (iv) prediction of the effect of segregation on solid cohesion energy based on ab-initio electronic structure computation.

The following description starts from the technical activities of the project i.e. work package 2.

2. METALLURGY BEFORE IRRADIATION WORK-PACKAGE 2

Most of the spallation elements are either not present in the initial chemical composition of the steels or exist in a very low and well controlled concentration range as it is the case for P and S (typically P < 350 appm, S < 100 appm). The main objective of the work-package "Metallurgy before irradiation" is to simulate the effects of some spallation elements like Ti or S or P or H on the physical metallurgy, microstructure and mechanical properties of the candidate materials in the non-irradiated condition, for a better understanding of the results obtained from simulation, neutron, and proton-neutron mixed spectrum irradiations.

The elements like Ti, P, S could be incorporated during melting and so, it is possible to have reasonable quantities of material to conduct mechanical tests with usual specimens and study their effects on the physical metallurgy of martensitic steels. For this purpose, several doped ingots were produced based in the 9Cr1Mo (EM10) and 9Cr2W steels.
The simulation of Hydrogen effects was studied by introducing this element by cathodic charging directly on tensile specimens of candidate steels and also of Ti-containing doped alloys to detect a possible Ti-hydride formation.

Other important objective of this work-package was the completion of existing data on conventional 9Cr candidate steels. For this purpose different actions were launched as : a) a metallurgical characterisation of candidate steels; b) a campaign of inter-labs comparison on tensile and mini-Charpy tests performed for 9Cr1Mo (EM10) steel to assess confident data obtained with different specimen dimensions and treatments of testing results; c) screening tests on creep and fracture toughness; d) determinations of cleavage properties.

This WP was carried out with the participation of CIEMAT, CEA, CNRS UMR6634, NRG, SCK•CEN, ENEA.
References of reports released in the WP2 are listed at the end of this section. The present summary is based on progress reports and especially on the final report (deliverable n° 41) provided by the work-package leader, A.M. Lancha, CIEMAT [12].

2.1 MATERIALS

Materials studied can be classed in three categories, where the nominal compositions are the following:

a) Reference (commercial) martensitic steels : 9Cr-1Mo (EM10) and 9Cr-1MoVNb (T91)

b) Experimental alternative steels : 9Cr-1W VTa, 9Cr-2W VTa

c) Doped alloys:
9Cr-1Mo (EM10) doped with Ti or (Ti, P, S) (EM10 Ti, EM10 TiPS)
9Cr-1Mo versions with S and low Mn (EM10 LMnS) and with Ti and low C (EM10 LCTi)
9Cr2W VTa + B; 9Cr2W VTa + low PSTi (750ppm*); 9Cr2W VTa + high PSTi (1600ppm*)
The last figures (*) indicate the total content on Ti, S and P. Details of chemical compositions could be found in [5, 8, 12].

Materials were supplied by CEA, in the case of EM10 and T91 conventional steels as well as Ti, P, S doped versions based in 9Cr1Mo alloy, and NRG for 9Cr(1&2W)VTa experimental martensitic steels and doped nuances based in 9Cr2WVTa alloy with additions of B^{10}, B^{11}, low and high content of Ti-P-S.

2.2 COMPLEMENTARY STUDIES ON CONVENTIONAL 9CR CANDIDATE MATERIALS

2.2.1 Metallurgical characterisation of conventional and experimental 9Cr martensitic steels

The microstructural characterisation of the conventional EM10 and T91 steels was mainly performed by CIEMAT [2]. The microstructure of these steels in the normalised & tempered (as-received) condition consisted on a lath packet structure of tempered martensite without δ ferrite. The size of Prior Austenite Grain (PAG) corresponds to ASTM 6-7 index for EM10 steel and 9-10 for T91 steel. During tempering, lath boundaries and prior austenitic grain boundaries are mainly the sites of an extensive precipitation of $M_{23}C_6$ carbides (where M is a metal such as Cr, Fe and Mo). Other types of precipitates were detected like M_2X (M being principally Cr, and X being C and/or N) in the EM10 steel and MX (where M is Nb or V, and X is C or N) in the T91 steel.
Experimental steels 9CrWVTa presented a homogeneous tempered martensitic structure with a small size of prior austenite grains described by the index 9 of ASTM scale [5].

The microchemistry of grain boundaries was extensively analysed by Auger Electron Spectroscopy (AES) on specimens broken inside the device. Phosphorus segregation (see figure 2-1) was detected on prior austenite grain boundaries of EM10 and T91 steels in the as-received condition [4]. On the contrary, no P-segregation was observed on 9Cr2WTaV experimental martensitic steels [9]. This fact is certainly related to the low P-content of experimental steels (< 50 ppm) compared to that of commercial EM10 (130 ppm) and T91 (200 ppm).

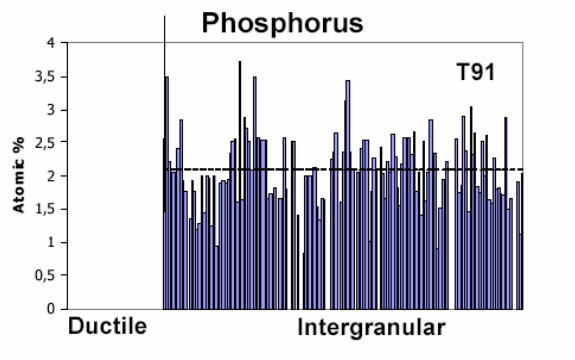

Figure 2-1 : Histograms showing the atomic concentration of P mainly found in intergranular regions of the fracture surface of T91 specimens in the as-received conditions [4].

2.2.2 Interlaboratory comparison of mechanical test results

In order to give a sound basis to compare the results from mechanical testing with specimens of various geometries used within the SPIRE project, an interlaboratory comparison programme was carried out. SCK•CEN defined and managed the inter-comparison programme, performed with the collaboration of CEA, CIEMAT, ENEA, NRG, PSI [1]. Tensile and impact tests were carried out with specimens of EM10 steel and results compared in order to assess the consistency of the experimental and analytical procedures used by the various partners**.**
Different types and sizes of tensile specimens were used: cylindrical and flat tensile specimens with cross sections ranging from 3.1 to 28.3 mm^2. The comparison showed that tensile strength values (yields and UTS) can be confidently assessed and compared, irrespective of the geometry and size of the tensile specimens used. Values of elongation and reduction of area should be treated with more caution on account of sample size.
Impact test results obtained from Charpy-V sub-size specimens (KLST type, overall length = 27 mm, thickness = 3 mm, width = 4 mm, notch depth = 1 mm) can be also compared and assessed with confidence, particularly in terms of absorbed energy and Shear Fracture Appearance (DBTT and USE) as shown in figure 2-2.

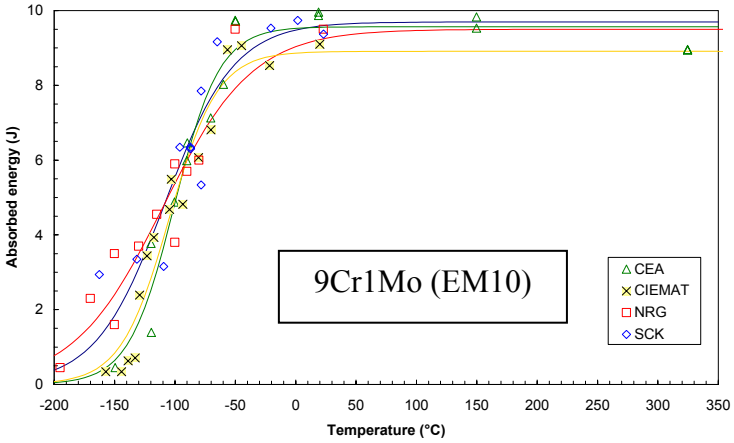

Figure 2-2: Inter-lab comparison of Charpy tests performed with sub-size (KLST) specimens of 9Cr1Mo (EM10) reference steel. In general, a good agreement was found from data provided by different labs [1].

2.2.3 Mechanical characterisation of EM10 and T91 reference steels

Besides tensile and impact properties, fracture toughness and small punch (SP) tests were performed on EM10 as well as creep tests on T91 steel [2]. Master Curve was determined testing 1/2TCT specimens following ASTM E1921-97, at temperatures corresponding to the transition region. Value of "To" parameter, determined by multi temperature technique, was –148ºC. The small punch (SP) tests showed that it was possible to predict the Ductile to Brittle Transition Temperature (DBTT) through the analysis of fracture energy. For EM10 steel, correlation set by CIEMAT between DBTT obtained from SP and DBTT from standard Charpy tests is in agreement with the literature.

Figure 2-3 compares the creep rupture strength determined for T91 steel that showed adequate level similar to those obtained for 9Cr reduced activation ferritic/martensitic steels developed for Fusion Technology applications.

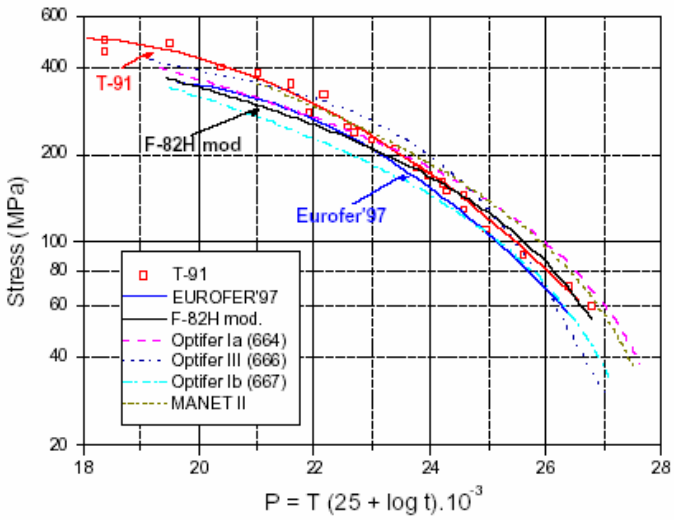

Figure 2-3: Larson-Miller representation of creep rupture strength obtained for 9Cr 1MoVNb (T91) steel compared to others 7-12Cr ferritic/martensitic steels from [2].

2.2.4 Modelling of fracture mechanisms of conventional 9Cr steels using the local approach

The main issues concerning the integrity and the lifetime of the spallation target structures are expected to be brittle fracture by decrease in ductility and fracture toughness. Therefore, the fracture properties of EM10 and T91 reference steels have been investigated in the brittle domain using tension tests on axisymetric notched specimens of NT2-type (6mm and 3.5mm in diameter). The objectives of this work, performed by CEA, were to characterize these materials in the as-received (unirradiated) condition and to apply a statistical model of brittle fracture (local approach) for the determination of fracture parameters [7].

In the temperature range studied, namely –170 to –150°C, cleavage was the main failure mechanism for both materials although some ductile cavities occur on the rupture surfaces. Isolated intergranular facets were observed as well. However, intergranular failure did not seem to influence the fracture properties in the temperature range investigated.

The fracture properties of 6mm notched tensile specimens were used to determine the Weibull parameters for the local approach of fracture according to BEREMIN model. Due to the low number of specimens tested in each condition, the confidence intervals for the Weibull parameters were large. Nevertheless, the prediction of size effect using the local approach to fracture was found to be in good agreement with the experimental results using specimens of 3.5 mm in diameter.
Moreover, a temperature dependence of the material parameters was observed from –170 to –150°C for T91 steel as shown in figure 2-4. This result might be related to the effect of some plastic strain on the fracture properties at –150°C. The rupture stress levels found represent the lower limit of the cleavage stress, which should be higher than 1700 to 2000MPa at -170°C for both materials.

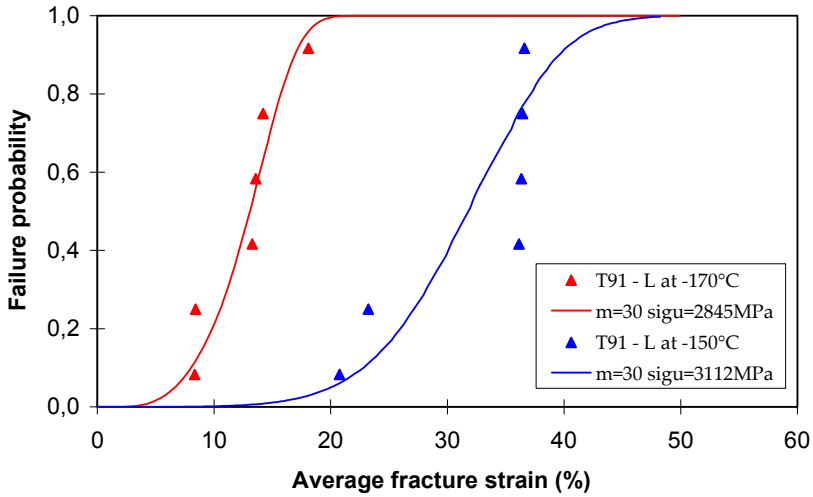

Figure 2-4: Experimental and calculated failure probability of T91 steel (NT2-6 specimens). Calculation of the temperature effect on the critical cleavage stress, σ_u, using BEREMIN model MMV with fixed Weibull modulus m=30 [7].

2.3 EFFECTS OF SPALLATION ELEMENTS LIKE TI, P, AND S ON THE BEHAVIOUR OF 9CR STEELS

2.3.1 Effects on physical metallurgy

The beam window will be strongly irradiated during service and undergo continuous modifications of its chemical composition with the time. Consequently, progressive and significant changes in behaviour are expected as a function of the time.
To elucidate the effects of the spallation elements and allow the determination of classical mechanical properties, different heats were produced based in 9Cr1Mo (CEA task) and 9Cr2W (NRG task) steels doped with the elements which could be introduced in the material by conventional melting techniques like Ti, P and S. Details of chemical compositions are given in [5, 8, 12].

Under mixed proton-neutron spectrum, elements produced by spallation reactions are mostly produced in solid solution and the first concern was to reproduce this condition. For that, several heat treatments were applied in order to evaluate the possibility to put these elements in solid solution and analyse their subsequent evolution to segregation, precipitation or modification of existing phases.

The different phase fields were determined for all doped steels with the thermodynamic software "MT DATA" and the experimental results were in good agreement with calculated phase diagrams [8]. Table 2-1 presents the secondary phases, predicted and observed, that will be induced by Ti, P and S. Whatever the heat treatment applied, quenching from high temperature at very high rates, tempering or step-cooling, these precipitated phases appeared very stable and their precipitation kinetics was very fast. Analysis by tomographic atom probe showed that it was not possible to obtain more than a few tens of S appm in solid solution at room temperature in a 9Cr steel, even with a low Mn content (to avoid the occurrence of MnS) and after performing an efficient quench from the upper limit of the austenitic field.

Thus, these results show that the normal trend of these doping elements should be the segregation or precipitation on interfaces and grain boundaries during in service conditions, where accelerated diffusion is expected due to the contribution of irradiation-induced point defects.

Table 2-1 : Comparison calculations/experiments for the secondary phases in Ti, P, S doped steels [8].

	EM10LCTi	EM10Ti	EM10TiPS	EM10LMnS
Prediction	TiN, TiC	TiN, TiC	TiN, TiC, $Ti_4C_2S_2$, MnS, Cr_2P	$Cr_{1.17}S$, MnS
Experiment	TiN, Ti(Mo)C	TiN, Ti(Mo)C	TiN, Ti(Mo)C, Ti_xS_y, $Ti_xS_yAl_z$, MnS	Cr_xS_y

A "step-cooling" heat treatment, which consisted in a cooling performed step by step to accelerate segregation of different elements, was applied to some specimens. According to analysis performed by Auger Electron Spectroscopy, doped alloys after step-cooling exhibited a concentration of Phosphorus on the intergranular facets, about twice higher, compared to similar measurements performed in undoped materials [4, 9]. Titanium and molybdenum tend also to segregate in grain boundaries.

2.3.2 Mechanical properties of Ti, P, S doped steels

The main effects observed in doped alloys is the decrease of ductility and the degradation of fracture toughness properties with coexisting impurities (P,S) and (Ti, P, S). These effects were found in doped materials based in 9Cr1Mo and 9Cr2W matrix whatever the metallurgical condition.

NRG investigated the effects of the (Ti, P, S) impurities (with a total content of 750 ppm) incorporated to 9Cr2WTaV steel. The energy transition curves from Charpy tests showed an increase of the Ductile-Brittle Transition Temperature (DBTT) of 50°C associated to a decrease of the Upper Shelf Energy (USE) for the doped alloy compared to the undoped material. Also, a loss of toughness of about 30-40% was measured at 20, 250 and 450°C and attributed to the presence of (Ti, P, S) elements as described in [5].
Nearly the same conclusions could be drawn from doped materials based in the EM10 (9Cr1Mo) matrix, especially for those containing (P,S) or (P,S,Ti) not matter the condition considered (as-quenched, tempered, step-cooled or ferritic state) [11].

2.4 EFFECTS OF HYDROGEN ON THE TENSILE PROPERTIES OF CANDIDATE STEELS AND DOPED MATERIALS

Hydrogen will be generated in large amounts from spallation reactions by the direct impingement of protons in the beam window material. The objective of the study performed by ENEA [10] was to investigate the susceptibility of candidate alloys to embrittlement induced by hydrogen and assess the effect of Ti, S and P spallation elements on hydrogen damage. The studied materials were the T91 and

EM10 reference steels and the experimental 9Cr2WTaV including the (Ti, P, S) doped versions to simulate the main detrimental spallation elements produced in service.
The experimental technique used was the Constant Extension Rate Tests (CERT) under dynamic electrochemical charging, at room temperature, to compare the relative resistance against hydrogen embrittlement. The hydrogen content introduced by this technique ranged from 2 to 8 wppm (about 110-450 appm).

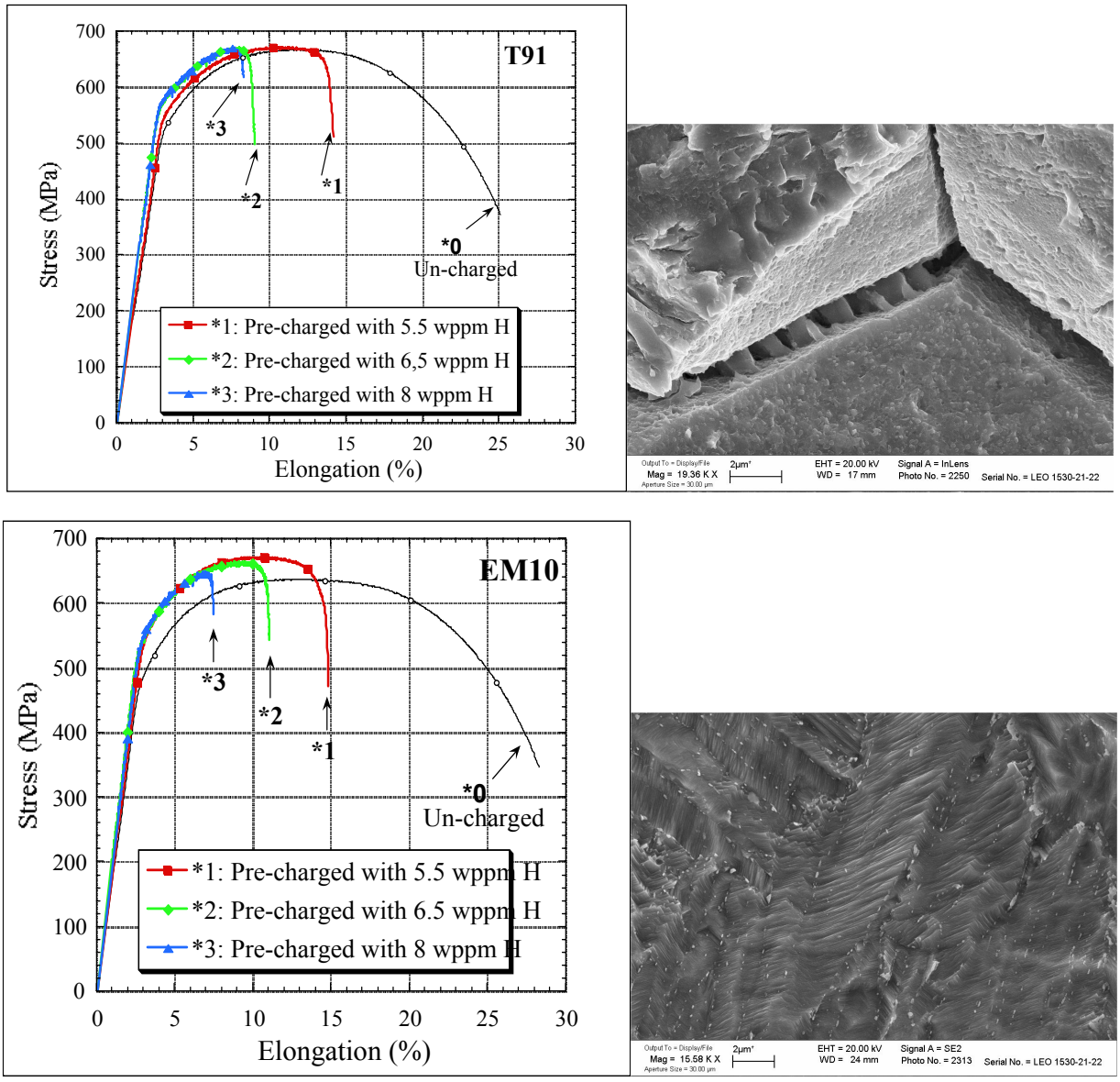

Figure 2-5: Effects of hydrogen content on T91 and EM10 tensile properties (Representative curves are the average of 2 or 3 tests) [10]. (Description of picture needed)

The introduction of hydrogen results in a slight increase of the tensile strength and a reduction of ductility as shown in figure 2-5. The fracture mode changes with increasing hydrogen content from ductile to intergranular decohesions and transgranular cleavage mode. Compared to uncharged conditions, hydrogen induced various degrees of ductility loss and hardening depending on H-content and material's microstructure. Accordingly, T91 exhibited the higher resistance to changes induced by hydrogen followed by EM10 and 9Cr2WTaV. The most important embrittlement was found for 9Cr2WTaV (TiPS) doped alloy.

From microstructural observations, it could be deduced that small grain size and primary precipitation with reversible trapping characteristics appeared as a beneficial microstructural combination for mitigating hydrogen embrittlement sensitivity of 9Cr martensitic steels. Phosphorus segregation did not seem to impart any further detrimental effect.
In spite of the questionable microstructural simulation, the response of doped steels to CERT under dynamic charging indicated that coarse, incoherent inclusions should be strictly avoided due to the poor cohesion of their interface under hydrogen action.

2.5 SUMMARY AND CONCLUSIONS

WP2 *"Metallurgy before Irradiation"* has been focussed: a) on complementary studies on 9Cr conventional and experimental martensitic steels and b) on the effects of addition of some spallation elements like Ti, P, S and H on these materials. An important database has been generated in both fields.

The main conclusions and the most import results are:

- A successful interlaboratory comparison of results on tensile and impact tests (Round-Robin) was carried out on the conventional 9Cr 1Mo (EM10) steel. The inter-comparison showed a good agreement and a satisfactory confidence level on the obtained data.

- The metallurgy of conventional and experimental 9Cr steels before irradiation was thoroughly studied. Their microstructure consists of tempered martensite without δ–ferrite where the major precipitated phase is $M_{23}C_6$ (M is Cr, Fe and Mo or W) carbides.

- The grain boundary microchemistry of as-received conventional and experimental steels was characterized by means of Auger Electron Spectroscopy (AES). Clear phosphorus segregation on grain boundaries was detected for EM10 and T91 steels, this segregation being most significant in T91. The 9CrWTaV experimental steel did not show any segregation on grain boundaries and this fact is probably related to its lower phosphorus concentration.

- Tensile, impact and fracture toughness properties were determined on both conventional EM10 and T91 steels, as well as on the experimental steel. In addition, small punch tests were carried out on EM10 steel and creep properties were investigated on T91 material. The whole data showed that the conventional 9Cr (EM10 and T91) and experimental (9Cr2WVTa type) steels, studied in the non-irradiated condition, present adequate properties for applications to ADS systems.

- Fracture properties of T91 were evaluated in the brittle domain and a statistical model of brittle fracture (local approach) was applied for the determination of fracture parameters. The values of the cleavage stress at –170ºC should be higher than 1700-1900 MPa.

- Effects of the spallation elements, like P, S and Ti, on the physical metallurgy of conventional and experimental 9Cr martensitic were investigated. The stability fields of different phases in conventional EM10 steel doped with Ti, S and P were determined using thermodynamic predictive software and corroborated by experimental results. The significant susceptibility of these elements to segregate or precipitate was evidenced.

- Concerning mechanical behaviour of doped steels, the concurrent presence of titanium, sulphur and phosphorus on conventional and experimental steels induces an important degradation of toughness and impact properties.

- Studies of hydrogen embrittlement were performed on EM10, T91, 9Cr2WTaV and Ti-P-S-doped 9Cr2WTaV. The effects of hydrogen on tensile properties were investigated at room temperature for hydrogen contents in the range 2-8wppm (about 110-450appm) introduced by cathodic charging. The main effects are related to a decrease of ductility and the occurrence of increasing intergranular and transgranular quasi-cleavage rupture modes with increasing hydrogen content. T91 steel exhibited the higher resistance to hydrogen degradation properties compared to the other materials.

From the point of view of ADS programme, the outcomes of these investigations will permit to go deeply into the irradiation mechanisms and to support the results obtained from simulation, neutron and proton-neutron mixed spectrum irradiations. In addition, all the obtained results are considered basic for conceptual design purposes.

2.6 REPORTS PRODUCED IN THE FRAME OF SPIRE PROJECT - WP2

1. "Preliminary intercomparison of mechanical tests results". Rev.01. E. Lucon. SCK•CEN (Belgium). Deliverable nº 4, month 12 (2001).

2. "Metallurgical characterization of conventional 9Cr steels". G. Diego, M. Serrano, F.J. Perosanz, A.M. Lancha. CIEMAT (Spain). Deliverable nº 4, month 12 (2001).

3. "Mechanical Response to Irradiation at 200 °C for EM10, T91 and HT9 Steels – Final Report: Specimens Irradiated to 2.6 and 3.9 dpa". E. Lucon. SCK•CEN Report BLG-986, August 2004.

4. "Auger analysis on EM-10 and T-91 steels in the as-received condition". M. García-Mazarío, A.M. Lancha. CIEMAT (Spain). Deliverable nº 33 (part 1 of 2), month 36 (2002).

5. "Mechanical properties of unirradiated 9Cr martensitic steels". J.B.J. Hegeman, J. Rensman. NRG (Holland). Deliverable nº 16 (part 1 of 2), month 24 (2002).

6. "Microstructure of experimental 9%Cr F-M steels". J.W. Hooijmans, E.W. Schuring, J. Rensman. NRG (Holland). Deliverable nº 16 (part 2 of 2), month 24 (2002). (This reference not cited in the text)

7. "Modelling of the fracture properties of conventional 9Cr steels using the local approach". P. Lamagnere, J. Pecego, G. Perez, V. Rabeau. CEA (France). Deliverable nº 27, month 30 (2003).

8. "Effects of iron spallation products, Ti, P and S on the physical metallurgy of 9Cr martensitic steels", O. Danylova, Y. De Carlan, D. Hamon, J.C. Brachet, J. Henry, A. Alamo. CEA (France). Deliverable nº 12, month 18 (2002).

9. "Auger analysis on doped steels". M. García-Mazarío, A.M. Lancha. CIEMAT (Spain), Deliverable nº 33 (part 2 of 2), month 36 (2004).

10. "Tensile properties of conventional and doped 9Cr steels under hydrogen charging". M.F. Maday. ENEA (Italy). Deliverable nº 34, month 36 (2004).

11. "Tensile and impact properties in the as-received condition and after step cooling of 9Cr martensitic steels doped with titanium, phosphorus and sulphur". Y. de Carlan, S. Urvoy, Y. Tournée, P. Wident. CEA (France). Deliverable nº 16, month 24 (2003).

12. « WP2 Metallurgy before irradiation – Final Report », A. M. Lancha, M. Garcia-Mazario, G. de Diego. CIEMAT (Spain). Deliverable nº 41, month 40 (2004).

3. EXPERIMENTAL SIMULATION OF IRRADIATION EFFECTS IN A SPALLATION SPECTRUM

WORK-PACKAGE 3

High quantities of gaseous products (about 6 at% H and 0.5 at% He) as well as significant amounts of solid spallation products (up to about 0.1 at% for elements such as Ca or Ti) will be generated in the spallation target window. It was anticipated that the impurity production should lead to additional hardening and embrittlement of the window material.

Therefore, the goal of WP3 is to simulate the effects of spallation elements on the microstructural evolution and mechanical properties of 9Cr martensitic steels via implantation of appropriate elements. The implantation technique allows reproducing in a realistic manner the creation of spallation particles inside the beam window. Furthermore, the implantation parameters (temperature, implantation rate, total implanted content etc) can be well controlled and modified in a relatively easy way. As a result, a parametric experiment can be carried out, which is not the case for irradiations with fission neutrons or high energy protons. However it must be mentioned that this simulation differs from the real case in a number of ways. For instance, the impurity loading rates and damage rates obtained in the implantation experiments are higher than those expected in the window.

WP3 was divided into two separate tasks, which focus on the effects of specific species which had been identified as potentially detrimental to mechanical properties: Helium (Task 1) and Ca, S, Ti (Task 2).
The contributors to this task were Forschungszentrum Jülich (FzJ), CEA, CNRS–UMR6634 and CNRS–IN2P3.

3.1 HE IMPLANTATION OF 9CR-1MO STEELS AND RELATED EXAMINATIONS

Among the various species produced in the window by spallation reactions, He is a particular concern. Apart from hydrogen, He has the highest production rate. Furthermore, unlike hydrogen, once produced, helium is retained in the steel. Helium is known to have embrittling effects when this element is introduced in steels at temperatures above approximately 0.45 T_m, where T_m is the melting temperature : this is the so-called "high temperature helium embrittlement" phenomenon which manifests itself for instance by premature failure during creep tests, due to the formation and growth of large helium bubbles at grain boundaries.

However, until recently, the data relative to the effects of helium when introduced at lower temperatures and more generally on the effects of high quantities of helium on the mechanical properties of martensitic steels were relatively scarce.
This is why an experimental programme, which constitutes Task 1, was set up in order to characterize the effects of helium on mechanical properties (mainly the tensile behaviour) of 9Cr martensitic steels and try to interpret the observed changes in mechanical behaviour based on microstructural investigations.

3.1.1 Materials, implantation and testing conditions

Two martensitic steels were used in this study: unstabilised 9Cr-1Mo (EM10 grade) and Mod 9Cr-1Mo VNb (T91 grade) obtained in the normalised and tempered condition. Two types of specimens were cut by spark erosion from sheets of 100 μm in thickness: miniature tensile specimens, with a gauge length of 12 mm and 2 mm width, and "H-shaped" specimens of overall dimensions 30 x 10 mm used for Small Angle Neutron Scattering (SANS) experiments.

The specimens were implanted with 23 MeV ^{4}He particles using the Jülich compact cyclotron. The α particle beam was degraded by a rotating wheel made of aluminium foils to achieve uniform helium loading throughout the specimen depth [1]. The tensile specimens were implanted at temperature ranging from 150 to 550°C up to a maximum concentration of 0.5 at% He [2]. This corresponds to a displacement damage of about 0.8 dpa per 0.5 at% He (based on TRIM-code calculations) and a displacement rate of

2.5 10^{-6} dpa/s. SANS specimens were implanted only at 250°C and 550°C with 0.5 at% He. After SANS analysis, these specimens were cut into "thread-like" samples with a 0.1 mm x 0.1 mm cross section [3] and sent to Rouen University (CNRS-UMR6634) for preparation of "tips" suitable for Atom Probe examinations.

Tensile tests were performed at FzJ in a vacuum furnace, with strain rates around 10^{-4}/s at both room and implantation temperatures [1]. Scanning Electron Microscopy (SEM) was used to examine fracture surfaces [2]. Following tensile testing, discs of 2mm in diameter were punched from specimens implanted at 250°C and 550°C to 0.5 at% He. TEM and SANS analyses were performed at CEA.
An investigation of helium effects on the fracture properties of T91 was also started to demonstrate the feasibility of implantation of Charpy sub-size specimens with 34 MeV ^{3}He particles, whose range in steel is about 240 μm. Following implantation at FzJ, the specimens were submitted to static bending tests at room temperature in the CEA-Saclay hot laboratories [4]. In the frame of SPIRE, only a feasibility study had been foreseen, as this type of experiments had not been previously performed.

3.1.2 He-effects on tensile properties

Typical examples of tensile curves measured at room temperature on implanted 9Cr martensitic EM10 and T91 steels are shown in Figure 3-1. For the same implanted helium concentration, the tensile behaviour was markedly different depending on the implantation temperature: following implantation at 250°C, both steels displayed a very high degree of hardening together with a total loss of ductility and a predominantly intergranular fracture mode, as shown in Figure 3-2. Implantation at 550°C to the same concentration induced some hardening; however the steels retained significant ductility [2].

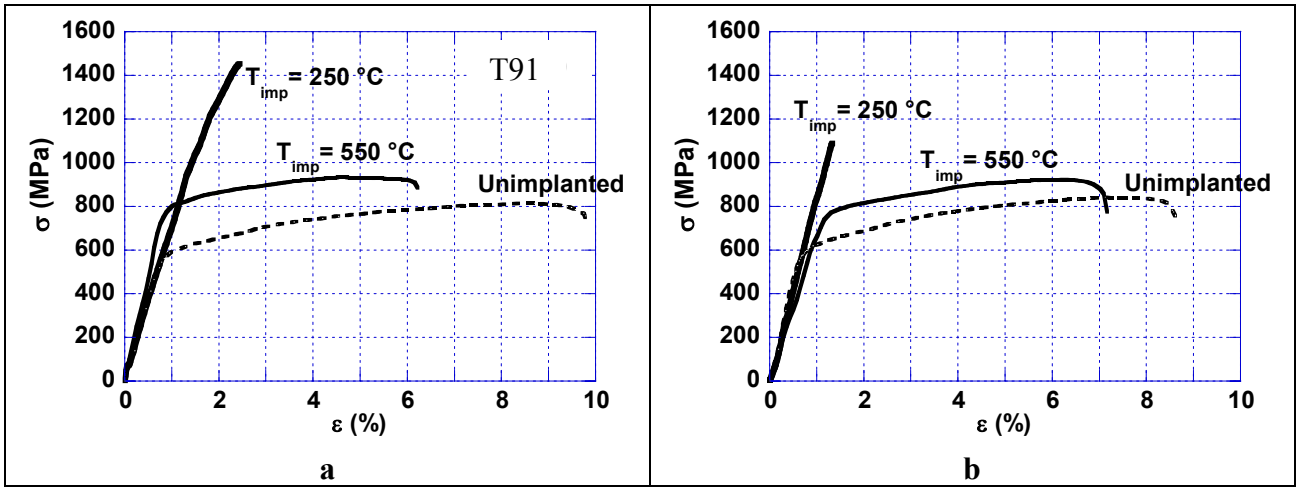

Figure 3-1 : Engineering stress-strain curves of EM10 (a) and T91 (b) steels, measured at 25°C after implantation with 0.5 at% He at 250°C and 550°C. The dotted line corresponds to the unimplanted reference specimen.

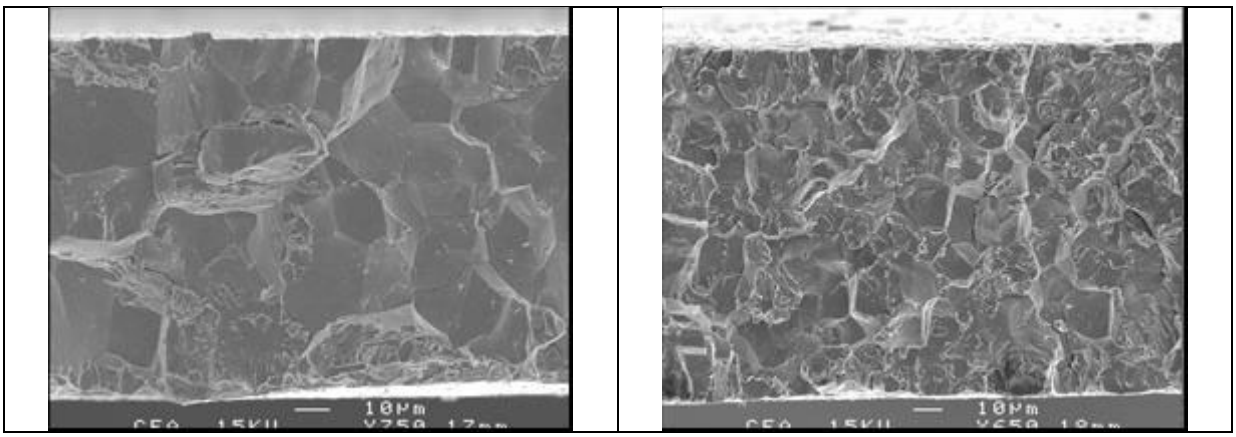

Figure 3-2 : SEM micrograph showing the fracture surface of EM10 (a) and T91 (b) specimens implanted at 250°C to 0.5 at % He and tested at 25°C

The tensile data measured at room temperature on implanted T91 specimens are presented in Figure 3-3 that shows respectively the evolution of the yield stress and the total elongation as a function of implanted helium content. As shown, the yield stress increases strongly with increasing helium concentration. The ductility following implantation at 250°C drops rapidly with increasing helium content. For a given helium concentration, the ductility increases with increasing implantation temperature, whereas the induced hardening decreases.

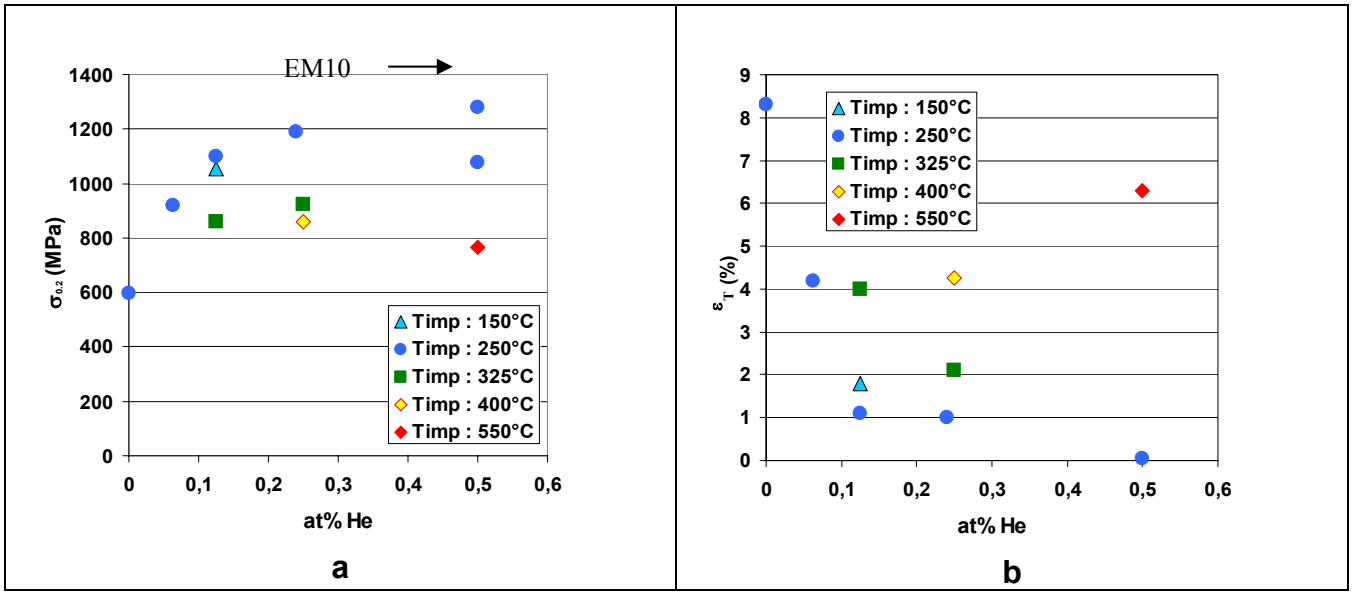

Figure 3-3: Graph showing the evolution of the yield stress (a) and the total elongation (b) of T91 measured at room temperature as a function of implanted helium content and implantation temperature. The data point corresponding to EM10 implanted to 0.5 at% He at 250°C was also added.

3.1.3 He-effects on the microstructure

Microstructural analysis was carried out at CEA by TEM and SANS on EM10 and T91 samples implanted with 0.5 at% He at 250°C and 550°C. This analysis revealed the presence of helium bubbles in the case of both implantation temperatures as well as black dots (i.e. clusters of point defects induced by the implantation) in the samples implanted at 250°C [2]. In the samples implanted at 550°C, the bubbles are relatively large and heterogeneously distributed. As shown in Figure 3-4, they are located on Prior Austenite Grain Boundaries, on lath and subgrain boundaries as well as on the dislocations inside the laths and on the carbide-matrix interfaces.

In the samples implanted at 250°C, the bubbles are tiny (bubble radius close to 1 nm) as shown in Figure 3-5, with a very high number density. Furthermore, the analysis of the SANS data indicates that, for both implantation temperatures, the helium bubbles are close to thermodynamic equilibrium, i.e. their internal pressure is balanced by their surface tension.

Following SANS analysis, the specimens were prepared for characterization using Atom Probe. Bubbles were detected by Field ion microscopy in samples implanted at 550°C, but not in the samples implanted at 250°C probably due to the small size of the bubbles formed at this temperature. In addition, tomographic Atom Probe experiments revealed silicon clustering in the samples implanted at 250°C. A possible interpretation of this finding could be silicon segregation on helium bubbles [8].

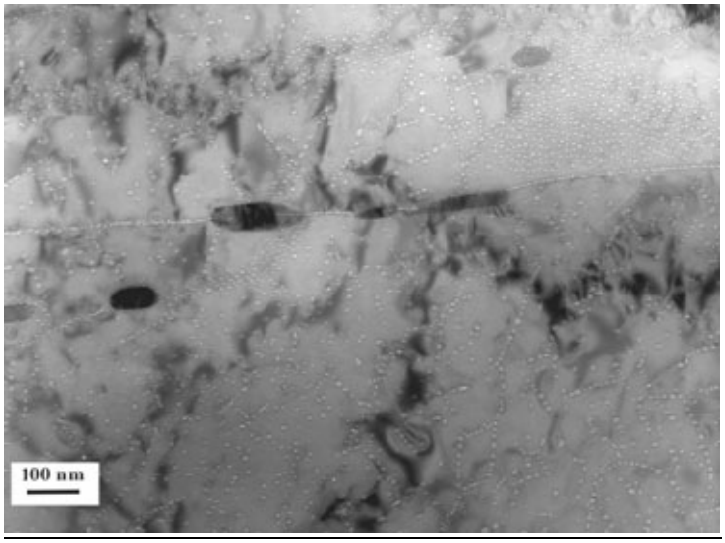

Figure 3-4: TEM micrograph showing the bubble microstructure in EM10 implanted with 0.5 at% He at 550°C. Under-focus imaging conditions (δf = - 1000 nm).

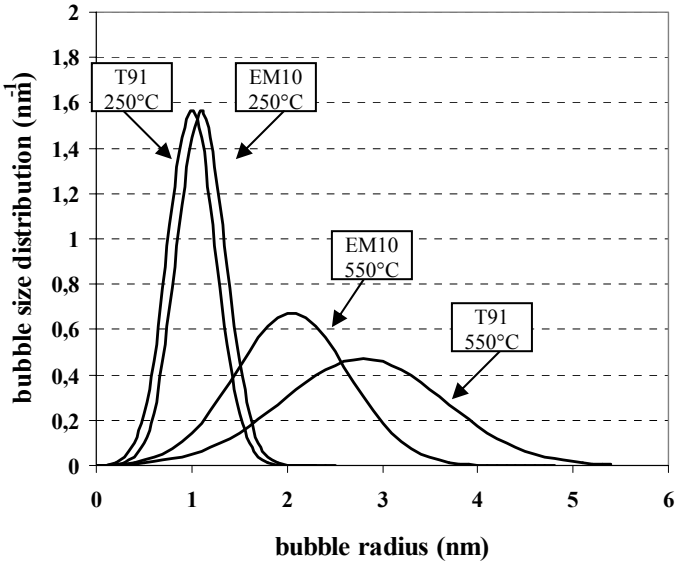

Figure 3-5 : Bubble size distributions, determined using SANS spectra, measured on EM10 and T91 specimens implanted with 0.5 at% He at 250 and 550°C.

Based on the microstructural results, it could be shown that the high degree of hardening of the specimens implanted at 250°C is mainly due to the high density of small bubbles they contain. However, hardening alone can not explain the complete ductility loss and the intergranular fracture mode. Ab-initio electronic structure calculations performed as part of WP6 (R. Gupta) have shown that helium drastically decreases grain boundary cohesion in iron. Therefore, it was suggested that the brittle intergranular fracture mode displayed by the specimens implanted at 250°C results from the combined effects of pronounced intergranular hardening and weakening of prior austenite grain boundaries due to helium.

3.1.4 He-effects on fracture properties

In order to investigate the effects of helium on fracture properties, it was decided to carry out static bending tests on sub-size Charpy specimens implanted in the notch with helium to prove the feasibility of this kind of tests. As part of SPIRE project, only a feasibility study was foreseen.

The objective is to determine the local stress/strain values at which cracking initiates in the implanted layer below the notch, based on bending tests results and finite elements (FE) calculations with as input data the tensile behaviours of the steel in un-implanted and implanted conditions.

This would allow, using a so-called "local approach of fracture model", to evaluate quantitatively the effect of helium on the fracture properties as a function of helium concentration and implantation temperature. Charpy specimens were implanted at 250°C with 100 appm He and submitted to bending tests at room temperature. FE calculations of the tests demonstrated that the slight difference between the bending behaviour of implanted and unimplanted specimens was due to the hardening of the steel as a result of implantation. It was concluded that these trial experiments successfully proved that the technique can be applied to higher helium concentrations to determine He-induced modifications of fracture properties.

3.2 IMPLANTATION OF VARIOUS SPALLATION PRODUCTS (CA, S, TI) AND RELATED EXAMINATIONS

As mentioned before, in addition to H and He, other spallation products are accumulated in the window. In this work, we have chosen to study the effects of calcium, sulphur and titanium. Calcium is totally insoluble in iron and therefore should be prone to clustering/precipitates formation, which could lead to hardening and embrittlement of the steel. Sulphur also has a low solubility below 500°C and might form CrS or FeS or possibly segregate to grain boundaries. Due to their high affinity for hydrogen, calcium or titanium hydride formation is also a possibility and so is the formation of titanium carbide precipitates.

The possible effects of these elements on microstructural evolution and hardening of 9C martensitic steels was investigated by implantation experiments of the selected species. Microstructural characterization was performed by TEM and Tomographic Atom probe. The induced hardening was measured using nanoindentation experiments, which is the only possible technique due to the small range of the injected particles in the steels.

EM10 steel was used either in the standard metallurgical condition (i.e. tempered martensite) or in a recrystallised condition to facilitate the detection by TEM of tiny clusters that should form during implantation [5]. Most implantation experiments were carried out with ions delivered by the IRMA medium energy accelerator of CSNSM-Orsay (CNRS-IN2P3), with ion energies of 90 to 180 keV corresponding to a range in the steel smaller than 100 nm. However, for nanoindentation experiments the ARAMIS 2MV tandem accelerator of CSNSM was used, since higher ion ranges, and therefore higher implantation energies are required [5-8].
Needle like specimens (see Figure 3-6) were also implanted before being characterized using the Atom Probe technique.

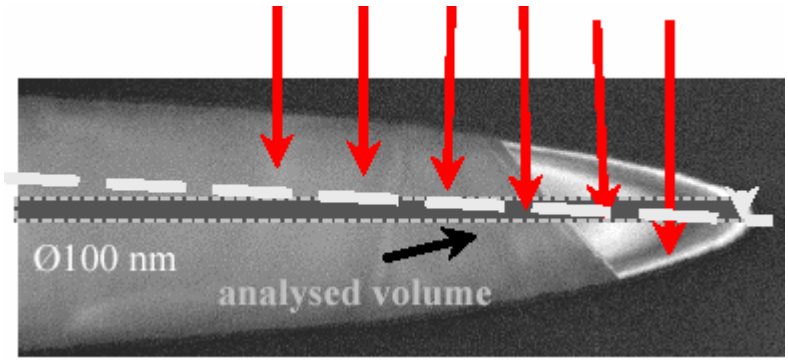

Figure 3-6 : Ion implantation in a EM10 needle. The needle is then analysed by 3D Atom Probe. The energy of the implanted elements is chosen as a function of the needle thickness.

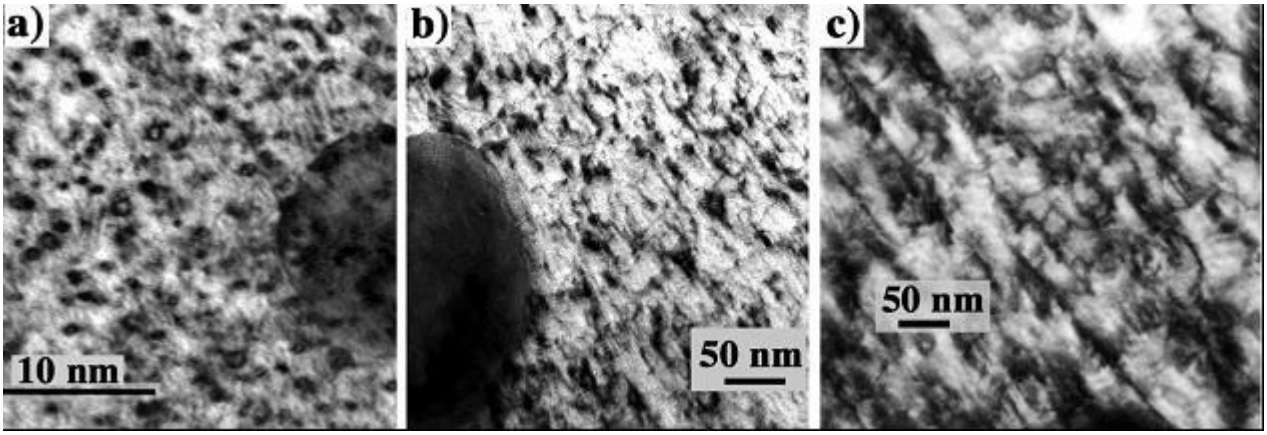

Figure 3-7 : In situ study of defect structure evolution under 90 keV Ca implantation at 500°C, with a constant flux of 3x10^{11} ions/cm^2/s and a fluence of a) 10^{15}, b) 3x10^{15} and c) 4x10^{15} ions/cm^2 in the EM10 steel [5].

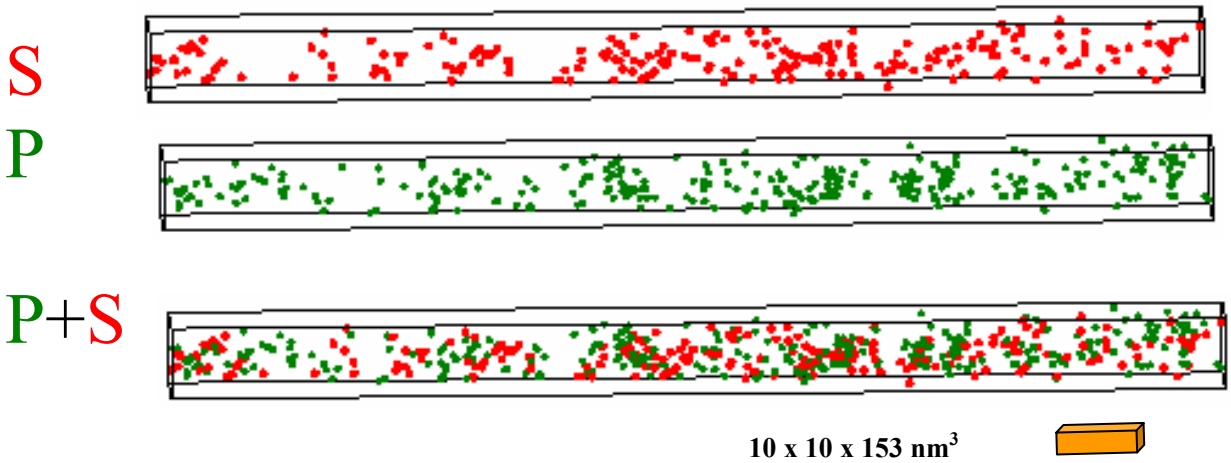

Figure 3-8 : Three dimensional reconstruction of the probed volume of EM10 steel implanted with sulfur at 300°C (4 10^{14} ions/cm^2, i.e. 0.4 dpa and 0.02 at% S implanted). Only sulphur and phosphorus atoms are represented for clarity [6, 8].

Figure 3-7 presents a typical example of the microstructural evolution under single-ion implantation, as revealed by the TEM in-situ study.

At this temperature and for the damage rate used in theses experiments (about 1. 10^{-3} dpa/s), a high density of dislocation loops are formed, leading to a dislocation network as the fluence is increased. Also, depending on the implantation temperature and damage rate, the $M_{23}C_6$ carbides were found to be either totally/partially amorphised or remained fully crystalline, in agreement with previous experiments. Using TEM, it was not possible to detect any clustering of the implanted species, even for Ca or S concentrations of about 1%. Also, neither calcium nor calcium hydride precipitation was detected.

The chemical evolution at the nanometer scale of EM10 under single ion implantation (S, Ti, Ca) was also studied using Atom Probe after implantation experiments carried out at 300°C and 500°C. Figure 3-8 corresponds to the reconstructed volume of one analysis following sulphur implantation.

The spatial distribution of sulphur is not homogeneous in the analysed volume. Furthermore, it is also the case for phosphorus, initially present as an impurity in the EM10 matrix, and which was found to be homogeneously distributed before implantation. Both elements are spatially correlated as shown in Figure 3-8. This experiment indicates that sulphur has a tendency to aggregate.

Several needles were implanted sequentially with Ca and H. Figure 3-9 shows the reconstructed volume of one analysis, where calcium atoms are homogeneously distributed. Neither calcium hydrides nor calcium clusters were detected in these experiments.
These results are somewhat puzzling since calcium is known to be totally insoluble in iron. In order to investigate whether the absence of calcium clustering could be due to the high implantation rates used in the present experiments, calculations using a rate theory model were performed]. This model, describing both the clustering of points defects as well as that of an impurity, predicts that under the implantation conditions used in this work, an insoluble impurity should form a high density of nanoclusters, in contrast to the experimental atom probe results.

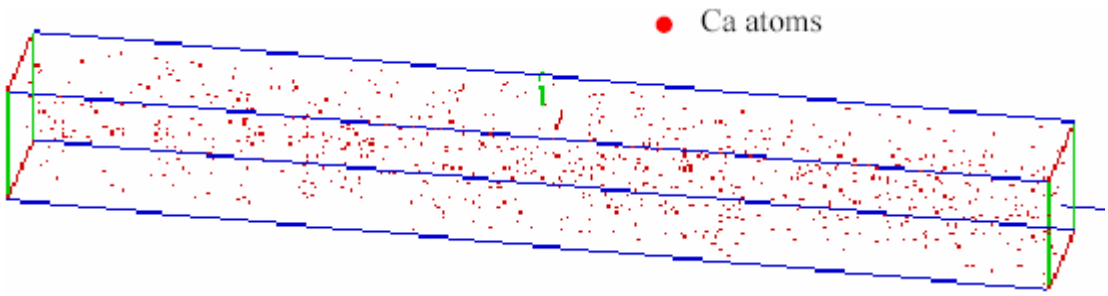

Figure 3-9 : Three dimensional reconstruction of the probed volume of EM10 sequentially implanted with Ca and H. Dimensions of the volume are : 10x10x75 nm^3. Only calcium atoms are represented for clarity [8].

Nanohardness measurements were also carried out following implantation at 500°C with 2.5 MeV Ca-ions delivered by the ARAMIS tandem accelerator. At this energy, the particle range is approximately 800 nm in the EM10 steel [7]. A maximum of dose of 5 10^{15} ions/cm^2 was implanted, which corresponds to a peak calcium concentration of about 0.2 at% and a peak damage value close to 4 dpa. Hardness values were deduced from the recorded load versus indentation depth curves.

Although there is some scatter in the hardness data, the effect of implantation on the hardness of EM10 steel is negligible: no hardening is observed but rather a slight decrease in hardness. Thus, if tiny Ca clusters were formed during implantation, they do not lead to significant hardening of the EM10 steel [9].

3.3 CONCLUSIONS

Irradiations effects in a spallation environment on the microstructure and mechanical properties of 9Cr-1Mo steels were experimentally simulated via the implantation of specific spallation elements (Ti, S, Ca, H, He) :

- The microstructural evolution of EM10 steel induced by single ion (Ti or S or Ca) implantations or by sequential implantations (Ca and H) was characterized by Tomographic Atom Probe (TAP) and Transmission Electron Microscopy (TEM). Onset of clustering was evidenced by 3D Atom Probe following sulphur implantation. In all other cases the implanted species were found to be homogeneously distributed in the steel matrix. Segregation of implanted atoms at grain boundaries or at interfaces was not observed either. In addition, no hardening was measured using nanoindentation on Ca implanted specimens.
- These experimental results are not fully understood: in particular, it is not clear why clustering of a species like calcium which is totally insoluble in iron, was not observed following implantation.

Nevertheless, the results obtained in the frame of SPIRE tend to indicate that solid spallation products are not a major source of degradation of mechanical properties under spallation irradiation conditions.

- T91 and EM10 miniature tensile specimens 100 μm in thickness were implanted with alpha particles in order to study the effects of helium on the tensile properties of 9Cr-1Mo steels. The corresponding microstructural evolution was characterized by TEM, SANS and Atom Probe.
- The existence of a "low temperature helium embrittlement" phenomenon was demonstrated. It was shown that following helium implantation at 250°C of T91 steel, the ductility quickly drops with increasing helium content while the material is drastically hardened. For a helium content of 0.5 at%, a complete loss of ductility was observed together with a brittle intergranular fracture mode.
- Based on the results of the microstructural characterization, it was shown that the high degree of hardening of specimens implanted at 250°C to 0.5 at% is due to the high density of tiny bubbles they contain. It was furthermore suggested that the brittle intergranular fracture mode, displayed by these specimens, results from the combined effects of pronounced intragranular hardening and decrease of grain boundary cohesion due to the presence of helium.
- Furthermore, for a given helium content, increasing the implantation temperature leads to an increase of ductility and a decrease of the induced hardening. These results indicate that the window operation temperature should not be too low otherwise the lifetime of this component would be significantly reduced.
- In addition, there is a need to characterize the effects of helium on the fracture properties of T91. To this end, trial implantation experiments in the notch of subsize Charpy specimens and static bending tests were carried out as part of SPIRE. They demonstrated the feasibility of this approach based on finite elements calculations and analysis of test results using a "local approach of fracture model". Additional experiments will be performed in the framework of the IP-EUROTRANS/DEMETRA programme in order to evaluate quantitatively the effect of helium on the fracture properties as a function of helium concentration and implantation temperature

3.4 REPORTS PRODUCED IN THE FRAME OF SPIRE PROJECT – WP3

1. P. Jung, J. Chen, H. Klein, W. Schmitz, Helium implantation and testing of tensile specimens, SPIRE deliverable 3, month 9
2. J. Henry, P. Jung, J. Chen, J.C. Brachet, Tensile properties and microstructure of 9Cr-1Mo martensitic steels containing a high helium concentration, SPIRE deliverable 11, month 15
3. J. Henry, T. Van den Berghe, P. Pareige, Fabrication of specimens for Tomographic Atom Probe examinations using He implanted samples, SPIRE deliverable 13, month 18
4. J. Henry, X. Averty, L. Vincent, P. Jung, P. Coffre, J.J. Espinas, He implantation in the notch of 9Cr-1Mo subsize Charpy specimens : demonstration of feasibility, SPIRE deliverable 28, month 30
5. G. Amiri, M-H. Ruault, J. Henry, H. Bernas, E. Cadel, P. Pareige, Consequences of calcium and sulphur spallation product recoils in 9Cr-1Mo steel : simulation by ion implantation, SPIRE deliverable 23, month 24
6. E. Cadel, P. Pareige, M.O. Ruault, Experimental simulation of spallation elements production in a 9Cr-1Mo martensitic steel : 3D atom probe characterisation, SPIRE deliverable 23, month 24
7. M.O. Ruault, O. Kaitasov, J. Henry, H. Bernas, S. Collin, Microstructural evolution of 9Cr-1Mo steel under sequential H and Ca ions : an in-situ TEM study, SPIRE deliverable 35, month 36
8. H. De Monestrol, P. Pareige, Tomographic Atom Probe analyses of the microstructure of 9Cr-1Mo steel after sequential Ca and H ions implantation, SPIRE deliverable 35, month 36
9. J. Henry, Experimental simulation of irradiation effects in a spallation spectrum: SPIRE WP3 final report, SPIRE deliverable 43, month 48.

4. NEUTRON-IRRADIATION AND POST-IRRADIATION EXAMINATION WORK-PACKAGE 4

Fast neutron irradiations allow simulating reasonably well the atomic displacements that will be produced with spallation spectrum. Work-package 4, "Neutron irradiation and Post-Irradiation Examinations (PIE)", was mainly devoted to assess the effects of neutron irradiation on the mechanical properties of structural materials. In particular, the range of low irradiation temperature 200-400°C was investigated because of the quite limited existing data on hardening, embrittlement and irradiation behaviour of 9Cr martensitic steels.

The irradiations were designed to complete the data base regarding the effect of displacement damage on mechanical properties at low temperatures (below 400°C) including their evolution at high dose, comparable to dose that should be received by the window of the target. For these purposes, three experiments were performed using Materials Testing Reactors (MTR) like BR2 and HFR, and a Fast Reactor (FR), BOR60, to reach high doses.
The tasks developed in the frame of WP4 were the following:

1. Irradiation in BR2 at 200°C and associated PIE (SCK•CEN)
2. Irradiation in HFR at 250°C and associated PIE (NRG)
3. Irradiation in BOR60 at 325°C and associated PIE (CEA, RIAR)

4.1 IRRADIATION IN BR2 REACTOR AT 200°C AND ASSOCIATED PIE (SCK•CEN)

The contribution of SCK•CEN within WP4 consisted in the irradiation at 200°C of conventional 9Cr (EM10 and T91) and 12Cr (HT9) martensitic steels with two different doses of about 2.6 and 3.9 dpa. Materials were included as tensile, Charpy and fracture toughness specimens. All steels have been irradiated with an environment of flowing water and without tailoring spectrum.
All details of experiments and PIE are described in [1, 2].

4.1.1 Materials, specimens and irradiation conditions

Three martensitic steels, 9Cr1Mo (EM10), 9Cr1MoVNb (T91), 12Cr1MoW V (HT9), were irradiated as specimens for tensile tests (cylindrical cross section, overall length = 27 mm, gauge length = 12 mm and diameter = 2.4 mm); Charpy-V sub-size samples (KLST type, overall length = 27 mm, thickness = 3 mm, width = 3 mm, notch depth = 1 mm) for determination of impact energy transition curves and Charpy-V (KLST type) pre-cracked specimens for determination of fracture toughness.

The irradiation experiment was conducted in BR2 reactor in Mol at 200°C ± 5°C. Two capsules were irradiated, one for 6 cycles and the second for 8 cycles, the fast flux being of about 3.5×10^{14} n/cm^2.s. Specimens were in contact with flowing water. The fission neutron flux was measured using Fe and Ti dosimeters located at 5 different levels of the rig. The average fast neutron fluence and doses reached in each case were respectively 1.73×10^{21}n/cm^2 - 2.60 dpa and 2.57×10^{21}n/cm^2 - 3.86 dpa.

4.1.2 Tensile properties

The evolution of tensile properties after irradiation at 200°C for EM10, T91 and HT9 steels are summarised in Table 4-1, for tests performed at the irradiation temperature. As expected irradiation induced hardening, evaluated from the increase of yield stress, and ductility loss. Figure 4-1 compares the stress-strain curves obtained for EM10 steel before and after irradiation.
In general, hardening and ductility loss increase with the dose. On the other hand, the amount of irradiation effects depends also on the material. EM10 steel exhibited the lower hardening and decrease of ductility followed by T91.

Table 4-1. Evolution of tensile properties with the dose for irradiations performed at 200°C.

Material	Dose (dpa)	T_{test} (°C)	$\sigma_{0.02\%}$ (MPa)	σ_{UTS} (MPa)	ε_u (%)	ε_t (%)	Z (%)
EM10	0	200	449	585	8	21	79
			450	574	7	20	80
	2.95		666	693	2	15	59
	4.36		710	718	2	14	77
T91	0	200	494	616	6	19	72
	2.95		835	838	2	12	79
	4.36		835	840	2	11	65
HT9	0	150	562	745	9	17	61
			561	743	10	19	62
	2.55	200	951	989	4	9	33
	4.33		981	1037	5	10	34

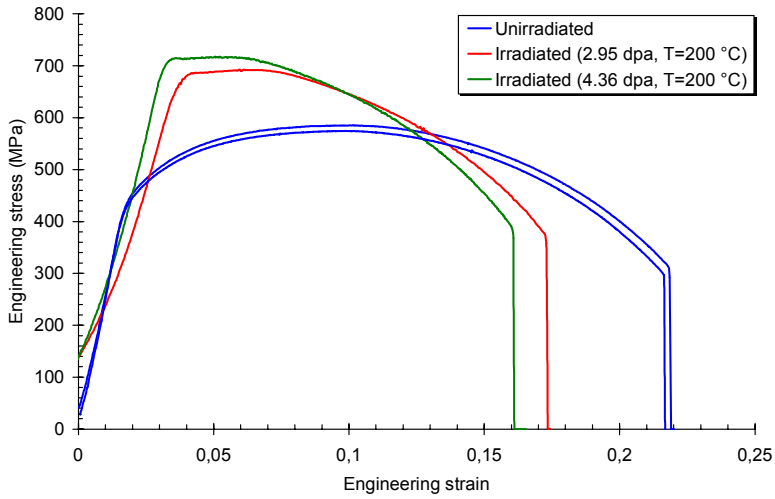

Figure 4-1: Engineering stress-strain curves of EM10 specimens irradiated and tested at 200°C.

4.1.3 Impact properties

Figure 4-2 illustrates the evolution of the impact properties determined from Charpy-V specimens of T91 steel irradiated at about 2.4 and 3.6 dpa. These irradiation conditions induced an important DBTT shift of 110 and 130°C compared to the unirradiated condition. For both doses, the values of DBTT (determined from absorbed energy curves) after irradiation are higher than room temperature. The upper shelf energy exhibited a relatively moderate decrease of about 7% in the case of T91 steel.

As given in table 4-2, EM10 displayed a lower increase of DBTT with values of the irradiated state ranging from -40°C up to 0°C. This material displayed an increase of USE values from 9.7J to 11.3J after irradiation.
The most important DBTT shift and reduction of USE level is obtained for HT9 steel. However, this alloy presented before irradiation quite poor impact properties (DBTT: ~ 0°C, USE: ~ 5J) compared to the other unirradiated steels.

Considering the important embrittlement degradation of impact properties occurring at 200°C for the relatively low fluence levels applied, the use of this temperature during in-service conditions appears as a major concern.

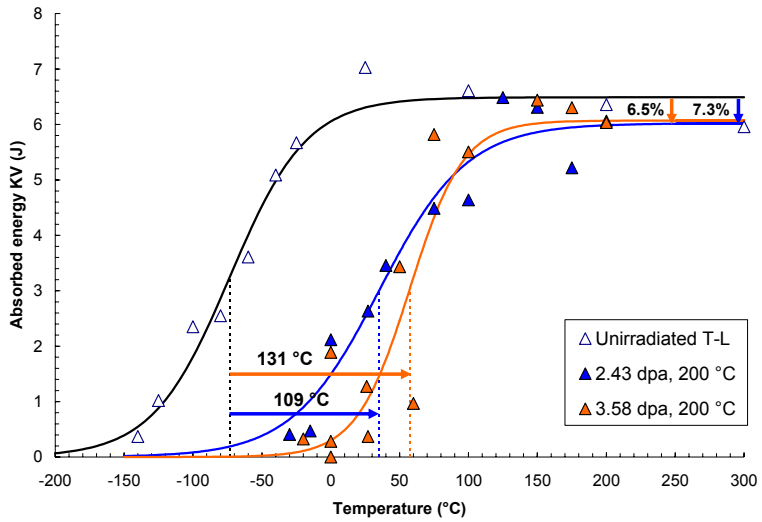

Figure 4-2: Absorbed energy values determined for T91 steel in the unirradiated and irradiated conditions (specimens with TL orientation)

Table 4-2. Summary of impact properties and fracture toughness determined for EM10, T91 and HT9 steels after irradiation in BR2 reactor at 200°C.

Type of test	Steel	Mean dose (dpa)	T_{test} (°C)	Main results
Charpy	EM10 (or.TL)	0 2.53 3.76	-120 ÷ 27 -20 ÷ 200 -60 ÷ 200	$DBTT_{KV}$ = -84 °C – $DBTT_{SFA}$ = -69 °C – USE = 9.7 J $DBTT_{KV}$ = 0 °C – $DBTT_{SFA}$ = 1 °C – USE = 11.3 J $DBTT_{KV}$ = -42 °C – $DBTT_{SFA}$ = -38 °C – USE = 11.0 J
	T91 (or.TL)	2.43 3.58	-30 ÷ 200 -20 ÷ 200	$DBTT_{KV}$ = 35 °C – $DBTT_{SFA}$ = 65 °C – USE = 6.0 J $DBTT_{KV}$ = 57 °C – $DBTT_{SFA}$ = 68 °C – USE = 6.1 J
	HT9 (or.LT)	2.47 3.70	27 ÷ 275 75 ÷ 260	$DBTT_{KV}$ = 169 °C – $DBTT_{SFA}$ = 186 °C – USE = 2.9 J $DBTT_{KV}$ = 164 °C – $DBTT_{SFA}$ = 177 °C – USE = 3.1 J
Fracture toughness	EM10 (or.TL)	0 2.91 4.29	-160 ÷-115 -60 ÷ -10 -90 ÷ -60	T_o = -135 ± 6.4 °C T_o = -31 ± 10.4 °C T_o = -41 ± 6.7 °C
	T91 (or.TL)	0 2.51 3.74	-125 ÷ -115 -20 ÷ 28 -40 ÷ 31.5	T_o = -113 ± 6.0 °C T_o = 32 ± 6.1 °C T_o = 46 ± 7.7 °C
	HT9 (or.LT)	2.51 3.71	80 ÷ 200 130 ÷ 180	T_o = 211 ± 6.7 °C T_o = 192 ± 7.7 °C

4.1.4 Fracture toughness

Charpy-V sub-size (KLST) specimens, pre-cracked by fatigue before irradiation, have been tested in three-point bend mode in order to determine the fracture toughness of the investigated steels in the ductile-to-brittle transition regime. The Master Curve analysis has been applied according to the ASTM E1921-03 standard, to obtain the value of the reference temperature To. This value corresponds to a median toughness of 100MPa√m for 1 TCT specimens. This temperature could be best used to quantify material toughness in alternative to the Charpy-based DBTT.

Figure 4-3 shows the experimental data points and associated Master Curves determined for T91 steel. The difference between the values of To for the two irradiated conditions is statistically not significant. Therefore, results indicate a similar degree of embrittlement, given by the shift of To, for both doses. Compared to Charpy tests, the magnitude of embrittlement shown by fracture toughness tests is significantly larger (see table 4-2) for all materials.
The ranking by increasing susceptibility to irradiation embrittlement (EM10-T91-HT9) is the same as found by impact tests.

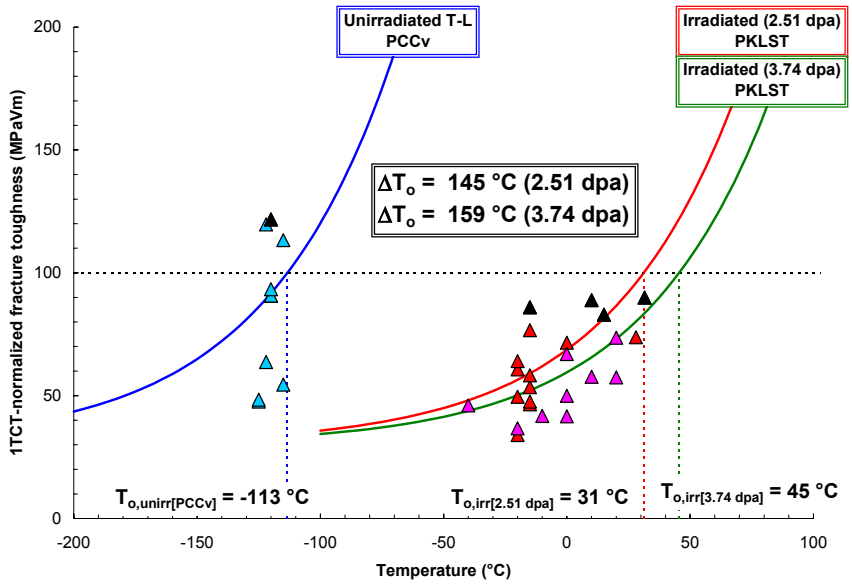

Figure 4-3: Fracture toughness experimental points and corresponding Master Curves obtained for T91 steel.

4.2 IRRADIATION IN HFR REACTOR AT 250°C AND ASSOCIATED PIE

Experiments managed by NRG and performed in HFR reactor at 250°C aimed to irradiate candidate materials and doped versions up to nominally 2.8 dpa using two devices - SUMO and CASHIR – the first leading to a mixed spectrum irradiation. The second design had a cadmium shield giving a higher ratio of fast to thermal neutron flux and hence a faster spectrum.

A commercially available martensitic steel, EM10 (9Cr1Mo) has been investigated as well as some experimental steels like 9Cr(1-2W) VTa.
The simulation of spallation products generation have been roughly approximated by doping materials with ^{10}B , intended to produce Helium by (n, α) reactions, and also by alloying with the most detrimental elements like Ti, P and S.
All details of experiments and PIE are described in [3].

4.2.1 Materials, specimens and irradiation conditions

Different heats of 9Cr ferritic-martensitic steels were irradiated in these experiments. They were: EM10 (9Cr1Mo) commercial steel; 9Cr1W VTa and 9Cr2W VTa experimental steels; doped alloys based in 9Cr2W VTa and EM10 with (S, P, Ti) impurities; 9Cr2W VTa + 50 wppm ^{10}B to produce He by (n, α) reactions and 9Cr2W VTa + 50wppm ^{11}B, that was the reference for ^{10}B-containing material. All materials were produced in the normalised and tempered condition.

Three types of specimens for mechanical tests were irradiated: tensile (gauge length 20mm, diameter 4mm), Charpy-V (KLST) to establish impact energy transition curves and CT (29 x 27 x 5 mm^3) specimens. The last ones have been destined to determine the fracture toughness (J-Δa curves) in the ductile regime domain.

Specimens were irradiated in contact with liquid sodium in both devices. The SUMO-05 irradiation was performed at an average irradiation temperature of 248°C, with specimen temperatures ranging from 234-258°C. The average irradiation dose level was 2.66 dpa.

The CASHIR-01 sample holder has been irradiated at an average temperature of 242 °C, with specimen temperatures ranging from 233-252°C. Because of heat transfer problems through the Cadmium shield this device was transferred to a peripheral core position of HFR with the lowest neutron flux and consequently the lowest gamma heating. The irradiation of CASHIR-01 went very slowly (~0.1 dpa/month) and lasted 28 months. The dose level is about 3.3 dpa on average. This position had a more important thermal spectrum than the original position. The fast to thermal fluence average ratio is 1.26 for SUMO-05 and 3.34 for CASHIR-01. For the last one, the ratio initially planned was 12-13, that is a factor 10 higher than for the SUMO-05.

4.2.2 Evolution of tensile properties

Tensile tests were performed at the irradiation temperature (250°C) and 20°C. The post-irradiation tensile curves for EM10 steel are different from the tensile curves for 9CrW VTa materials. While the yield stress of both materials is very similar, the uniform elongation is very different. Up to the dose level achieved, EM10 retains its capacity to strain harden uniformly, but 9Cr2WVTa irradiated heat seems to show immediate instability after yielding with localised deformation only.

Hardening of different classes of materials, measured at room temperature and for doses varying from 2.1 to 3.9 dpa, is in the range of 250-350 MPa for EM10 and 9Cr2W VTa steels, 280-380 MPa for B-containing materials, 350-450 MPa for (Ti, P, S) doped alloys. Figure 4-4 shows the general trend of hardening with the dose for 9Cr martensitic steels irradiated in HFR and BR2 reactors.

The calculated He concentrations from ^{10}B doped heat are around 250 appm for SUMO samples and 80 appm for CASHIR specimens. To detect a possible effect of Helium on ductility, the total elongation is plotted versus the thermal fluence. As shown in figure 4-5, no significant effects are detected.

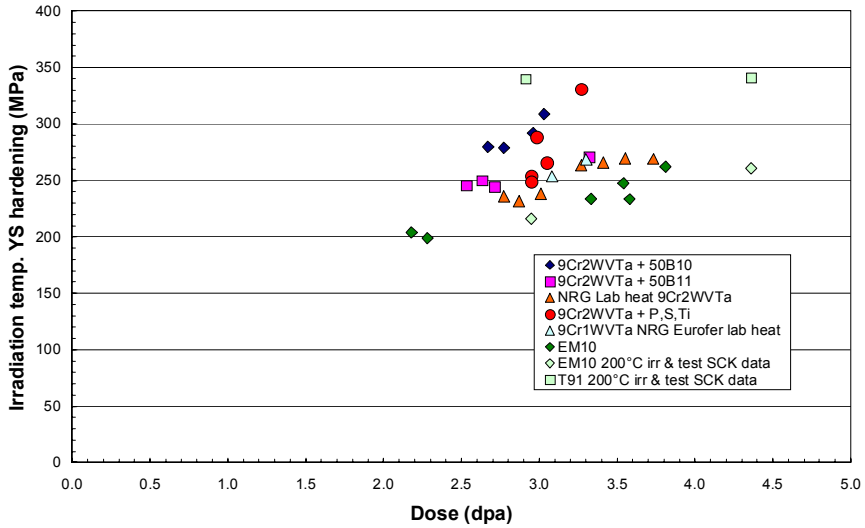

Figure 4-4: Hardening, measured by the increase of yield stress at the irradiation temperature, as a function of dose for 9Cr steels irradiated at 200°C (BR2, SCK data) and 250°C (HFR, NRG data).

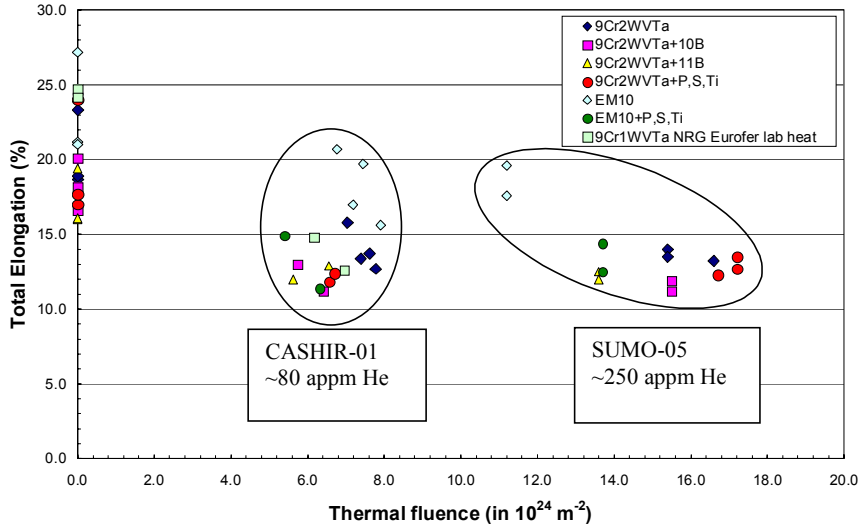

Figure 4-5: Total elongation, measured at room temperature and 250°C, versus thermal fluence for 9Cr steels irradiated at 250°C.

4.2.3 Evolution of impact properties

Energy transition curves have been determined for all materials and both irradiation conditions. Figure 4-6 illustrates the evolution of the impact properties of 9Cr1WTaV and 9Cr2WTaV steels irradiated at 250°C with doses of about 2.8 and 3.4-3.7 dpa. The transition region of these irradiated materials is around 100°C higher compared to the unirradiated condition and a slight decrease of the upper shelf energy level is observed. EM10 displayed lower DBTT values, which range from -50°C up to -10°C after irradiation. Energy values are in good agreement with that obtained after irradiation in BR2 reactor at 200°C [2].

The most important DBTT shift and reduction of USE level is obtained for EM10-(Ti,P,S) specimens which seem more sensitive to irradiation-induced embrittlement than 9Cr2W-(Ti,P,S) doped alloys as shown in figure 4-7. In these doped alloys, DBTT values are largely exceeding room temperature.

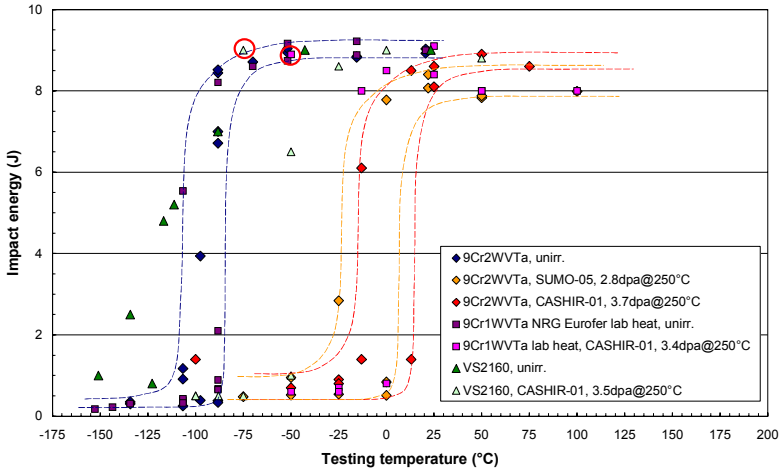

Figure 4-6 : Impact energy transition curves obtained for 9Cr (1-2W)VTa experimental steels irradiated at 250°C with doses ranging from 2.8 to 3.7 dpa.

Concerning B-containing materials, they behave in such a way that the same impact energy curves were obtained for both materials after irradiation for equivalent doses, even they displayed different initial impact properties. So, no significant He-embrittlement could be demonstrated for B-doped 9Cr2W VTa with He contents up to 250 appm.

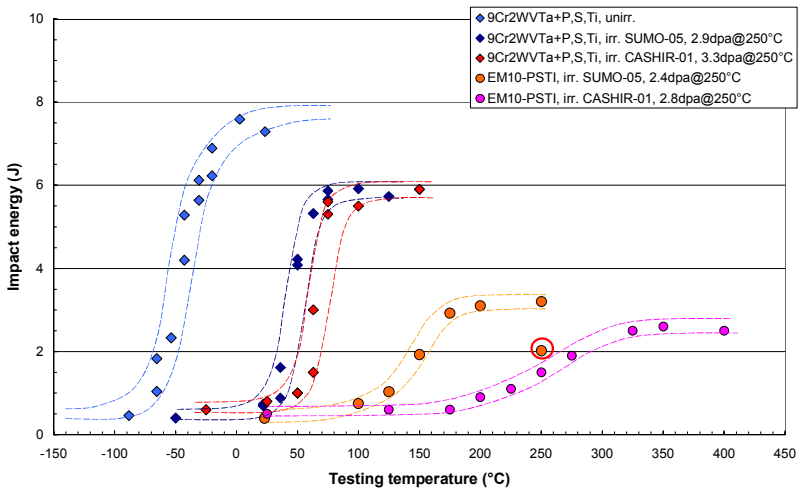

Figure 4-7: Evolution of energy transition curves of (Ti, P, S) doped alloys, based on 9Cr2W and EM10, irradiated at 250°C for doses ranging from 2.4 to 3.3 dpa.

4.2.4 Fracture toughness

Materials were tested at room temperature, 125°C and 250°C according to procedures described in [3]. J-curves determined for 9Cr2W VTa experimental steel are given in figure 4-8. As shown, toughness is reduced about 25-30% after irradiation regardless of testing temperature.
In the unirradiated condition, doped alloys reached approximately 60-70% of the fracture toughness of the base metal 9Cr2W VTa at room temperature and 250°C. In the irradiated state the difference is still of the same order.

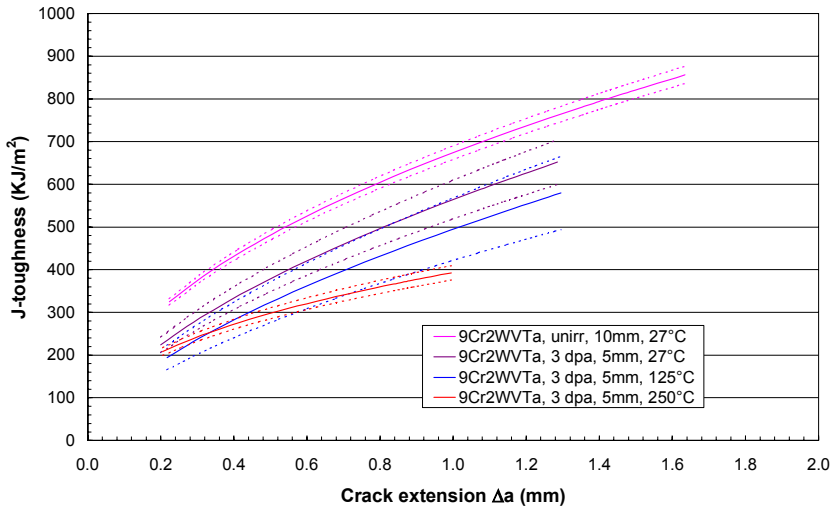

Figure 4-8: J-R curves determined for 9Cr2W VTa steel before and after irradiation.

4.3 IRRADIATION IN BOR60 AT 325°C AND ASSOCIATED PIE

To study the irradiation behaviour of 9Cr martensitic steels at high dose in the low range of temperature foreseen for the spallation target, CEA decided to perform an irradiation experiment in the fast reactor BOR60 (Research Institute of Atomic Reactors (RIAR), Dimitrovgrad, Russia) at 325°C for a dose of about 40 dpa, close to the displacement damage foreseen for the beam window and structures of the spallation target. The experiment, named "ALTAIR", started in May 2000 and finished on 15 October 2002.

Different 9Cr materials were included in this experiment: 9Cr1Mo reference (commercial) martensitic steels; 9CrW V Ta experimental alternative steels; 9Cr1Mo-(Ti, P, S) doped alloys.

All details of experiments and PIE are described in [4].

4.3.1 Materials, specimens and irradiation conditions

Materials irradiated in ALTAIR experiment are: a) 9Cr1Mo (EM10) and 9Cr1MoVNb (T91) reference martensitic steels; b) 9Cr-2W VTa and 9Cr-2W VTaB (from NRG), 9Cr-1W VTa (Eurofer97, Fusion Technology) experimental alternative steels; c) doped alloys, to simulate the effects of spallation elements, that were obtained by addition of elements such as S, P and/or Ti during re-melting 9Cr1Mo (EM10) heat; some variants with low carbon (EM10 LCTi) or low Mn content (EM10 LMnS), to avoid the precipitation of Ti and S respectively, were also included. All materials were produced in the Normalized and Tempered (N&T) conditions, except some specimens of doped alloys obtained in the as-quenched or ferritic condition.

Usual tensile (diameter 2mm, 12mm gauge length) specimens were irradiated as well as pressurised tubes of reference and experimental martensitic steels to estimate the irradiation creep modulus. These

tubes of 6.55 mm of external diameter, 0.45 mm in thickness contain Argon pressure to induce hoop stress levels of 150 and 220 MPa at the irradiation temperature. Charpy-V (KLST) specimens were also included but results are not yet available.

The irradiation rig was constituted of 7 stages. Samples were directly in contact with liquid sodium. The irradiation temperature was 325°C ± 5°C. The dose was about 42 dpa on stages 1 to 4, and decreased from 40 dpa in stage 5 to 32.5 dpa in stage 7.

4.3.2 Tensile properties

Irradiated specimens were tested at 20°C and at the irradiation temperature (325°C) using a strain rate of $1.4x\ 10^{-3}s^{-1}$. Tests were also performed on control (unirradiated) samples for comparison.
The tensile properties of reference materials, EM10 and T91 commercial steels, are compared to those of 9CrWTaV experimental martensitic steels as shown in figures 4-9 for tests performed at the irradiation temperature. These materials reached a dose in the range 40-42 dpa, except for 9Cr2WTaV specimens where the dose was 32.5 dpa.

As expected all materials exhibited a degradation of mechanical behaviour in the irradiated condition. However, the susceptibility to hardening and embrittlement was found to be different for examined materials, which presented before irradiation quite similar tensile properties. As shown in figure 4-9, EM10 and T91 reference steels seem to harden earlier than the experimental alloys like 9Cr1WTaV (Eurofer) and 9Cr2WTaV.

The same situation was found concerning the evolution of ductility. After irradiation at 42 dpa, both 9Cr1Mo steels exhibited some ductility at 325°C but nearly no plasticity is obtained for tests performed at 20°C as shown in figure 4-10. The values of total elongation and reduction in area, measured at 20°C, reached a level as low as 1.4% and less than 4% respectively for EM10. These values are even lower for T91. So, the ductility seems to decrease much faster in the case of 9Cr1Mo steels compared to 9Cr(1-2W)TaV alloys. However, regarding the uniform elongation, very low values in the range 0.3-0.5% were obtained for all materials and both test temperatures.

As shown in figure 4-9, the yield stress and the ultimate tensile strength (U.T.S.) reach the same values after irradiation, which means a reduction of the strain hardening capability of all materials. Specimens tested at room temperature exhibit an irradiation-induced hardening of about 10-20% higher than that determined at 325°C.

The total lost of ductility of EM10 and T91 at 20°C should indicate an important shift of the Ductile Brittle Transition Temperature (DBTT) beyond the room temperature and this point will be assessed by in progress Charpy tests.
The results described previously, from irradiations performed by SCK and NRG at 200°C and 250°C respectively and for doses relatively low (2.4-3.8 dpa), have shown important shifts of DBTT values, which are sometimes higher than room temperature in the case of 9Cr1Mo steels.

In general, the behaviour of doped alloys is quite similar to that of 9Cr1Mo conventional steels. The irradiation-induced hardening is about 500-600MPa at 325°C, around 700MPa at 20°C for all materials. At 325°C, the ductility level is comparable to that obtained for EM10 reference steel. But at 20°C, total, uniform elongations and reduction in area reached practically nil values for all materials in as-quenched or tempered or ferritic condition.

No significant effects of doping elements could be detected, especially after irradiation. The main contributions to hardening and ductility loss seem to be defined by the matrix behaviour. However, some possible second order effects should be also due to sulphur and phosphorus.

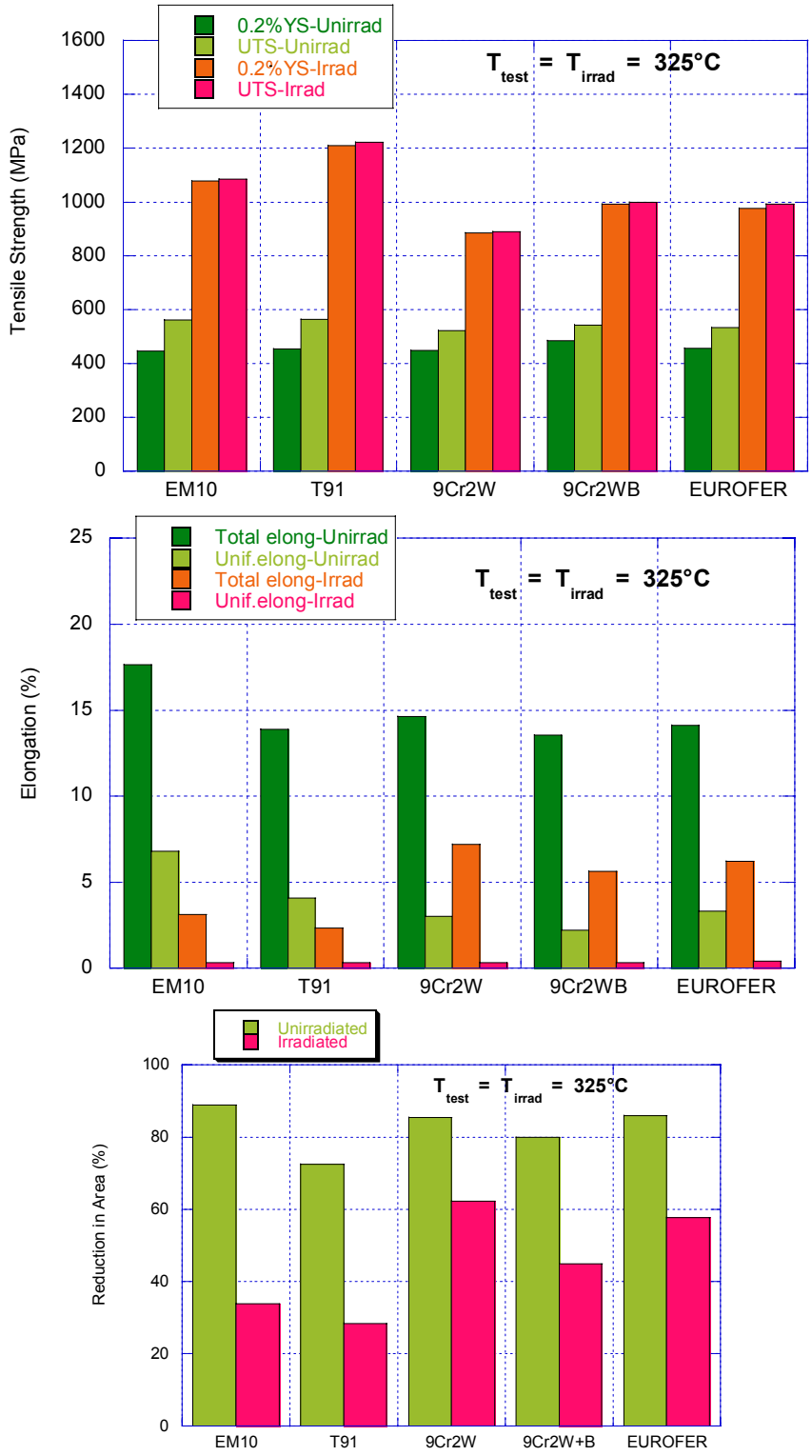

Figure 4-9: Evolution of the tensile properties of 9Cr martensitic steels irradiated at 325°C with a dose of about 40-42dpa (except 9Cr2WTaV, 32.5 dpa). Tests performed at the irradiation temperature.

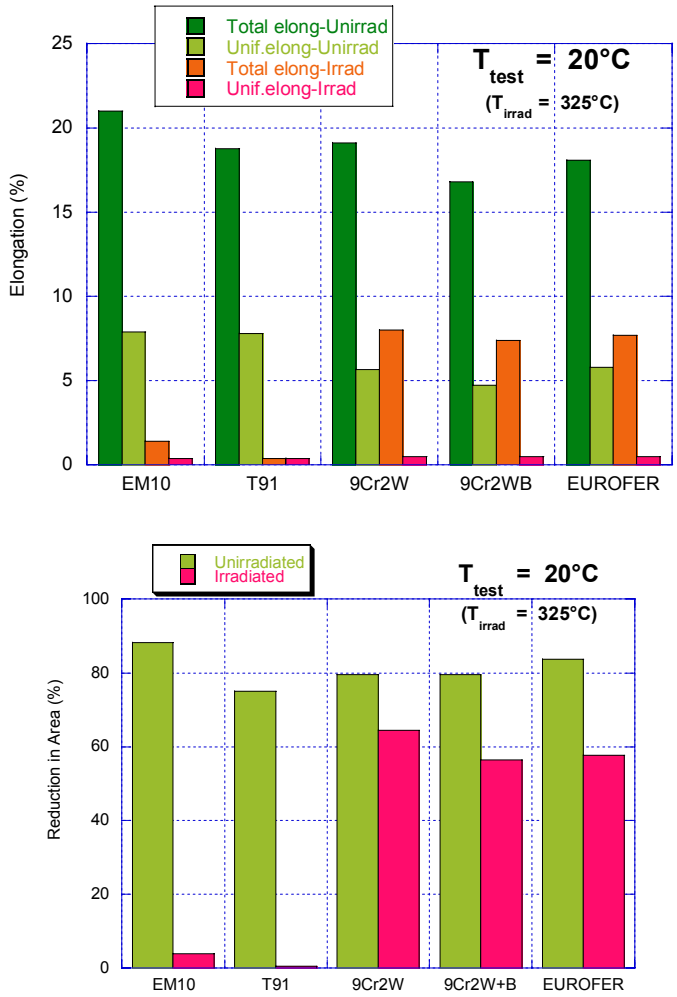

Figure 4-10: Elongations and reduction in area values of 9Cr martensitic steels irradiated at 325°C with a dose of about 40-42dpa (except 9Cr2WTaV, 32.5 dpa) determined from tensile tests performed at room temperature.

4.3.3 Irradiation Creep

Pressurised tubes of EM10, T91, 9Cr1WTaV (Eurofer) and 9Cr2WTaV were irradiated to determine the deformation due to irradiation-creep as a function of the dose and the applied stress. The measurement of the external diameter is performed by profilometry to determine accurately the strain in the central region of tubes.

Measurement were performed before irradiation and at the doses of 19.3 dpa, 41.9 dpa and 62 dpa, the last obtained for tubes re-irradiated in a Fusion Programme experiment at the same temperature. The weight of pressurised specimens is also measured at each step to guarantee that there is not leakage of argon pressure. The average diametral strains determined for each material are shown in figure 4-11. No meaningful data were obtained for T91 because of gas leak, which was attributed to failed welds.

In all the cases, the strains measured are very low ($\leq$0.9%) after about 62 dpa, confirming that 9Cr martensitic steels display at 325°C a rather good dimensional stability as already determined for equivalent doses and higher irradiation temperatures (400-550°C) on several conventional ferritic-martensitic steels.

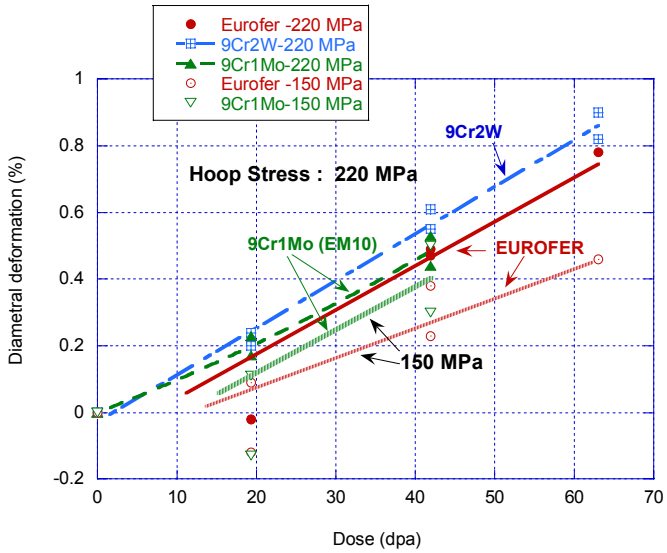

Figure 4-11: Diametral strain of 9Cr1Mo(EM10), 9Cr2WTaV and 9Cr1WTaV (Eurofer) steels as a function of the dose determined for applied hoop stresses of 150 and 220 MPa.

Values of the creep modulus were estimated assuming that the contributions of thermal creep and swelling were negligible. EM10, 9Cr2WTaV and Eurofer present nearly the same average value of the irradiation-creep modulus, which is $(0.7 \pm 0.1) .10^{-6}$ $(dpa.MPa)^{-1}$. This value is in good agreement with those already determined at higher temperatures (400-550°C) for EM10 and other ferritic-martensitic steels and should indicate no temperature dependence for the irradiation-creep modulus.

4.4 SUMMARY AND MAIN CONCLUSIONS

Within the WP4 of SPIRE project, several important irradiation experiments were performed to complete the missing data on usual mechanical properties (tensile, impact, fracture toughness, irradiation creep) in the range of low temperatures (T < 400°C). For this purpose, two complementary experiments were performed in BR2 and HFR reactors at 200 and 250°C respectively, covering the range of low doses (2.0-4.5 dpa) to study the early stages of hardening and embrittlement phenomena that should occur in candidate structural materials.
On the other hand, one irradiation experiment was carried out in BOR60 fast reactor at 325°C in order to investigate the effects of irradiation at higher doses (32-42 dpa), close to that planned for the spallation target and other irradiated structures.

The main following conclusions could be drawn from these experiments.

For low doses:

- 9Cr1Mo-EM10 commercial steel presented the lowest sensitivity to irradiation-induced hardening and embrittlement. This material retains its strain hardening capacity and exhibits the highest level of uniform elongation after irradiation at 200 and 250°C, both in a mixed and thermal-neutron-shielded spectrum.

- Compared to EM10, T91 shows larger irradiation embrittlement, that is larger DBTT shift, USE drop and decrease of fracture toughness. The ranking of increasing sensitivity to irradiation-induced effects is EM10, T91 and HT9 according to results of SCK●CEN.

- The shift of reference temperature T_o, determined from toughness tests, is systematically larger than DBTT shift measured from Charpy tests for 9-12Cr steels. This fact, not observed for other classes of steels (for ex. RPV steels), has important implications for both designers and safety authorities. Other

linked item, which requires further research and discussion, is related to the applicability of the Master Curve approach to high Cr F/M steels.

- In general, an excellent agreement and consistent results were obtained in experiments performed at BR2 (200°C) and HFR (250°C).
- Experimental steels of 9CrW VTa type presented also a moderate hardening and embrittlement, even if some tensile instability (localised deformation) are observed.
- Materials containing ^{10}B to generate He by nuclear reactions during irradiation did not show evidence of He-effects for contents up to 250 appm at 250°C.
- All heats doped with (Ti, P, S) or boron showed more irradiation yield stress increase per dpa and higher DBTT shifts than undoped materials. The largest DBTT shift was obtained for EM10-(Ti, P, S) doped alloys.

For high doses:

- After irradiation at 325°C in BOR60 reactor, dissimilar levels of tensile strength and ductility were obtained for the reference and experimental 9Cr martensitic steels, which presented comparable tensile properties before irradiation.
- The commercial 9Cr1Mo (EM10) and 9Cr1MoVNb (T91) martensitic steels seem to be more sensitive to the irradiation induced hardening. A near total loss of ductility was observed for irradiated 9Cr1Mo steels for tensile tests performed at 20°C, which is probably associated to a high increase of DBTT.
- 9CrWTaV experimental martensitic steels displayed a lower level of hardening and higher ductility at 325°C and also at 20°C. Thus, they showed more delayed irradiation effects than 9Cr1Mo irradiated in the same conditions.
- No clear effects of doping elements were observed after irradiation at high doses (32-42 dpa), the main contribution to hardening and ductility loss seems to be defined by the metallurgical condition of specimens.
- The profilometry of pressurised tubes showed a very low irradiation-creep deformation, less than 1% after 63 dpa at 325°C, for EM10, 9Cr1WTaV (Eurofer) and 9Cr2WTaV martensitic steels

4.5 REPORTS PRODUCED IN THE FRAME OF SPIRE PROJECT – WP

1. "Mechanical response to irradiation at 200°C for Three high-Cr martensitic steels (EM10, T91, HT9) - Intermediate Report : 1st Specimen Batch (2.6 dpa)", E. Lucon, A. Almazouzi, SCK•CEN Report BLG -973, **Deliverable n° 44 (a)**, February 2004.

2. "Mechanical response to irradiation at 200°C for EM10, T91 and HT9 steels - Final Report : Specimens irradiated to 2.6 and 3.9 dpa", E. Lucon, A. Almazouzi, SCK•CEN Report BLG-986, September 2004, **Deliverables n° 31 and 44(b)**.

3. "NRG SPIRE contribution: Mechanical Test Results from MTR Irradiation up to 3 dpa at 250°C", J.W. Rensman, F. Schmalz, R. d. Boef, F.P. v.d. Broek, J. Boskeljon, Report NRG 20564/04.62317/P, October 2004, **Deliverables n° 32 and 45**.

4. "PIE of 9Cr martensitic steels irradiated up to 42 dpa in BOR-60 reactor at 325°C – CEA contribution to SPIRE Project –WP4 : Final Report", A. Alamo, J.L. Bertin, CEA Report, January 2005, **Deliverable n° 46**.

5. IRRADIATION UNDER MIXED PROTON-SPECTRUM AND POST-IRRADIATION EXAMINATION WORK-PACKAGE 5

The irradiations under mixed proton-neutron spectrum and the corresponding PIE are the purpose of the work-package 5 of SPIRE project. This part of the programme is very important, since the spectrum is prototypical to that planned for the beam window of the spallation target.

The goal of WP-5 is to characterise the microstructure and mechanical properties of structural materials after irradiation in a prototypical mixed flux of protons of energy in the range 500 MeV to 1 GeV and neutrons produced by spallation. The methodology relies on an international irradiation program carried on in SINQ facility at the Paul Scherrer Institut (PSI), Switzerland.

Samples for the SPIRE program were included in two irradiations in SINQ targets Mark –II and Mark-III, namely SINQ Target Irradiation Programs STIP-I and STIP-II, which operated in 1998-1999 and 2000-2001, respectively. The irradiation experiments were prepared and performed by PSI, while the post-irradiation examinations (PIE) of SPIRE samples have been conducted at both PSI and CEA hot labs.
The experiments were carried out in nearly the same range of irradiation temperatures used in neutrons and implantation experiments, which allow comparing the behaviour of 9-12Cr martensitic steels in different environments. Details of experiments and achievements are given in references [1-3].

5.1 IRRADIATIONS OF SPIRE MATERIALS IN SINQ FACILITY

Specimens for SPIRE programme were integrated in two experiments performed in SINQ facility with protons of about 520 MeV, which produced spallation neutrons and also, hydrogen and helium. The main characteristics of these irradiations are :

- STIP I (MARK-II): the irradiation temperature ranged from 90 up to 360°C, the doses up to 12 dpa and the maximale concentration in He was 1130 appm.
- STIP II (MARK-III): the irradiation temperature ranged up to 400°C and the dose up to 20.3 dpa, the maximal He-content was 1695 appm.

In the SPIRE project, the main concerned materials are 9Cr-1MoVNb (T91) and 9Cr-1Mo (EM10) martensitic steels. However, other advanced 9%Cr steels such as F82H (8Cr-2W VTa) and Optifer (9Cr-1W), from the fusion materials program, were also investigated.
The T91 steel used in STIP-I was received from Oak Ridge national laboratory. The T91 steel used in STIP-II was obtained from CEA, which is the common material for all SPIRE partners.

Specimens were placed in tubes of 9.25mm of inner diameter, which limited the size of samples. On the other hand, since the proton beam had roughly a two dimensional Gaussian distribution with σ_x=2.12 cm and σ_y=3.56 cm, the specimens had to be as short as possible, to avoid large dose variation along their length, and should be close packed for good heat transfer. Consequently, only small specimens were used in these experiments: TEM discs of 3mm in diameter for microstructure studies; discs (3mm in diam.) for small punch (SP) tests that could provide information on tensile and fracture toughness; miniature tensile specimens of 12mm total length; Charpy sub-size (ASTM sub-size and KLST) specimens.

5.2 PIE OF SPECIMENS IRRADIATED IN STIP-I

5.2.1 Investigation on the microstructure of martensitic steels T91 and F82H

TEM samples of both materials were irradiated at different positions in STIP I experiment to get a series of irradiation conditions in the range 90-360°C with doses ranging from 2.7 to 11.8 dpa and the corresponding helium concentration from 145 to 1115 appm.

The results showed that in general the microstructure of the T91 steel was very similar to that of the F82H steel at the same conditions. Before irradiation both steels have a typical martensitic lath structure containing dislocations with a density of approximately 1×10^{14} m^{-2}. $M_{23}C_6$ type carbide precipitates were identified mainly along prior austenite grain boundaries and martensite lath boundaries. The size of precipitates varies from few tens nanometers to ~2 µm.

In the both steels, the defect size increases while their density drops rapidly with irradiation temperature above about 250°C as shown in figure 5-1.

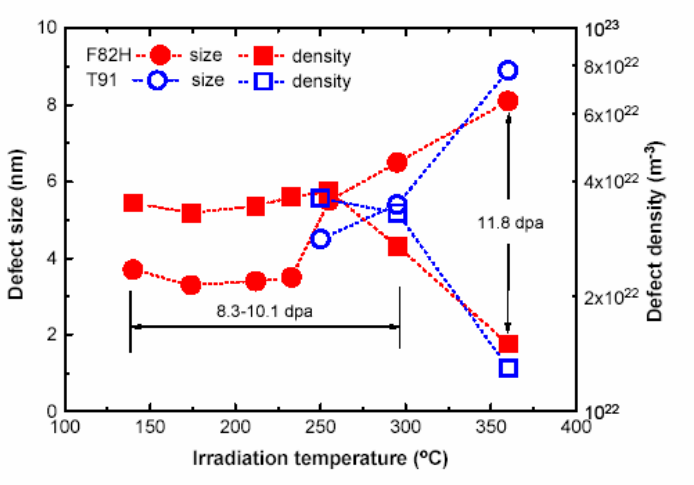

Figure 5-1: Irradiation temperature dependence of the density and the size of defect clusters for T91 and F82H samples irradiated to 8.3-11.8 dpa.

High-density of helium bubbles of around 1 nm size were observed in the both steels when the samples reached a dose of about 10 dpa and 550 appm He at 175°C or above. The helium bubbles observed in the T91 steel have a slightly higher density and a smaller size as compared to those in the F82H steel irradiated at the same conditions as shown in figure 5-2.

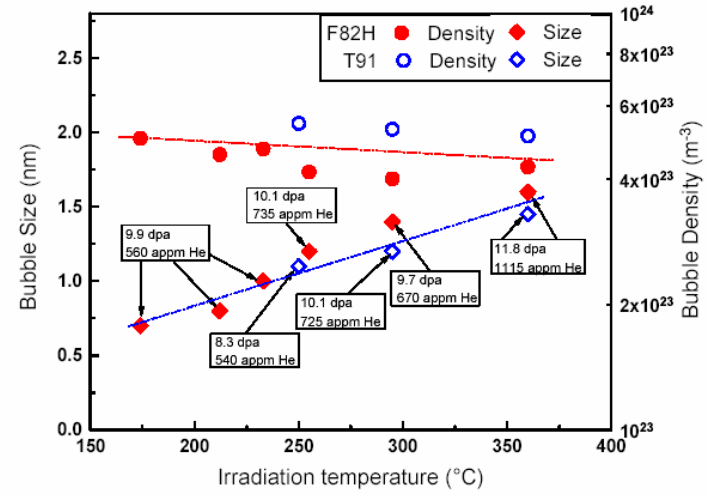

Figure 5-2: Irradiation temperature dependence of size and density of helium bubbles for T91 and F82H. Doses and helium concentrations are indicated for each experimental point.

The amorphisation of M23C6 precipitates was observed systematically in the T91 and F82 samples irradiated at temperatures T ≤ 200 °C, which is consistent with previous observations on other martensitic steels irradiated with 800 MeV protons at low temperatures. However, no amorphisation was detected at 250°C and beyond as illustrated in figure 5-3.

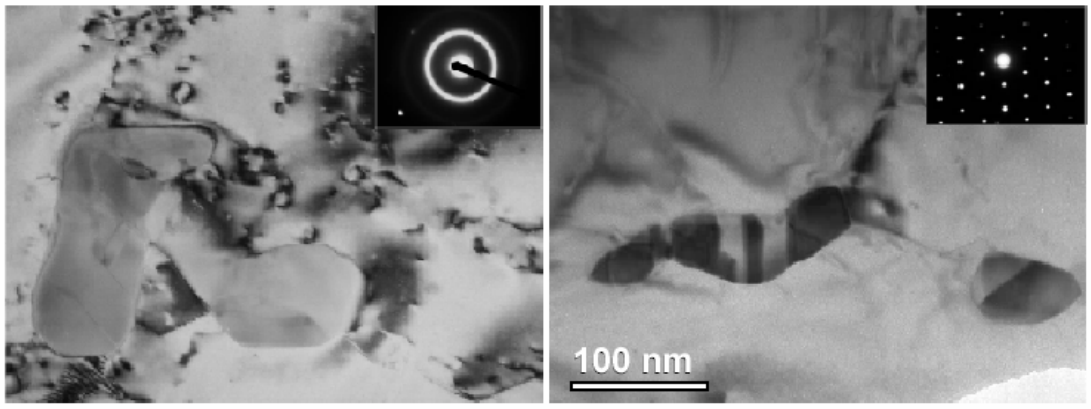

Figure 5-3: TEM bright field images and diffraction patterns, in upper-right corners obtained from the corresponding precipitates, showing the amorphisation of precipitates (left) in T91 steel for 5.8 dpa/205°C, whereas at right no changes in the crystallographic structure are observed for 8.3 dpa/250°C.

5.2.2 Mechanical properties of T91 and others F/M specimens irradiated in STIP-I

Tensile properties of T91 and F82H steels were investigated as a function of the dose and irradiation temperature. To study the ductile-brittle transition of mechanical behaviour, small punch tests and Charpy impact tests were performed as well.

- Tensile properties

Specimens of the martensitic T91 and F82H steels were irradiated in a temperature range of 90 to 360 °C up to 12 dpa. Tensile tests, performed at 22, 250 and 350 °C, demonstrated that the irradiation hardening increases with increasing dose as displayed in figure 5-4 for samples irradiated up to 300°C. The uniform elongation drops to less than 1%, while the total elongation is greater than 5% in all cases. However, all the samples ruptured in ductile fracture mode after irradiations and tests carried out in the whole range of temperatures investigated [1].

For specimens irradiated at higher temperatures than 300°C, higher ductility levels, total and uniform elongations, were obtained with increasing irradiation temperature. Thus, F82H sample irradiated to 12.3 dpa at 360°C presented higher elongation values than specimens irradiated to 10 dpa at 300°C when tested at 350°C. Comparable behaviour was observed for EM10 irradiated and tested in the same range of temperature [2]. These facts seem indicate a possible change of operating mechanisms, which are defined by the irradiation temperature.

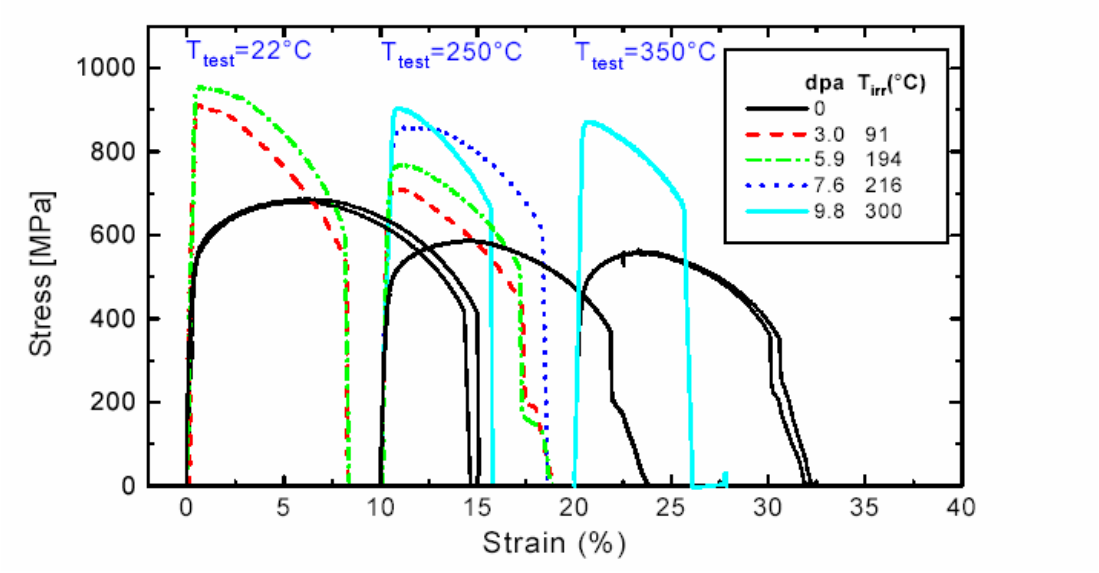

Figure 5-4: Engineering tensile stress-strain curves of T91 irradiated at SINQ / STIP-I and tested at 22, 250 and 350 °C. Samples were irradiated in the range 91-300°C with doses from 3 to about 10 dpa.

.

- Small punch tests

Small Punch (SP) tests were conducted in a temperature range from -190°C to 80°C on different martensitic/ferritic steels, T91, F82H, and Optimax, irradiated in the range 90-275°C up to 9.4 dpa.
The dependence of SP fracture energy with the test temperature and different irradiation doses is illustrated in figure 5-5. The ductile-to brittle transition temperature ($DBTT_{SP}$) values were defined by the temperature at the half value of the upper shelf energy.

The results demonstrated that the $DBTT_{SP}$ increases with increasing irradiation dose. In addition, the increase of $DBTT_{SP}$ should vary linearly with the helium content. These results should indicate that helium plays a significant role in DBTT shift after irradiation.

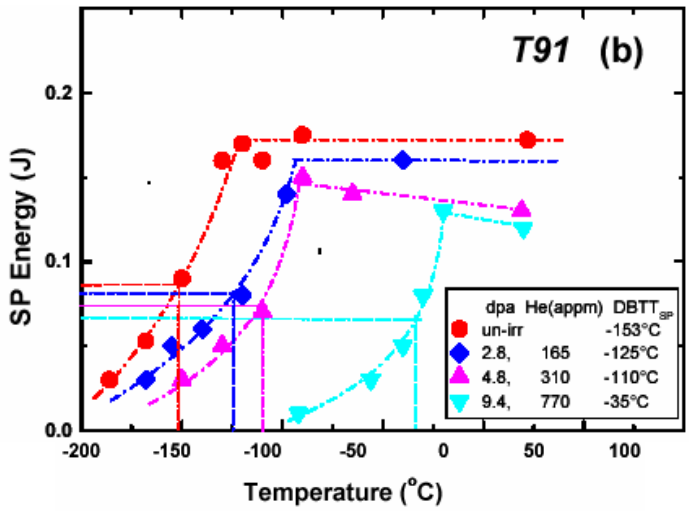

Figure 5-5: Fracture energy, determined from Small Punch tests, versus test temperature for T91 steel irradiated at different doses in the range 90-280°C.

- Charpy impact tests

Charpy impact tests were conducted on T91, F82H, Optifer-V and Optimax specimens irradiated to 7.5 dpa in the irradiation temperature range 120 - 195°C. Results obtained for T91 are shown in figure 5-6.
The variation with the dose of DBTT and Upper Shelf Energy (USE) values is shown in figure 5-7 for different 9Cr steels.
Small punch test and Charpy impact data can be correlated by the expression: $\Delta DBTT_{SP} = 0.4\ \Delta DBTT_{CVN}$. Values of DBTT shift ($\Delta$DBTT), corresponding to all investigated materials, fall into a linear band when they are plotted against helium content (see figure 5-8).

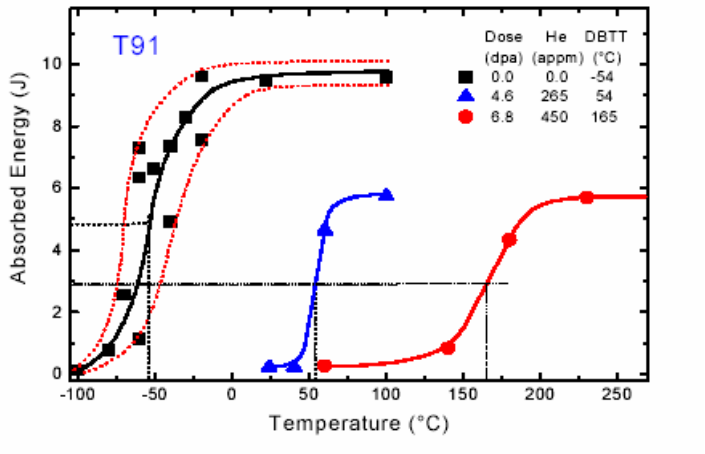

Figure 5-6: Impact energy transition curves determined for T91 steel irradiated at 122 and 185°C with doses of 4.6 and 6.8 dpa respectively.

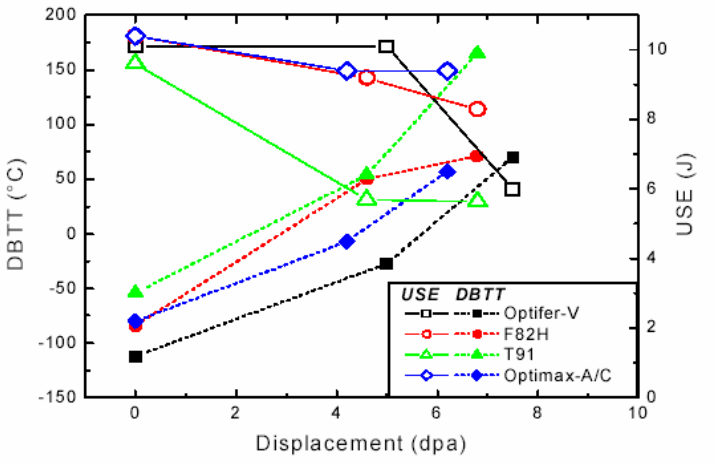

Figure 5-7: Dependence of DBTT and USE values with the dose for T91, F82H and other 9CrW-type martensitic steels.

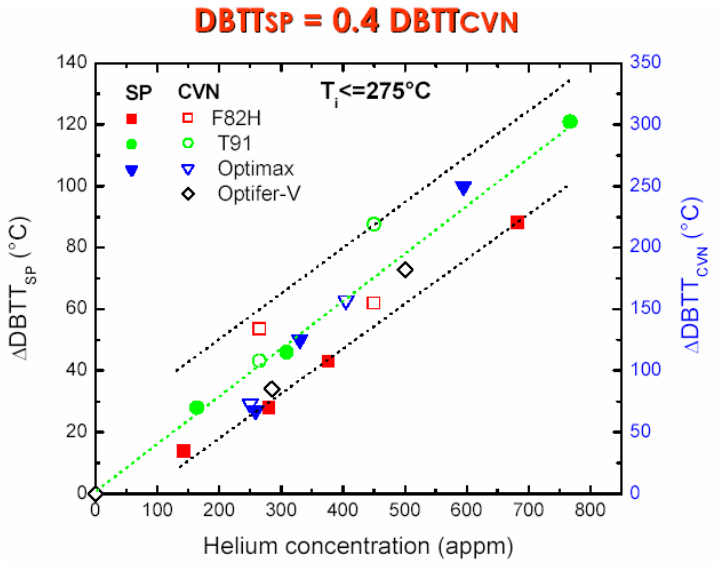

Figure 5-8: Correlation of DBTT shift values, determined by Small Punch (SP) and Charpy tests (CVN), and Helium concentration produced during irradiation.

5.3 PIE OF SPECIMENS IRRADIATED IN STIP-II

STIP-2 irradiation experiment was conducted in 2000 and 2001 and the samples were retrieved in 2003. Limited post-irradiation work has been done due to high radioactivity of the samples and limited time. Nevertheless, some preliminary PIE on selected samples were carried out at PSI.

TEM observations have been performed on a F82H sample irradiated at 400±50ºC to the highest dose of 20.3 dpa and 1695 appm He. The distribution of helium bubbles in the matrix shows a clearly bimodal behaviour. Small bubbles of few nanometers size distributed rather homogeneously in the matrix with some segregation along dislocation lines.
Large helium bubbles or voids with a size up to 50 nm were observed in some locations with relatively high precipitate density. Fig. 5-9 shows the He bubble distribution and dislocation loops induced by irradiation. Furthermore, some new precipitates also appeared.

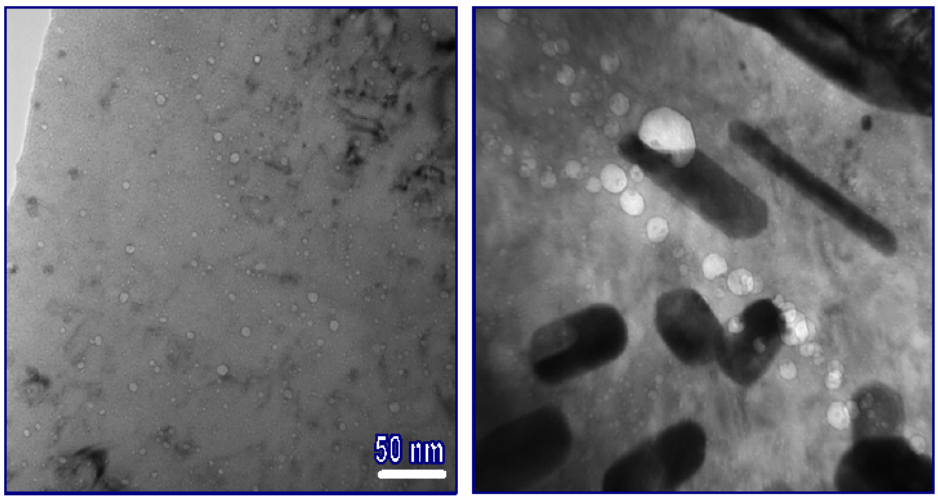

Figure 5-9: The distribution of He-bubbles observed in a F82H sample irradiated at 400±50°C to 20.3 dpa and 1695 appm He. The scale is the same for both pictures.

Preliminary Charpy tests were conducted in T91 specimens as well as small punch tests in F82H steel. Both types of tests indicated that the irradiation–induced embrittlement continued to increase with the dose. Figure 5-10 presents the first results for T91 specimens, which were irradiated at 210°C for a dose of 12.8 dpa. All of them were broken in a brittle manner from for all tests performed from 250 up to 400°C. T91 specimens irradiated in STIP 2 were obtained with the TL-orientation. This orientation display a more important DBTT shift if compared with figure 5-6 for an equivalent dose level (6-7 dpa). Effects of specimens' orientation is also observed in the unirradiated condition as shown in fig. 5-10 for samples of STIP 2 and STIP 3 obtained respectively with TL and LT orientations.

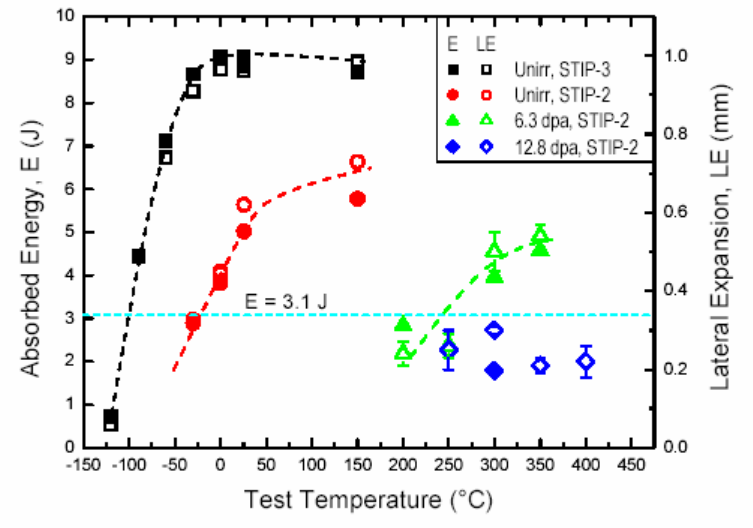

Figure 5-10: Impact energy curves obtained after irradiation of T91 specimens at 118°C for 6.3 dpa (300 appm He) and at 210°C for 12.8 dpa (785 appm He).

5.4 SUMMARY AND MAIN CONCLUSIONS

Martensitic steels T91, F82H and other 9CrW-type steels were irradiated in SINQ facility. Two experiments were carried out: STIP-I with doses up to 12 dpa and 1120 appm He at temperatures up to 360±30°C, and in STIP-II up to 20.3 dpa and 1695 appm He at temperatures up to 400±50°C. Dedicated post irradiation examinations have been performed on the STIP-I samples and limited investigations have been done on the STIP-II samples.

The following conclusions could be drawn:

- The dislocation and precipitate structures of T91 and F82H steels were largely investigated. After irradiation at $T_{irrad} \leq 360$°C, high-density defect clusters or dislocation loops occurred. The density and size of defect clusters in the T91 and F82H samples reached nearly the same values for equivalent doses. In the both steels, the size increases while the density drops rapidly with irradiation temperature above 250°C.

- High-density of helium bubbles of a diameter around 1 nm or larger were generally observed in the both steels above 200°C for a relatively high dose of about 10 dpa and 550 appm He. Non-uniformly distributed bubbles of a size up to 50 nm were observed in a F82H sample irradiated at 400±50°C up to 20.3 dpa and 1650 appm He.

- The amorphisation of M23C6 precipitates was systematically observed in the T91 and F82H samples irradiated at $T_{irrad} \leq 200$ °C.

- The irradiation hardening of T91 and F82H increases with increasing dose. For samples irradiated at 300°C and below, the uniform elongation drops to less than 1%, while the total elongation was greater than 5% in all cases.
- For all doses and irradiation temperatures investigated, the tensile specimens ruptured with a ductile fracture mode.
- The ductile-to-brittle transition temperature (DBTT) increased with irradiation dose and did not saturate at doses up to 12.8 dpa (with 730 appm He).
- T91 samples after irradiation to 12.8 dpa and 730 appm He at 210±24°C presented a brittle fracture appearance even at 400°C, which implies a very large DBTT higher than 400°C.
- Similar to the Charpy results, the ductile-to-brittle transition temperature (DBTT) determined from small punch tests, increases with irradiation dose and does not saturate at doses up to 18.4 dpa (with 1450 appm He).
- Small punch test data can be well correlated with the Charpy impact data using the expression: $DBTT_{SP} = 0.4\ DBTT_{CVN}$.
- The DBTT shift shows a linear dependence on helium concentration.

5.5 REPORTS PRODUCED IN THE FRAME OF SPIRE PROJECT – WP5

1. "Irradiation under neutron-proton mixed spectrum and related post-irradiation examination ", Y. Dai, PSI report TM-34-03-08, Deliverable n° 17.
2. "Tensile Properties of 9Cr-1Mo Martensitic Steel irradiated with high energy protons and neutrons", J. Henry, X. Averty, Y. Dai, P. Lamagnère, J.P. Pizzanelli, J.J. Espinas, P. Wident, CEA report NT SRMA 2003-2539, Deliverable n° 17.
3. "Irradiation under neutron-proton mixed spectrum in SINQ targets and related post-irradiation examinations – Final report", Y. Dai, X. Jia, R. Thermer, F. Groeschel, PSI report TM-34-04-08, October 2004, Deliverable n° 47.

6. BASIC STUDIES: NUMERICAL SIMULATION OF IRRADIATION EFFECTS WORK-PACKAGE 6

The objective of this work-package is to provide the basic understanding of phenomena occurring in a spallation environment. Because of the irradiation effects in structural materials can be studied up to limited doses under prototypical proton-neutron mixed spectrum, other important goal is the development of reliable tools for extrapolation to the conditions that has to be sustained by the window of the XADS spallation target.

For these purposes the following research subjects were selected: (i) Irradiation damage characterisation in the beam window, carried out by FZK, (ii) molecular dynamics prediction of irradiation damage in Fe-Cr alloys by KTH, (iii) modelling, on an atomic basis, of the hardening due to radiation defects, by CNRS-CECM and (iv) prediction of the effect of segregation on solid cohesion based on ab-initio electronic structure computations performed by CEA.

Basic understanding of binary Fe-Cr alloys is a prerequisite for future modelling of chromium bearing ferritic steels foreseen to be used in accelerator driven systems. Such understanding can be obtained using multiscale modelling, i.e. a combination of ab-initio, molecular dynamics and Monte Carlo simulations, where each approach is used at its appropriate length and time scale, providing input for simulations of larger systems and longer times.

6.1 DAMAGE CHARACTERISATION OF THE ADS BEAM WINDOW

The main objective of this task was the investigation of the irradiation damage for XADS structural materials and in particular to assess in-service conditions for the beam window. The study was performed using a detailed geometrical model, which includes a liquid metal spallation target, an active core with fissile isotopes, a beam window, which separates vacuum of accelerator tube and the spallation target, and a flow guide. Calculations were performed using Monte Carlo neutron, photon and charged particle transport code MCNPX. The code allows realistic simulation of spallation process and transport of generated nucleons including proton and neutron spatial and energy distributions as well as evaluation of various damage characteristics (displacement damage, heat deposition, gas and spallation element production rates).

This information can be used for experimental simulation of irradiation damage conditions expected for the XADS window and other elements of construction. It is necessary for performing calculations on temperature and stress distribution in the window and nearby materials as well as for liquid metal flow simulation, preliminary selection of material capable to sustain these conditions for a necessary period of time. The primary knocked-on atom energy spectra will be used for subsequent multiscale modelling of iron-chromium alloys.
Detailed description of the simulations, carried out by FZK, is given in ref. [1, 2, 3].

6.1.1 Displacement damage

In the process of proton transport, complex energy spectra of protons and neutrons are formed in the beam window, the flow guide and other construction elements of ADS. These spectra result in production of point defect and defect clusters, which degrade mechanical properties of construction materials. Considering different energy ranges one can conclude that at high particle energies (E > 150 MeV) displacement damage is produced solely by protons due to the processes of spallation and multi-fragmentation, while at low particle energies (E < 150 MeV) damage is produced mainly by neutrons.

The maximum damage rate at the beam window centre amounts to 32 dpa/fpy. From this value, 19 dpa/fpy come from the contribution of neutrons (En < 150 MeV), while 13 dpa/fpy are coming from protons (Ep > 150 MeV). From the total neutron contribution to damage, about 4 dpa/fpy is produced by fission

neutrons generated in the active core (see figure 6-1). This last contribution to the window damage is practically position independent. However it depends on the k_{eff}, which is reducing with irradiation time.

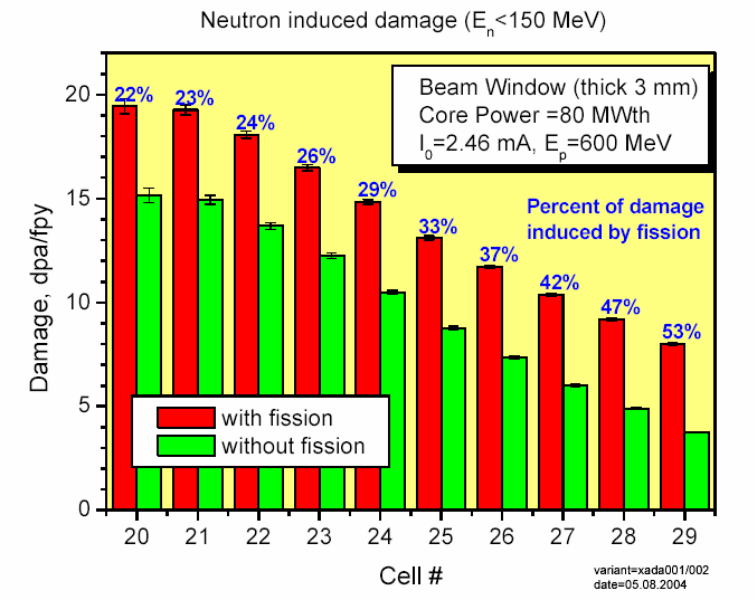

Figure 6-1: Contribution of fission neutrons on neutron induced damage in the beam window from the centre to the periphery of the beam window.

6.1.2 Heat production

Heat deposition profile in the beam window was calculated using MCNPX. This calculation takes into account all possible particles produced in spallation intranuclear cascades. The maximum heat deposition at the beam window centre amounts to 60 W/g. Protons contribute 93%, neutrons and gamma gives 3-4% to heat deposition and the rest of 3-4% is generated by other types of particles.
It was confirmed that the amount of heat deposited in the beam window by protons can be estimated using a simple analytical formula.

6.1.3 Gas and spallation elements production rates

The MCNPX results on gas production obtained in this work correspond well with those calculated using experimentally measured cross sections.
Spallation element production rates agree well with those obtained using various semi-empirical formulae (Silberger and Tsao) and systematic (Weber) fitted to the recent experimental data.

Total gas production in the beam window is given in figure 6-2. The maximum gas production rates in the centre of the beam window are 9300 appm H/fpy and 1400 appm He/fpy. The ratios of hydrogen and helium produced per displaced atom are about 430 appm H/dpa and 35 appm He/dpa, which are about ten and three times respectively higher than those expected for the DEMO fusion reactor first wall.

Spallation element production rates were calculated as follows: 57 appm Ca/fpy, 69 appm Ti/fpy, 88 appm V/fpy, 12 appm P/fpy, 17 appm S/fpy, 133 appm Cr/fpy, 110 appm Mn/fpy. These rates agree well with those obtained using MCNPX neutron and proton spectra and experimentally measured spallation element yields for iron (see figure 6-3).

6.1.4 Conclusions

The calculated spallation element production rates are significantly lower than the limits specified in the initial SPIRE proposal. Therefore it seems that, at least for the beam parameters used in this study, the spallation element production will not significantly affect mechanical properties of structural materials.

Very high gas production rates in the beam window can stimulate hydrogen and helium embrittlement of structural material. At present the elevated helium production as well as the high ratio of helium produced per dpa is, besides liquid metal embrittlement, the major factor of concern with respect to deterioration of structural material properties.

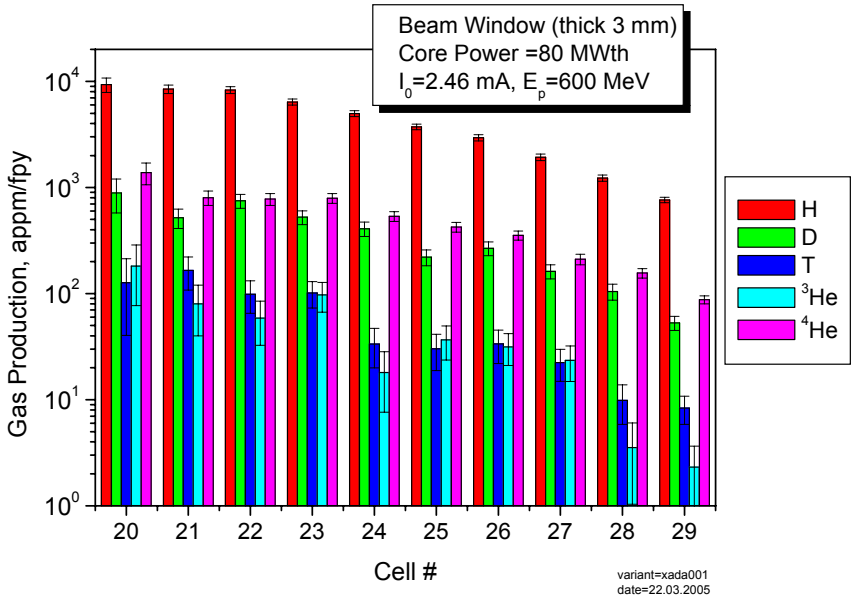

Figure 6-2: Total gas production in the hot window.

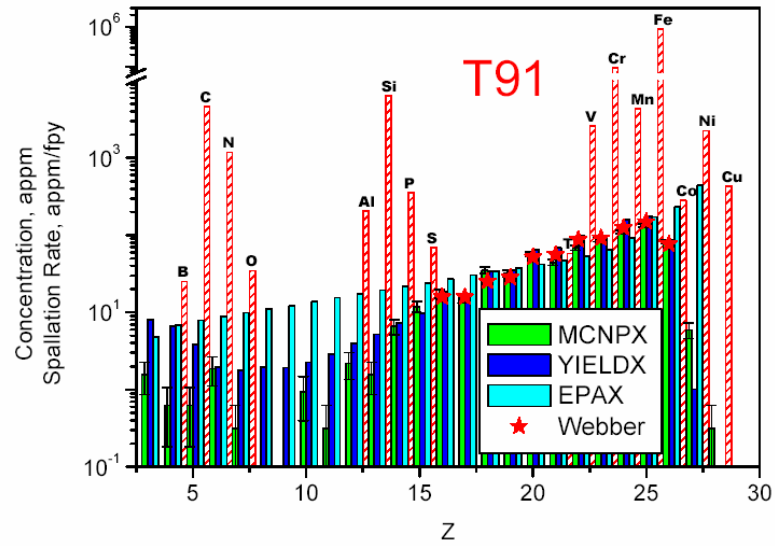

Figure 6-3: Spallation element production in the beam window after one year of irradiation as calculated with MCNPX, using two empirical formulae and experimental cross sections of R. Weber. The composition of T91 is shown with hatched red bars for comparison.

6.2 MOLECULAR DYNAMIC SIMULATION OF DEFECTS PRODUCTION AND MIGRATION RATES IN FECR ALLOYS

The WP 6 intends to investigate and model fundamental phenomena (embrittlement, segregation, swelling) that characterize the evolution of ferritic steels subject to irradiation of protons and neutrons. In particular, the primary goal of this task was to study defects production in atomic collision cascades and their subsequent migration in Fe-Cr binary alloys.

The first step consisted on the development of a many body potential and cohesion model for FeCr alloys. For this purpose, a new embedded atom method potential was developed by joint efforts of the groups from KTH and CNRS-CECM.
In fact, the development of the appropriate set of potentials for Fe-Cr system was made in several steps described in [4-7]. The procedure consisted in fitting systematically a selection of measured and calculated properties of the pure elements and the alloy, using a consistent approach based on Finis-Sinclair formalism. Thus, an improved set of potentials have been implemented that are able to reproduce elastic constants, thermal expansion coefficients and vacancy migration properties of ferromagnetic iron and paramagnetic chromium.

Modelling of chromium precipitation occurring during vacancy assisted thermal ageing as well as cooling down of recoil cascades have been performed with molecular dynamics and Kinetics Monte Carlo (KMC) methods, using the appropriate set of potentials derived for Fe-Cr system.
The simulations of thermal ageing showed that there is no sign of precipitation at any temperature when using a potential fitted to the mixing enthalpy of Fe-5Cr. But, the KMC simulations using the potential fitted to the mixing enthalpy of Fe-20Cr yield formation of Cr clusters on a time and temperature scale in good agreement with measurements of hardening in high Cr binary alloys. In Fe-10Cr it was found that spinoidal decomposition of the initially random alloy into a binary phase occurred at temperatures below 400K [5-7].

Applied to recoil cascade simulations, the alloy potential predicted a higher stability of mixed <110> Fe-Cr and Cr-Cr dumbbells with respect to the Fe-Fe dumbbells. Consequently, Cr tends to accumulate in interstitial defect clusters formed during cooling down of recoil cascades. These defects will be less mobile than pure iron defects, acting as obstacles for dislocation motion with the resulting hardening of material. In pure iron and Fe-10 Cr system, the fraction of interstitial defects located in clusters is estimated to 0.45 ± 0.05 for recoil energies of 2, 5 and 10 keV [6, 7].

6.3 MODELLING OF THE OBSTACLE FORCES DUE TO IRRADIATION DEFECTS AND THE ASSOCIATED HARDENING

Microstructural investigations of irradiated materials show a wide spectrum of defect clusters and precipitates. The high number density of very small (nano-sized) features results in significant material hardening. Because of their small size, the applicability of the elasticity theory to the modelling of the interaction of dislocations with obstacles becomes questionable. Therefore, atomic scale simulations were performed to investigate the details of dislocation-obstacle interaction (a plot of obstacle-force versus distance to dislocation). The main goal of the task was to identify the obstacles responsible for irradiation induced hardening and rank them. The results of the task depended on the interatomic potential for Fe-Cr alloys developed in the frame of the task previously described.

The Monte Carlo code for simulation of the grand-canonical ensemble has been developed to calculate equilibrium and non- equilibrium thermodynamic and mechanical properties of binary alloys. The code has been tested with the first version of Fe-Cr potential.
The MD codes and graphical visualization tools for the study of dislocation core in Fe-Cr alloys were successfully developed and tested for the case of pure Fe. The following results were obtained [8, 9]:

- the configuration of the dislocation core with and without external stresses,
- the force-distance plot of dislocations in Peierls valleys and the corresponding dislocation glide behaviour,
- macroscopic elastic limits and their temperature dependence,
- binding energies of point defects with screw dislocation core and

- the force-distance plot for the interaction of point defects with screw dislocation.

6.4 COHESION ENERGY OF SEGREGATED BOUNDARIES BASED ON ELECTRONIC STRUCTURE

During service many new elements, that were not already present, will be produced in the spallation target window due to spallation reactions. These new elements, and the impurities already present, will very likely segregate to the grain boundaries of the steel and thus affect their cohesive properties. It is clear that all the new elements produced will not be behaving in a similar manner.

In order to understand the long term reliability of the Fe-9Cr structural material, it is important to know how the grain boundary cohesion is affected by various impurities. For this purpose, ab initio electronic structure calculations concerning the behaviour of impurities on the grain boundary cohesion were performed using two different methods: the Linear Muffin Tin Orbitals (LMTO) method and the Full Potential Linearised Augmented Plane Wave (FP-LAPW) method. No empirical parameters were used in these calculations, the crystal potentials were constructed starting from the atomic numbers Z and iterated to self-consistency [10, 11,12].

The following impurities were considered in the present work: H, He, P, S, Cl, Ti, V, Cr, Zr, Nb, Mo, co-segregation of H and Ti, co-segregation of H and He.
The grain boundaries in realistic Fe-9Cr steel are necessarily complex and incoherent, especially in the presence of continuous irradiation. Simplified models were therefore used to understand the basic mechanisms and the origin of the effects of various impurities on the grain boundary behaviour.

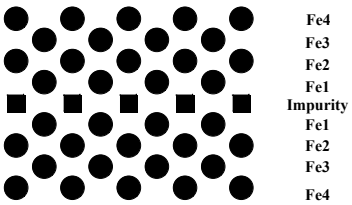

Figure 6-4: Simplified model of a grain boundary in bcc Fe.

Basically the grain boundary was represented by a (100) type slab geometry of a bcc lattice consisting in (100) Fe layers (Fe-9Cr steel is represented here by bcc Fe) and the impurity atom layer is inserted in the middle of these Fe layers as illustrated in Figure 6-4. The calculations have shown that:

- There is a significant loss in the grain boundary cohesion due to the presence of hydrogen due to the formation of metal-hydrogen bonds that decrease the metal-metal bonding.
- There is only a small dilatation due to helium in the grain boundary region, which does not decrease the grain boundary cohesion significantly (~0.17eV). But, helium is an inert closed-shell atom, and its chemical interaction with the neighbouring iron atoms is basically repulsive resulting in an enormous decrease in the grain boundary cohesion (~1.32eV). This is a new mechanism, and has to be considered in addition to the classical helium-induced embrittlement due to bubble formation.
- Ferromagnetism of iron has practically no effect on the grain boundary embrittlement due to helium.
- Calculations of the grain boundary electronic structure in the presence of P, S, and Cl show that all these metalloid elements are extremely detrimental to the grain boundary cohesion, and their potency increases in the order P, S, Cl.
- Calculations with the transition metal elements of the 3d series (Ti, V, Cr) and the 4d series (Zr, Nb, Mo) show that all these elements are beneficial to the grain boundary cohesion.
- Regarding co-segregation of Ti and H to the grain boundary, it is found that the beneficial effect of Ti is suppressed by the hydrogen atoms due to the formation of the Ti-H bonds.

- Calculations for the co-segregation of H and He to the grain boundary show that the synergistic effect of co-segregation is small.

6.5 REPORTS PRODUCED IN THE FRAME OF SPIRE PROJECT – WP6

1. A. Möslang, P. Vladimirov, Primary results on irradiation damage characterisation of the XADS beam window, Progress Report, Deliverables n° 1 and n° 5, December 2001.

2. A. Möslang, P. Vladimirov, Damage characterisation of the XADS beam window, Progress Report, Deliverables n° 14 and n° 18, November 2002.

3. A. Möslang, P. Vladimirov, Damage characterisation of the ADS beam window, Final Report, Deliverable n° 29, December 2004.

4. R. Chakarova, J. Wallenius and V. Pontikis, Development of Fe(bcc)-Cr many body potential and cohesion model, KTH report, Deliverable n° 6, June 2002.

5. J. Wallenius, C. Lagerstedt, N. Sandberg, R. Chakarova, V. Pontikis, Modelling of Chromium precipitation in Fe-Cr alloys, KTH report, Deliverable n° 19, December 2003.

6. J. Wallenius, C. Lagerstedt, V. Pontikis, Effect of PKA energy on defect cluster formation, KTH report, Deliverable n° 21, August 2004.

7. J. Wallenius, C. Lagerstedt, V. Pontikis, Molecular dynamics simulation – Final Report, KTH, Deliverable n° 26, September 2004.

8. B. Amarouchene, V. Pontikis, Lattice friction: force-distance plot determination, Deliverable n° 20, October 2002.

9. B. Amarouchene, V. Pontikis, Development of FeCr many body potentials/Distribution of their species inFeCr alloys/ Lattice friction: force-distance plot determination, Deliverable n° 6, 7 & 20, 2004.

10. R. Gupta, "Effect of spallation products on grain boundary cohesion – I", Deliverable n° 8, October 2001.

11. R. Gupta, "Effect of spallation products on grain boundary cohesion – II", Deliverable n° 22, December 2002.

12. R. Gupta, "Effect of spallation products on grain boundary cohesion – III", Deliverable n° 39, CEA report NT SRMP 2004-8, March 2004.

7. DISCUSSION

During the development of SPIRE project, an important experimental programme and theoretical simulations were implemented aiming to study the microstructure and the mechanical behaviour of 9-12%Cr martensitic steels in conditions simulating the spallation target environment. A huge volume of results were obtained in comparable conditions of dose and irradiation temperature as described in chapters 2 to 6. Some comments could be added in the form of discussion.

MECHANICAL PROPERTIES OF REFERENCE MATERIALS

To complete data concerning the mechanical behaviour of unirradiated reference steels tensile, impact, creep, fracture toughness tests have been performed including round robin tests that documented the high confidence level of results. The cleavage stress was also evaluated (about 1700-1900MPa at -150°C) for 9Cr1Mo (EM10) and 9Cr1MoVNb (T91) steels.

EXPERIMENTAL SIMULATION OF SPALLATION ELEMENTS

Helium effects

Besides the atom displacement damage, one of the most important concerns is the gas production and in particular Helium. The effects of He were mainly investigated by ion implantation experiments performed in the FZJ cyclotron at various and well controlled He-contents and implantation temperatures. In this case, the displacement damage was relatively small, about 0.8 dpa for the maximum content implanted (5000 appm He), giving a He-production rate of several 1000 appm He/dpa. The maximum content investigated corresponded to the He-concentration initially foreseen for the window after 1 year of service.

Results have clearly shown the effects of helium on tensile properties of both materials investigated, 9Cr1Mo (EM10) and 9Cr1MoVNb (T91), and demonstrated the existence of a "low temperature helium embrittlement" after implantations at $T \leq 250°C$. At these temperatures, the ductility drops very quickly with He-content simultaneously to the important increasing hardening of the material. A total loss of ductility and a brittle intergranular fracture mode were observed after implantation of 5000 appm He at 250°C. At higher temperatures, lower hardening and lower degradation of ductility was obtained.

Based on microstructural results investigated by TEM, SANS and TAP, it could be shown that the high degree of hardening of the specimens implanted at 250°C is mainly due to the high density of small bubbles they contain. However, hardening alone can not explain the complete ductility loss and the intergranular fracture mode. Ab-initio electronic structure calculations performed as part of WP6 by R. Gupta (deliverables n° 22, 39) have shown that helium drastically decreases grain boundary cohesion in iron. Therefore, it was suggested that the brittle intergranular fracture mode displayed by the specimens implanted at 250°C results from the combined effects of pronounced intergranular hardening and weakening of prior austenite grain boundaries due to helium.

On the other hand, the feasibility of He-implantation in sub-size Charpy specimens, to study the effects on the fracture properties of T91, was demonstrated and will be investigated in a future programme.

Hydrogen effects

The susceptibility to hydrogen embrittlement was investigated at room temperature in reference and experimental steels as well as in some doped versions. The method of electrochemical charging let to introduce H-content in the range 100-500 appm (2-8 wppm), in tensile specimens tested at room temperature. The hydrogen damage is evidenced by some hardening and a trend to intergranular decohesions and intragranular cleavage with the increasing content. T91 presented the higher resistance to this type of damage followed by EM10 and 9Cr2WTaV. The small size of prior austenitic grains and a fine carbide distribution seem beneficial to delay H-effects.

One open point is related to hydrogen effects at higher temperature. It is generally assumed that the high diffusivity could prevent the accumulation of H in the lattice. However, recent results seem indicate that

even low H-content (below 300 appm) could have significant impact in fatigue life of martensitic steels at 300°C after proton irradiation [1].

Effects of other spallation elements (Ca, Ti, P, S)

Simulation of solid elements like Ca, Ti, P, S were performed via ion implantation experiments or introducing them (Ti, P, S) during melting to produce doped heats.

Except for Ca implanted samples where neither clustering nor hardening was detected, experimental investigations have evidenced the high susceptibility of elements like P, S and Ti, to segregate in grain boundaries or to prone the precipitation of several complex compounds (carbides, nitrides, sulphides). Spallation reactions will produce these elements in solid solution. But, the present investigations showed that their normal trend should be the segregation or precipitation on interfaces or grain boundaries during in-service conditions, phenomena that could be enhanced by the accelerated diffusion due to the contribution of irradiation-induced point defects.

Concerning the mechanical behaviour of containing (Ti, P, S) materials, the concurrent presence of these elements resulted in a significant degradation of toughness and impact properties of 9Cr1Mo as well as experimental 9CrWTaV steels. After irradiation, doped alloys based in 9Cr1Mo matrix displayed a more important DBTT shift and USE decrease compared to 9Cr2WTaV (see figure 4-7), probably associated to higher contents of impurities in the former material. At high doses, all irradiated doped steels based in 9Cr1Mo matrix exhibited no plasticity during tests performed at room temperature.

EFFECTS OF IRRADIATION UNDER PROTOTYPICAL MIXED PROTON-NEUTRON SPECTRUM

Irradiations performed in SINQ facility under mixed spectrum, constituted of protons of high energy and spallation neutrons, are rather representative of conditions foreseen in the spallation target window. Compared to irradiations in nuclear fission reactors, the specific features of SINQ experiments come mainly from the high production of helium and hydrogen. Displacement damage, induced by neutrons and protons, and gas production occur simultaneously and both contribute to hardening and embrittlement of materials.

The experiments under prototypical spectrum reached up to 12 dpa and He-content of 1130 appm in the first (STIP I, 90-360°C) and 20 dpa and 1695 He-appm in the second one (STIP II, up to 400°C). The irradiation temperature, dose and gas production are interconnected variables, which are somewhat difficult to control because of variations of beam current and frequent beam trips. Thus, the interpretation of obtained data is sometime rather complex. However, a clear trend of mechanical behaviour was observed for 9Cr martensitic irradiated in this environment.

Important modifications of the microstructure occurred during irradiation: amorphisation of $M_{23}C_6$ precipitates, development of irradiation defect clusters of several nanometres size, high density (one order of magnitude higher than defect clusters) of He-bubbles (1nm size for doses lower than 12 dpa), which become large voids at higher doses.

Regarding the irradiation induced effects on mechanical properties, the amount of hardening obtained in SINQ experiments is comparable with that evaluated after neutron irradiation in fission reactors in the range of low doses (< 10 dpa) and for similar irradiation temperatures (T<350°C). Figure 7-1 compares the increase in yield stress of different materials determined in BR2, HFR and SINQ-STIP I experiments and in previous work [2, 3].

So, it appears that the displacement damage should provide the main contribution to hardening. In this case, the effects attributed to helium should be of second order at least for He-concentrations lower than 1000 appm. A ductile fracture mode was observed in all tested tensile specimens.

But, the most important concern is related to the high degree of embrittlement displayed by 9Cr martensitic steels as shown by the results from impact and small punch tests. An important increase of DBTT as well as a significant decrease of USE values was obtained with the increasing dose. In particular, T91 specimens irradiated to 12.8 dpa at about 210°C±30°C present a very brittle behaviour even for tests performed up to 400°C. So, one of the important issues is to evaluate how much helium contributes to the degradation of material properties in addition to displacement damage.

The evolution of impact properties from SINQ irradiations looks comparable up to 4.5 dpa with data from neutron experiments. Nevertheless, at higher doses the increase of DBTT seems to be accelerated above 6 dpa (see figure 5-7). This fact is in contrast with results of impact tests performed in T91 and other high Cr steels after neutron irradiations performed in the range 290-420°C, which indicated that the increase in DBTT saturated for doses higher than 5 dpa [4, 5].

This difference in impact behaviour observed in SINQ experiments and neutron irradiations was tentatively attributed to He-effects. A linear relationship was established between DBTT shifts and He-content.

But, comparing with STIP I, the degradation of impact properties from STIP II (6.3dpa-300appm He-ΔDBTT:300°C, 12.8dpa-800appm He-ΔDBTT:800°C) are even more important than that predicted by the linear relation previously established in figure 5-8. One contribution to this difference comes from the orientation of specimens (LT in STIP-I, TL in STIP-II), since the TL-orientation display higher DBTT and lower USE even in the unirradiated condition.

Nevertheless, the serious degradation of impact properties of T91 irradiated at 12.8 dpa and 210°C in STIP II needs further confirmation, since only 4 specimens were available for one irradiation condition because of the significant thermal gradient in SINQ devices.

Another important point to investigate in SINQ environment is the relationship between the degree of hardening and embrittlement and the irradiation temperature, parameter that has a strong influence in the material behaviour as shown by the implantation experiments and neutron irradiations.

EFFECTS OF IRRADIATION UNDER NEUTRON SPECTRUM

To evaluate the effects of atomic displacements on the behaviour of 9-12Cr martensitic steels, several irradiation experiments were carried out in fission reactors to complete the missing data on usual mechanical properties in the range of low irradiation temperatures (T < 400°C).

To investigate the first stage of the neutron damage in the range of low doses, experiments were performed in BR2 (200°C) and HFR (250°C) reactors. An excellent agreement and consistent results were obtained in both facilities.

For the investigated doses (2-4 dpa) and irradiation temperatures in the range 200-250°C, materials can be ranked in 3 groups considering their increasing sensitivity to hardening and embrittlement:

- 9Cr-1Mo (EM10) and 9Cr2WTaV displayed the lower increase of yield stress (200-270 MPa), DBTT lower than or about 0°C and a reduced DBTT shift (ΔDBTT = 75-85°C). In particular, EM10 retains a high strain hardening capacity as in the unirradiated condition. Fracture toughness values corresponding to the upper shelf region decreased 25-30% after irradiation.
- 9Cr-1MoVNb (T91) exhibited a hardening of about 350°C, a DBTT shift of 110-130°C giving final values of DBTT higher than room temperature (35-60°C). From fracture toughness tests performed in the ductile-brittle transition regime and the application of the Master Curve analysis, a quite important increase of the reference temperature T_o (*) was found (145-160°C), higher than the DBTT shift.
- 12Cr1MoWV (HT9) presented the most important level of degradation of properties compared with 9Cr steels at 200°C. For the same doses, the increase of yield stress was 440MPa, DBTT shifted 170°C whereas the reference temperature T_o was increased 230-250°C. It should be pointed out that this material presented before irradiation poor toughness properties.

This classification is in good agreement with previous irradiations performed in OSIRIS reactor (CEA-Saclay) at 325°C for various doses in the range 1-9 dpa, which lead to the same ranking of 9-12Cr steels according to their increasing sensitivity to irradiation induced hardening and ductility loss [2-YdC, 5 AA].

(*) *Related to fracture toughness properties, two important points need further investigation and discussion. The first is linked to the applicability of the Master Curve approach to high Cr ferritic-martensitic steels. In the affirmative case, the second item is related to the shift of reference temperature T_o, determined in the transition regime, which seems systematically larger than DBTT shift measured from Charpy tests for 9-12Cr steels. More experimental data is needed to confirm it, but this fact, not observed*

for other classes of steels (for ex. RPV steels), should have important implications for both designers and safety authorities.

To investigate the effects of neutron irradiation at higher doses, close to the maximum dose expected for the spallation target structures, an experiment was performed in BOR60 fast reactor at 325°C for 32-42 dpa. In this case, different susceptibility to hardening and embrittlement was also found for 9Cr steels, which presented before irradiation quite similar mechanical properties. But, the rank is different compared to the behaviour at low doses.

9Cr1Mo (EM10) and 9Cr1Mo9Cr1MoVNb (T91) reference steels seem to harden earlier and their ductility decreases much faster than the experimental alloys like 9Cr1WTaV (Eurofer) and 9Cr2WTaV (see figures 4-3 and 4-4). Both 9Cr1Mo steels exhibited some ductility at 325°C but nearly no plasticity is obtained for tests performed at 20°C for doses in the range 32.5- 42 dpa.

Previous experiments performed in OSIRIS reactor at 325°C showed that 9Cr1Mo (EM10) steel displayed up to 9 dpa high values of total, uniform elongations and reduction in area measured at 20°C [3].

Regarding the evolution of hardening with the dose, figure 7-1 shows a good agreement with data obtained at BR2, HFR and SINQ at lower temperature (100-250°C) and those corresponding to 325°C. A continuous decrease of the hardening rate is observed with the increasing dose. Nevertheless, even the hardening rate decreases, the ductility of materials diminish continuously to reach a nearly zero level at 32.5 dpa in the case of EM10 and T91. The main concern is the determination of this "threshold dose" for the total ductility loss for each material and each irradiation temperature.

The nearly total ductility loss of EM10 and T91 at 20°C should indicate an important shift of the Ductile Brittle Transition Temperature (DBTT) beyond the room temperature. The first Charpy tests (in progress) seem to confirm this point. Irradiations performed in BR2 and HFR have shown that the DBTT increased sometimes further than room temperature for relatively low doses, in particular for T91.

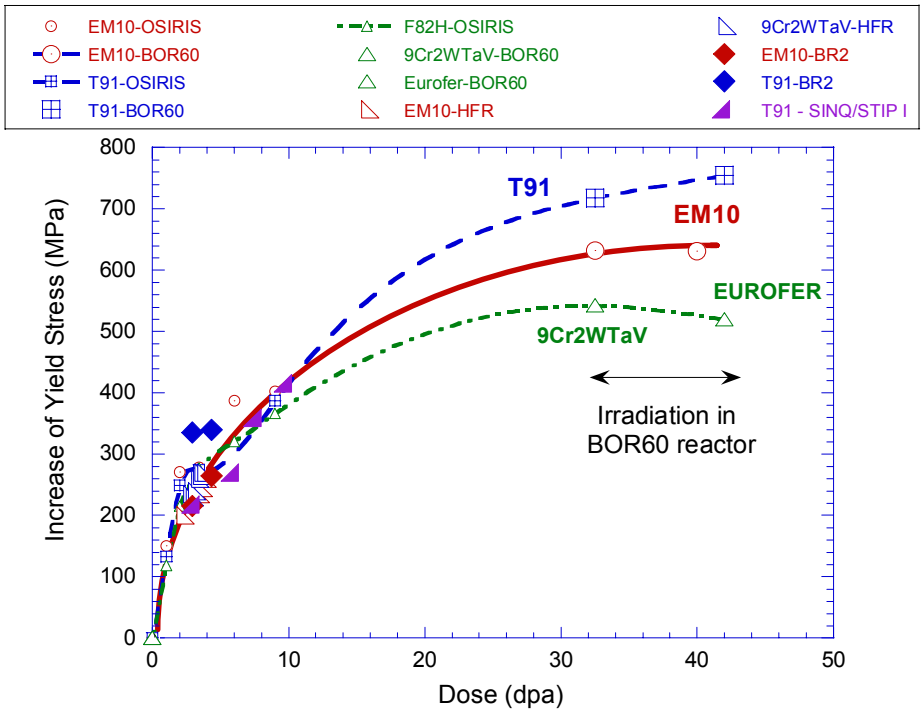

Figure 7-1 : Irradiation-induced hardening, measured at the irradiation temperature, as a function of the dose. Comparison of data obtained in experiments performed in BR2 (200°C), HFR (250°C), OSIRIS and BOR60 (325°C) reactors and SINQ facility (STIP I, T_{irrad} : 90-300°C, measured at 250°C).

On the other hand, previous results obtained for EM10 and T91 irradiated in Phenix fast reactor in the range 380-550°C for high doses (about 68 dpa for T91, 97 for EM10) showed DBTT values below room temperature in all the cases [6]. Therefore, the present results suggest a preponderant effect of the irradiation temperature as already observed for low doses [2, 7, 8]. This important outcome is illustrated in figure 7-2, which compares the induced hardening for EM10 specimens irradiated in Phenix reactor at several temperatures and comparable doses to that measured after irradiation in BOR60.

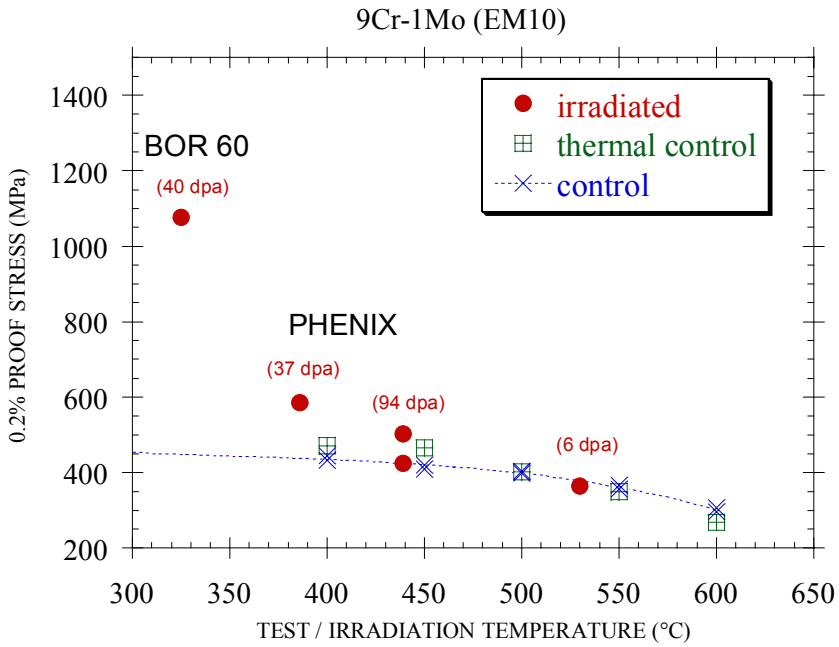

Figure 7-2 : Effects of the irradiation temperature on the irradiation-induced hardening determined for 9Cr1Mo (EM10) martensitic steel.

It is important to emphasize the improved behaviour of 9CrWTaV steels which showed more delayed irradiation effects. Thus, their DBTT values should be significantly lower compared to 9Cr1Mo materials irradiated in the same conditions. To enhance the performance of structural materials, further investigations are necessary in the future to get insight into the mechanisms responsible of the improved behaviour of 9CrWTaV steels.

One of the reasons is certainly related to the more restricted chemical composition specification and a better control during manufacturing of 9CrWTaV experimental martensitic steels of impurities detrimental for mechanical behaviour. As shown by Auger Electron Spectroscopy (see figure 2-1), significant phosphorus-segregation has been detected in the grain boundaries of both T91 and EM10 steels in the unirradiated condition that was not observed in 9Cr2WTaV.

The first recommendation is the reduction of specified P-content (and also S) from the present values in 9Cr1Mo steels, 130-200 ppm, to the level required in 9CrW experimental steels (< 50 ppm P).

DAMAGE CHARACTERISATION OF THE SPALLATION TARGET WINDOW

New calculations were carried out to update the first estimations of irradiation damage that will undergo the XADS beam window. For this purpose, the damage for structural materials was calculated using a detailed geometrical model, which includes a liquid metal spallation target, an active core with fissile isotopes, a flow guide and a beam window of 3mm in thickness to separate the accelerator vacuum and the liquid lead alloy.

Calculations were performed assuming a 600 MeV proton beam of 2.5 mA, a proton current density lower than 28μA/cm^2 and a full calendar year of operation for a core power of 80MWth. These values are in general lower than those used in the preliminary estimations performed before the start of SPIRE programme (assumed protons of 1GeV with a current density of ~ 70μA/cm^2).

Results obtained for these conditions showed that the maximum damage rate corresponding to the beam window centre is about 32 dpa/fpy, that is nearly 3 times lower than initially considered. From this value, 19 dpa/fpy come from neutrons (E_n < 150 MeV), while 13 dpa/fpy are coming from protons (E_p > 150 MeV). About 4 dpa/fpy from the total neutron contribution to damage is produced by fission neutrons generated in the active core (see figure 6-1).

The maximum heat deposition at the beam window centre was evaluated on 60W/g, where 93% comes from protons contribution, neutrons and gamma gives 3-4% and the complement from other particles.

The maximum gas production rates are 9300 appm H/fpy and 1400 appm He/ fpy, with ratios of about 430 appm H/dpa and 35 appm He/dpa, which are respectively around ten and three times lower than the initial considered values.

Concerning the solid spallation elements (Cr, Mn, Ti, Ca, V, P, S) their production rate was at least one order of magnitude lower compared to the first estimates, so less than 100-150 appm/fpy, whatever the considered element. Consequently, no quite severe contribution is expected from solid spallation elements.

Even the new estimates for the gas production are lower than those initially foreseen, their level remains significantly high. So, the main concern is however the high gas production rates and especially the He/dpa ratio, parameter that will contribute to the determination of the lifetime and performances of spallation target structures, in particular for the beam window.

OTHER CALCULATIONS

Other important achievements in this field are related to the development of FeCr many body potential to model the configuration and migration of radiation defects, clustering/ precipitation of chromium.
The evaluation of cohesion energy of segregated boundaries was performed taking into account different elements (H, He, Ti, V, Cr, Zr, Nb, Cl,…). In particular for helium, calculations have concluded to the significant loss in grain boundary cohesion due to the chemical interaction of helium, which is essentially repulsive with neighbouring atoms. Calculations for the co-segregations of H and He in the grain boundary show that the synergistic effect is small.

REFERENCES

1. P. Marmy and B.M. Oliver, J.Nucl.Mater, 318 (2003) pp132-142.
2. A. Alamo, M. Horsten, X. Averty, E. I. Materna-Morris, M. Rieth, J.C. Brachet, J. of Nuclear Materials 283-287 (2000) 353.
3. Y. de Carlan, X. Averty, J.C. Brachet, J.L. Bertin, J.L. Rozenblum, F. Rabouille, A. Bougault, Proc. of "Effects of Radiation on Materials: 22nd Int. Symposioum, June 8-10, 2004, Boston, USA, to be published in ASTM - STP 2005.
4. R. L. Klueh, D.J. Alexander, J. Nucl. Mater. 258-263, (1998) 1269.
5. M. Rieth, B. Dafferner, H.D. Röhrig, C. Wassilew, Fusion Eng. Design 29 (1995) 365.
6. J.L. Séran, A. Alamo, A. Maillard, H. Touron, J.C. Brachet, P. Dubuisson, O. Rabouille, J. of Nuclear Materials 212-215 (1994) 588-593.
7. M. Rieth, B. Dafferner, H.D. Röhrig, J Nucl. Mater. 258-263 (1998) 1147.
8. E.I. Materna-Morris, M. Rieth, K. Ehrlich, Effects of radiation on Materials : 19th Int. Symposium, ASTM STP 1366 (1999)

8. CONCLUSIONS

An important programme of R&D was developed in the frame of SPIRE project on 9Cr martensitic steels to study their microstructure and the mechanical behaviour in conditions simulating the spallation target environment.

- An important data set on mechanical properties was obtained for the reference and experimental steels in the unirradiated condition.
- Irradiations with prototypical proton/neutron spectrum carried out in the temperature range 100-350°C and for fluences up to 12 dpa, showed a very important degradation of the impact properties of 9Cr martensitic steels. Nevertheless, acceptable ductility was obtained in tensile tests for the investigated conditions (He < 1000 appm).
- Helium implantation experiments have demonstrated the existence of a "low temperature Helium-embrittlement" occurring for T ≤ 250°C, where a total loss of ductility and an intergranular fracture mode is obtained for He ≥ 2500 appm.
- Neutron irradiation experiments performed in the range 200-250°C for low doses (2-4 dpa) and at 325°C for high doses (32-42 dpa) have shown that 9-12Cr martensitic steels exhibit a significant degree of hardening and embrittlement when irradiated at these temperatures, even at low doses.
- 9Cr1MoVNb (T91) and 9Cr1Mo (EM10) displayed a higher degree of embrittlement compared to 9CrWTaV steels when irradiated at high doses (32-42 dpa). Among other reasons, the higher degradation of mechanical properties could be related to Phosphorus segregation detected in unirradiated specimens by Auger spectrometry.
- The simulations of other spallation elements like Hydrogen, introduced by cathodic charging, or (Ti, P, S) introduced during melting of special ingots, mainly resulted in the deterioration of toughness and impact properties before and after irradiation.
- Detailed calculations provided new estimates for the irradiation damage of the beam window, i.e., 32 dpa/fpy, He-content of 1400 appm He/fpy and 35 appm He/dpa, and a low production rate of solid spallation elements (< 150 appm/fpy).

All performed experiments have shown a very important degree of embrittlement in the temperature irradiation range of 100-325°C. This is a common feature to irradiations with mixed spectrum where both displacement damage and He-effects contributions operate, to neutron irradiations where only displacement damage is produced, or to He-implantations. The important conclusion that could be drawn is related to the major role of the temperature, in the range T<350°C, on the irradiation behaviour of materials.

Consequently, from the point to view of irradiation behaviour and to avoid a prohibitive level of hardening and embrittlement, in-service temperatures need to be higher than 350°C to optimise the lifetime of the beam window and other structures heavily irradiated of the spallation target or core components.

However, 9Cr experimental steels of 9Cr (1-2W) VTa appeared as promising candidates, with delayed effects of irradiation at high doses. One reason of the best behaviour these materials is certainly related to the low level of specified impurities and their good control during manufacturing.

On the other hand, the activities carried out in SPIRE project have improved the scientific and technological knowledge related to the metallurgy of 9Cr martensitic materials, have enhanced skills of staff and permitted the development of international cooperation in the field of structural materials for ADS systems.

The main outcomes of SPIRE constituted a basic input for the definition of the research programme concerning the structural materials irradiation behaviour of IP-EUROTRANS (6^{th} FP).
Also, connected fields such as materials community for fusion technology and advanced fission reactors will also benefit from the successful outcomes of the present work.

9. PROSPECTS FOR FUTURE PROGRAMME

During SPIRE project, an important experimental programme was carried out to investigate the susceptibility of martensitic steels to hardening and embrittlement in the low range of temperatures (200-325°C) where these phenomena could reach a prohibitive level. For this purpose, experiments were performed at BR2 (2-5.5dpa, 200°C), at HFR (about 3 dpa, 250°C) and in the fast reactor BOR60 at 325°C for 42 dpa. Irradiations under prototypical mixed proton/neutron spectrum (100-350°C, 12 dpa) were also performed in SINQ facility as well as He-implantation experiments for different He-contents (up to 5000 appm He) and implantation temperatures.
Results from these experimentations have confirmed the important degree of embrittlement reached for the main candidates, i.e., 9Cr1Mo (EM10 and T91) steels in the low range of temperatures.
These data have highlighted as well the preponderant effect of the irradiation temperature, which defines the irradiation behaviour and induces different performances of materials in the range 300-550°C.
One of the main concerns of a future R&D programme is to delimit the temperature range for utilisation of candidate materials for spallation target structures and core components. Other important issue is related to the synergistic effects of irradiation in presence of LBE on the degradation of structural materials properties.

Consequently, for future work, a comprehensive and consistent programme is proposed on the irradiation behaviour of the reference materials with the following objectives:

- To determine according to the design requirements, the relevant properties of the selected structural materials under irradiation conditions envisaged for components of the spallation target and sub-critical system, in the whole range of foreseen in-service temperatures.
- To assess the irradiation behaviour of alternative solutions (coated versions, high temperature resistant materials) compared to the present reference materials.
- To investigate the combined effects of irradiation in presence of LBE on structural materials as well as the Po production, release and deposition.
- Quantify the effects of spallation products, in particular He, on mechanical properties.
- To contribute to the modelling and development of experimental and theoretical tools to predict irradiation and spallation effects to high dose levels.

IRRADIATION STUDIES FORESEEN IN THE FRAME OF IP-EUROTRANS /DEMETRA – DM4 "TECHNOLOGY"

During the last year of SPIRE project, an important effort was devoted to discussion and meetings to prepare the domain 4 (DEMETRA) of the integrated project EUROTRANS (6th FP), related to the technology of structural materials and heavy liquid metals.

Based on the requirements from designers of ADS components, the main outcomes from SPIRE project and taking into account the facilities available in Europe, it was concluded that the main objectives of the future experiments should be:

1. To investigate the combined effects of neutron irradiation in presence of lead-bismuth liquid metal, covering a large range of irradiation temperatures (300-550°C).
2. To get data for high doses in a large range of irradiation temperatures (380-550°C) under irradiation with fast neutron spectrum.
3. To get data using mixed proton/neutron spectrum for doses and temperatures as close as possible to conditions foreseen for the spallation target structures.

Therefore, several experiments are planned to characterise the irradiation behaviour of 9Cr1MoVNb (T91) reference steel, 9CrW alternative martensitic steels and their versions with coating for corrosion protection.

Item 1 is related to a new type of irradiation experiment that will be performed for the first time in Europe, aiming to evaluate the contribution of corrosion mechanisms and the irradiation damage on the degradation of mechanical properties, as well as the evolution of LBE after irradiation.

Two complementary experiments are planned in BR2 and HFR reactors to develop this know-how and to obtain data for low doses in static LBE in the range 300 to 550°C.

Item 2 will be implemented by the experiment planned in Phenix reactor for various irradiation conditions: doses in the range 35-70 dpa and irradiation temperatures from 390°C to 520°C. These data will be a complement of results previously obtained in BOR60 (325°C, 32-42 dpa).

Concerning the item 3, a new experiment with mixed proton/neutron spectrum is carried out in SINQ facility for higher doses (~ 20 dpa) and higher temperatures (400-600°C) with the corresponding tests after irradiation.

To complete these experiments and separate the He-contribution to the evolution of mechanical properties, the investigation of He-effects on the fracture properties of T91 is also included.
Others experiments destined to provide basic understanding of observed phenomena and tools will be developed for reliable extrapolation of the results obtained in experiments to the conditions that have to be sustained by the window and other highly irradiated parts of the European Transmutation Demonstrator.

Figure 9-1 illustrates the complementarities of all experiments foreseen in IP EUROTRANS-DEMETRA. They were defined in such a way to cover as much as possible the parameters required by the design, to avoid duplication and to be complementary with those already performed during SPIRE project. The comparison is also given with approximate conditions foreseen by designers for the irradiated structures of ADS.

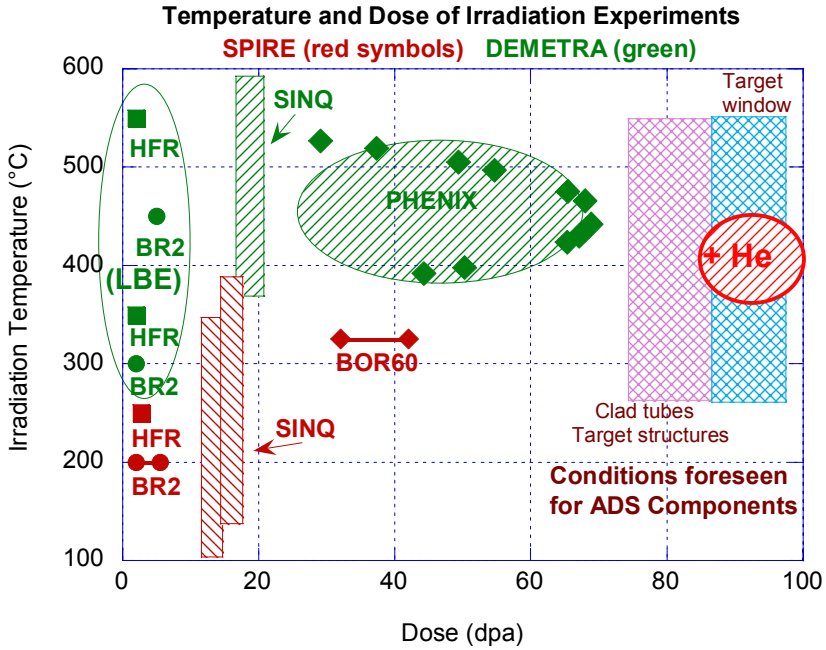

Figure 9-1 : Representation of temperature/dose conditions of irradiation experiments planned in the frame of IP-EUROTRANS-DEMETRA and performed in SPIRE project and comparison with approximate conditions foreseen for different ADS components.

10. LIST OF DELIVERABLES

Deliv. n°	Deliverable title	Deliv. date (month)	Report Title - Authors	Organisme
1	Definition of boundary conditions for calculation (Neutron and proton spectra)	6	Primary Results on Irradiation Damage Characterization of the XADS Beam Window - Deliv. N° 1 & 5 A. Möslang and P. Vladimirov	FZK/IMF-1
2	Management report	6	Semi Annual Management Report - Month 6 SPIRE Contract n° FICK-CT-2000-00058 J.L. Boutard	CEA
3	Mechanical properties of He implanted 9 Cr conventional steels	9	He Implantation and testind of Tensil Specimens (phase I) J. Chen, P. Jung, H. Klein, W. Schmitz	Forschungszentrum Jülich
			Mechanical properties and surface examination of He-implantes conventional 9Cr steels J. Chen, P. Jung, H. Klein, W. Schmitz	Forschungszentrum Jülich
4	Conventional 9 Cr : mechanical properties and inter laboratory Quality Assurance comparison	12	Mechanical properties of conventional 9Cr steels befor irradiation G. Diega, M. Serrano, F.J. Perosanz, A.M. Lancha	CIEMAT
			SPIRE PROJECT - Work Package 2 (WP2) : Preliminary Intercomparison of Mechanical test results E. LUCON	SCK CEN Mol (Belgium)
5	Implementation and adaptation of codes for SPIRE specific application	12	Primary Results on Irradiation Damage Characterization of the XADS Beam Window - Deliv. N° 1 & 5 A. Möslang and P. Vladimirov	FZK/IMF-1
6	Development of Fe(bcc)-Cr many body potential and cohesion model	12	Development of Fe(bcc)-Cr many body potential and cohesion model R. Chakarova, V. Pontikis and J. Wallenius	KTH and CNRS-CECM
7	Computation of equilibrium. & non-equilibrium species distribution. Irradiation defects clusters identification	12	Included in deliverable n° 40 - Final report	CNRS-CECM
8	P and S segregation effects on grain-boundaries cohesion (LTMO-ASA method)	12	Effect of spallation products on grain boundary cohesion R. Gupta	CEA
9	Management report	12	Semi Annual Management Report - SPIRE Contract n° FICK-CT-2000-00058 - Months 12&18 J.L. Boutard; A. Alamo	CEA
10	Scientific and technical report	12	First Annual Scientific and Technical Report - SPIRE Contract n° FICK-CT-2000-00058 Jean-Louis BOUTARD	CEA
11	FEGSTEM analysis of microstructure and segregation in 9Cr conventional steels	15	Tensile Properties and microstructure of 9Cr-1Mo Martensitic Steels containing a High Helium concentration J. Henry, P. Jung, J. Chen, J.C. Brachet	CEA
12	Doped steels : heat treatment definition, solubility boundaries determination	18	Effects of iron Spallation Products, Ti, P And S on the Physical Metallurgy of 9Cr Martensitic steels O. Danyloa, Yde Carlan, D. Hamon, J.C. Brachet, J. Henry, A. Alamo	CEA
13	Fabrication of needles for implantation and TAP examination	18	Fabrication of specimens for tomographic atom probe examinations using He Implanted samples J. Henry, T. Van Den Berghe, P. Pareige	CEA

Deliv. n°	Deliverable title	Deliv. date (month)	Report Title - Authors	Organisme
14	Progress report on damage characterisation of the beam window	18	Damage Characterization of the XADS Beam Window Deliverables n° 14 & 18 A. Möslang, P. Vladimirov	FZK/IMF-1
15	Management report	18	Semi Annual Management Report - SPIRE Contract n° FICK-CT-2000-00058 – Months 12&18 J.L. Boutard; A. Alamo	CEA
16	Doped steels : mechanical properties, in as received condition-Impact properties after step-cooling	24	Window materails for ADS NRG deliverable N°16, part1 of 2:Mechanical properties of unirradiated 9Cr martensitic steels J.B.J. Hegeman, J. Rensman	NRG
			Microstructure of experimental 9%Cr F-M steels NRG deliverable N0 16, part 2 of 2: Microstructure of unirradiated 9Cr martensitic steels J.W Hooijmans, E.W. Schuring, J. Rensman	NRG
			Tensile and Impact Properties in the as-received condition and after step cooling of 9Cr Martensitic steels doped with titanium, phosphorus and sulphur Y. De Carlan, S. Urvoy, I. Tournié, P. Wident	CEA
17	Mark II irradiation : PIE of tensile specimens. including SEM and FEGSTEM examination	24	Tensile Properties of 9Cr-1Mo Martensitic Steel irradiated with high energy protons and neutrons J. Henry, X. Averty, Y. Dai, P. Lamagnère, J.P. Pizzanelli, J.J. Espinas, P. Wident	CEA
			WP5: Irradiation under neutron-proton mixed spectrum and related post-irradiation examination	Paul Scherrer Institut
18	Progress report on damage characterisation of the beam window	24	Damage Characterization of the XADS Beam Window Deliverables n° 14 & 18 A. Möslang, P. Vladimirov	FZK/IMF-1
19	Modelling of Mo and Si effect on migration rates. Treatment of electronic excitation, *Content modified:modelling of Cr precipitation appeared as more relevant subject*	24	Modelling of Cr precipitation in Fe-Cr alloys J. Wallenius; C. Lagersterdt; N. Sandberg; R. Chakarova; V. Pontikis	KTH and CNRS-CECM
20	Force-distance plot determination . Ranking of irradiation. defects versus hardening	24	Lattice friction : force-distance plot determination. Classification of irradiation defects as a function of their efficiency as obstacles to dislocation glide. B. Amarouchene and V. Pontikis	CNRS-CECM
21	PKA energy effect on the number of vacancies number for high PKA energy	24	Effect of PKA energy on defect cluster formation. J. Wallenius; C. Lagersterdt; V. Pontikis	KTH and CNRS-CECM
22	Effect of other impurities (Mo & He) on grain boundaries cohesion	24	Effect of spallation products on grain boundary cohesion Work Package 6 (WP6) Basic Studies R. Gupta	CEA

Deliv. n°	Deliverable title	Deliv. date (month)	Report Title - Authors	Organisme
23	Ca, Ti and S single implantation of TEM discs and TAP specimens - TEM & TAP examination	24	Experimental simulation of spallation elements production in a 9Cr-1Mo martensitic steel : 3D Atom Probe Characterisation E. Cadel, P. Pareige, M.O. Ruault	CNRS-GMP & IN2P3
			Consequences of calcium and sulfur spallation products recoils in 9Cr-1Mo steel : simulation by ion implantation G. Amiri, M.H. Ruault, J. Henry, H. Bernas, E. Cadel, P. Pareige	CEA & CNRS-IN2P3
24	Management report	24	Semi Annual Management Report - SPIRE Contract n° FICK-CT-2000-00058 - Months 24&30 A. Alamo	CEA
25	Mid term report	24	Scientific and Technical Mid Term Report - SPIRE Contract n° FICK-CT-2000-00058 A. Alamo	CEA
26	Molecular dynamics simulation final report	27	Molecular dynamics simulation - final report J. Wallenius; C. Lagersterdt; V. Pontikis	KTH
27	Conventional 9 Cr steels : cleavage properties & identification of fracture mechanisms	30	Modelling of the Fracture Properties of Conventional 9Cr Steels using the local approach P. Lamagnere, J. Pecego, G. Perez, V. Rabeau, B. Marini, P. Wident	CEA
28	Feasibility of He – implantation in the notch of 9Cr1MoVNb conventional steel mini Charpy specimens	30	He implantation in the notch of 9Cr-1Mo subsize Charpy specimens :demonstration of feasibility J. Henry, X. Averty, L. Vincent, P. Jung, P. Coffre, J.J. Espinas	CEA
29	Final report on damage characterisation of the beam window	30	Final Report on Damage Characterization of the ADS Beam Window P. Vladimirov and A. Möslang	FZK
30	Management report	30	Semi Annual Management Report - SPIRE Contract n° FICK-CT-2000-00058 - Months 24&30 A. Alamo	CEA
31	Neutron dosimetry and temperature analysis for irradiation in MTR at 200°C	31	Included in deliverable n° 44b - Final report	SCK CEN Mol (Belgium)
32	Neutron dosimetry and temperature analysis for irradiation in MTR at 250°C	31	Included in deliverable n° 45 – Final report	NRG
33	Doped steels : evolution of microstructure after step-cooling. FEGSTEM, TAP and AES	36	Auger Analysis on EM-10 and T-91 steels in the as-received condition M. Garcia-Mazario, A.M. Lancha	CIEMAT
			Auger Analysis on Doped steels M. Garcia-Mazario, A.M. Lancha	CIEMAT
34	Doped steels : tensile properties after H cathodic charging	36	Tensile Properties of conventional and doped 9Cr steels under hydrogen charging M.F. Maday, G. Filacchioni, L. Pilloni, D. Ferrara, E. Casagrande, U. De Angelis	ENEA

Deliv. n°	Deliverable title	Deliv. date (month)	Report Title - Authors	Organisme
35	Successive implantation of Ca followed by H - TEM and TAP	36	Work Package N°3 Experimental simulation of irradiation effects in a spallation spectrum Tomographic Atom Probe analyses of the microstructure of 9Cr-1Mo steel after sequential Ca and H ions implantation Month 36 H. DeMonestrol, P. Pareige	CNRS - GPM
			Microstructural evolution of 9Cr-1Mo steel under sequential H and Ca ions : An in-situ TEM Study M.O. Ruault, O. Kaitasov, J. Henry, H. Bernas, S. Collin	CNRS - IN2P3
36	H and hydride effects on the host matrix and interface cohesion	36	Effect of spallation products on grain boundary cohesion R. Gupta	CEA
37	Management report	36	Semi Annual Management Report - SPIRE Contract n° FICK-CT-2000-00058 - Months 36&42 A. Alamo	CEA
38	Scientific and technical report	36	Scientific and Technical Report - Year 3 - SPIRE Contract n° FICK-CT-2000-00058 - A. Alamo	CEA
39	Final report : Cohesion energy of segregated boundaries	39	Effect of spallation products on grain boundary cohesion Work Package 6 (WP6) Basic Studies R. Gupta	CEA
40	Final report : Modelling of obstacles hardening	39	Development of Fe(bcc)-Cr many body potentials Distribution of species in FeCr alloys Lattice friction : force-distance plot determination. Classification of irradiation defects as a function of their efficiency as obstacles to dislocation glide. B. Amarouchene and V. Pontikis	CNRS-CECM
41	Final report WP2: Effects of spallation products on physical metallurgy of selected steels	40	Lattice friction : force-distance plot determination. Classification of irradiation defects as a function of their efficiency as obstacles to dislocation glide. B. Amarouchene and V. Pontikis	CIEMAT
42	Management report	42	Semi Annual Management Report - SPIRE Contract n° FICK-CT-2000-00058 – Months 36&42 A. Alamo	CEA
43	Final report WP3 : Experimental simulation of irradiation effects in spallation spectrum	48	Experimental simulation of irradiation effects in spallation spectrum: SPIRE WP3 - Final report - Deliverable n° 43 - J. Henry	CEA
44	Integrated data set report on PIE of specimens irradiated in MTR at 200°C	48	Mechanical Response to Irradiation for Three High-Cr Martensitic Steels (EM10,T91, HT9) Intermediate Report :1st Specimen Batch (2,6dpa) E. Lucon, A. Almazouzi	SCK CEN Mol (Belgium)
			Mechanical Response to Irradiation at 200°C for EM10, T91, HT9 Steels - Final Report: Specimen Irradiated to 2,6 and 3,9 dpa E. Lucon, A. Almazouzi	SCK CEN Mol (Belgium)

Deliv. n°	Deliverable title	Deliv. date (month)	Report Title - Authors	Organisme
45	Integrated data set report on PIE of specimens irradiated in MTR at 250°C	**48**	NRG SPIRE contribution : Mechanical Test Results from MTR irradiation up to 3 dpa at 250°C - Month 48 J. Rensman; F. Schmalz; R. d. Boef; F.P. v. D. Broek; J. Boskeljon	NRG
46	Integrated data set report on PIE of specimens irradiated in FBR at 325°C	**48**	Post-irradiation Examinations of 9Cr martensitic steels irradiated up to 42 dpa in BOR60 reactor at 325°C - Final Report- Deliverable n° 46 - Month 48 A. Alamo - J.L. Bertin	CEA
47	Mark III irradiation : PIE of specimens . including SEM and FEGSTEM examination	**48**	Irradiation under neutron-proton mixed spectrum in SINQ targets and related post-irradiation examination Y. Dai, X. Jia, R. Thermer, F. Groeschel	Paul Scherrer Institut
48	Management report	**48**	Semi Annual Management Report - SPIRE Contract n° FICK-CT-2000-00058 - Month 48 A. Alamo	CEA
49	Technology Implementation Plan	**48**	T.I.P. – J.L. Boutard, Updated , A. Alamo	CEA
50	List of reports and final report	**48**	Final Scientific and Technical Report - Year 4 - SPIRE Contract n° FICK-CT-2000-00058 - A. Alamo	CEA

11. PUBLICATIONS IN INTERNATIONAL SCIENTIFIC JOURNALS

1. Y. De Carlan, D. Hamon, J.C. Brachet, J. Henry, A. Alamo, "Effects of iron spallation products, Ti, P and S on the physical metallurgy of 9Cr martensitic steels", O. Danylova, CEA (France), J. Phys. IV France, vol. 12 (2002), Pr8-75.

2. G. Amiri, M-O. Ruault, J. Henry, H. Bernas, E. Cadel and P. Pareige, Consequences of calcium and sulfur spallation product recoils in 9Cr-1Mo steel : simulation by ion implantation, J. Phys. IV 12 (2002) 85

3. E. Cadel, P. Pareige and M.-O. Ruault, Experimental simulation of spallation elements production in a 9Cr-1Mo martensitic steel : 3D atom probe characterization, J. Phys. IV 12 (2002) 93

4. J. Henry, P. Jung, J. Chen and J-C. Brachet, Tensile properties and microstructure of 9Cr-1Mo martensitic steels containing a high helium concentration, J. Phys. IV 12 (2002) 103

5. P. Jung, J. Henry, J. Chen, J-C. Brachet, Effect of implanted helium on tensile properties and hardness of 9% Cr martensitic stainless steels, Journal of Nuclear Materials. Vol. 318, pp. 241-248 (2003)

6. J. Henry, M.H. Mathon, P. Jung, Microstructural analysis of 9% Cr martensitic steels containing 0.5 at% helium, Journal of Nuclear Materials. Vol. 318, pp. 249-259 (2003).

7. H. de Monestrol, P. Pareige, J. Henry, Atom Probe analysis and field ion microscopy of 9% Cr martensitic steels containing 0.5 at% He, to be published

8. P. Jung, J. Henry and J. Chen, " Tensile properties of candidate structural materials for high power spallation sources at high helium contents, to be published in Journal of Nuclear Materials, in 2005

9. X. Jia, Y. Dai, M. Victoria, "The impact of irradiation temperature on the microstructure of F82H martensitic/ferritic steel irradiated in a proton and neutron mixed spectrum", Journal of Nuclear Materials, 305 (2002) 1.

10. Y. Dai, X.J. Jia, K. Farrell, "Mechanical properties of T91 irradiated at ≤ 300°C in SINQ Target-3", Journal of Nuclear Materials, 318 (2003) 192.

11. X. Jia , Y. Dai, "Microstructure in martensitic steels T91 and F82H after irradiation in SINQ Target-3", Journal of Nuclear Materials, 318 (2003) 207.

12. X. Jia , Y. Dai, "Small punch tests on martensitic/ferritic steels F82H, T91 and Optimax-A irradiated in SINQ Target-3", Journal of Nuclear Materials, 323 (2003) 360.

13. J. Henry, X. Averty, Y. Dai , P. Lamagnère, J.P. Pizzanelli, J.J. Espinas and P. Wident, "Tensile properties of 9Cr-1Mo martensitic steel irradiated with high energy protons and neutrons", Journal of Nuclear Materials, 318 (2003) 215.

14. X. Jia and Y. Dai, "Microstructure and mechanical properties of F82H weld metal irradiated in SINQ Target -3", J. Nucl. Mater. 329-333 (2004) 309.

15. Y. Dai and X. Jia, "The behaviours of martensitic steels after irradiation in SINQ Target-3", American Nucl. Society, La Grange Park, ILL, (2004) 857.

16. Yong Dai and Pierre Marmy, "Charpy Impact Tests on Martensitic/Ferritic Steels after Irradiation in SINQ Target-3", J. Nucl. Mater. in press.

17. P. Vladimirov, A. Möslang, Comparison of material irradiation conditions for fusion, spallation, stripping and fission neutron sources, J. Nucl. Mat., 329-333(1), 2004, 233

18. P. Olsson, I.A. Abrikosov, L. Vitos and J. Wallenius, Ab Initio Formation Energies of Fe-Cr alloys, J. Nucl. Mat. 321 (2003) 84.

19. J. Wallenius, P. Olsson, C. Lagerstedt, N. Sandberg, R. Chakarova, V. Pontikis, Modelling of Cr precipitation in Fe-Cr alloys, Phys. Rev.B, 69 094103 (2004)

20. L. Malerba, D. Terentyev, P. Olsson, R. Chakarova and J. Wallenius; Molecular dynamics simulation of Fe-Cr of displacement cascades in Fe-Cr alloys, J.Nucl.Mater., 329-333 (2004) 1156

21. J. Wallenius, I. A. Abrikosov, R. Chakarova, C. Lagerstedt, L. Malerba, P. Olsson, V. Pontikis, N. Sandberg, D. Terentyev, Development of an EAM potential for simulation of radiation damage in Fe-Cr alloys, J. Nucl. Mater. 329-333 (2004) 1175

22. J.Wallenius, P. Olsson and C. Lagerstedt, Relation between thermal expansion and interstitial formation energy in pure Fe and Cr, Nucl. Instr. & Meth. B 228 (2005) 122.